

Exact and Asymptotic Analysis of EM-Wave Scattering in Cold Plasma



By

Ayesha Javaid

**Department of Mathematics
Quaid-i-Azam University
Islamabad, Pakistan
2022**

Exact and Asymptotic Analysis of EM-Wave Scattering in Cold Plasma



By

Ayesha Javaid

Supervised By

Prof. Dr. Muhammad Ayub

**Department of Mathematics
Quaid-i-Azam University
Islamabad, Pakistan
2022**

Exact and Asymptotic Analysis of EM-Wave Scattering in Cold Plasma



By

Ayesha Javaid

A THESIS SUBMITTED IN THE PARTIAL FULFILLMENT OF THE REQUIREMENT FOR THE
DEGREE OF
DOCTOR OF PHILOSOPHY
IN
MATHEMATICS

Supervised By

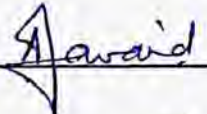
Prof. Dr. Muhammad Ayub

**Department of Mathematics
Quaid-i-Azam University
Islamabad, Pakistan
2022**

Certificate of Approval

This is to certify that the research work presented in this thesis entitled **Exact and Asymptotic Analysis of EM-Wave Scattering in Cold Plasma** was conducted by **Ms. Ayesha Javaid** under the kind supervision of **Prof. Dr. Muhammad Ayub**. No part of this thesis has been submitted anywhere else for any other degree. This thesis is submitted to the Department of Mathematics, Quaid-i-Azam University, Islamabad in partial fulfillment of the requirements for the degree of Doctor of Philosophy in field of Mathematics from Department of Mathematics, Quaid-i-Azam University Islamabad, Pakistan.

Student Name: **Ayesha Javaid**

Signature: 

External committee:

a) **External Examiner 1:**

Name: **Dr. Tariq Javaid**

Designation: Professor

Office Address: Department of Mathematics & Statistics,
International Islamic University, Islamabad.


Signature: 

b) **External Examiner 2:**

Name: **Dr. Muhammad Mushtaq**

Designation: Assistant Professor

Office Address: Department of Mathematics,
COMSATS University, Islamabad.

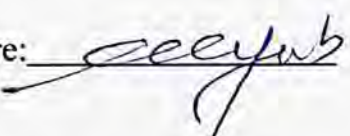
Signature: 

c) **Internal Examiner**

Name: **Prof. Dr. Muhammad Ayub**

Designation: Professor

Office Address: Department of Mathematics, Quaid-i-Azam University,
Islamabad.

Signature: 

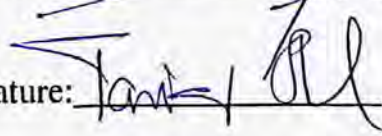
Supervisor Name:

Prof. Dr. Muhammad Ayub

Signature: 

Name of Dean/ HOD

Prof. Dr. Tariq Shah

Signature: 

Author's Declaration

I, **Ayesha Javaid**, hereby state that my Ph. D thesis titled **Exact and Asymptotic Analysis of EM-Wave Scattering in Cold Plasma** is my own work and has not been submitted previously by me for taking any degree from the Quaid-i-Azam University Islamabad, Pakistan or anywhere else in the country/world.

At any time if my statement is found to be incorrect even after my graduate the university has the right to withdraw my Ph. D degree.



Name of Student: **Ayesha Javaid**

Date: **16 Feb 2022**

Plagiarism Undertaking

I solemnly declare that research work presented in the thesis titled "**Exact and Asymptotic Analysis of EM-Wave Scattering in Cold Plasma**" is solely my research work with no significant contribution from any other person. Small contribution/help wherever taken has been duly acknowledged and that complete thesis has been written by me.

I understand the zero-tolerance policy of the HEC and **Quaid-i-Azam University** towards plagiarism. Therefore, I as an Author of the above titled thesis declare that no portion of my thesis has been plagiarized and any material used as reference is properly referred/cited.

I undertake that if I am found guilty of any formal plagiarism in the above titled thesis even afterward of Ph. D degree, the University reserves the rights to withdraw/revoke my Ph. D degree and that HEC and the University has the right to publish my name on the HEC/University Website on which names of students are placed who submitted plagiarized thesis.



Student/Author Signature

Name: **Ayesha Javaid**

Acknowledgement

All praises and glories be to Allah, the Creator, Who created everything from spinning electrons to spiraling galaxies with astonishing beauty and symmetry. I offer my humblest thanks to our Holy Prophet Muhammad (PBUH), who is forever a source of guidance and knowledge for humanity. Thank Allah Almighty for His uncountable blessings on Ummat-e-Musalma due to Ahl-e-Bait and all Sahaba-e-Karaam, Who urge us to unveil the truth behind the natural phenomenon which gives us motivation for research.

*I would also like to express my heartiest gratitude to my worthy supervisor **Sir Professor Dr. Muhammad Ayub** (Passionate and Great Mathematician) for his constant guidance, support, valuable discussions, and inspiring attitude throughout my research work. Here I especially like to mention that he has been very kind to me, without his motivational encouragement I would never be able to complete this dissertation. It was a great privilege and honor for me to work under his kind supervision. I thank him for housing me as a research student and providing me with all his valuable ideas and time.*

*At this great occasion, I can never forget my teachers what they have taught me, especially the thought provoking lectures and inspiring personality of **Prof. Dr. Tasawar Hayat** (Distinguished National Professor), **Prof. Dr. Sohail Nadeem**, **Prof. Dr. Tariq Shah**, **Dr. Babar Mirza**, **Dr. Khalid Saifullah**, and **Dr. Malik Yousaf**.*

*I want to convey my deepest thanks and compliments by the core of heart to my beloved father **Hafeez Jawaid Cheema** (Late). Despite facing many hardships, he supported and encouraged me continuously for completion of my Ph. D degree. And especially to my beloved **Phoophoo G Shamim Fardous** whose support has been as important for me as my father's. I also mention the Precious Duas given by my beloved mother **Tahira Fardous** (Late). I can never forget their sacrifice for me. Their unconditional love for me is priceless.*

*I want to say a very special thanks to my best and dearest husband **Nazam Ali Khan Dhudhi** for his cooperation and kindness. I am thankful to my colleague, **Dr. Sajjad Hussain** for his encouragement, cooperation and guidance during my research work. I would like to thank my all*

*kids Rida Fatima, Haya Fatima, Afifa Batool, Hadia Nazam and Muhammad Hamza Nazam
for giving me their time, true respect, love and pray in favor of me.*

Ayesha Javaid

I dedicate this thesis to my beloved

Parents (Late)

Contents

1	Introduction	5
1.1	Motivation	5
1.2	Background	6
1.3	Dissertation Catalog	9
2	Mathematical Preliminaries	12
2.1	Plane Wave	12
2.2	Electromagnetic Waves	12
2.3	Types of Electromagnetic Waves	12
2.3.1	Radio waves: Instant Communication	13
2.3.2	Microwaves: Data and Heat	13
2.3.3	Infrared Waves: Invisible Heat	13
2.3.4	Visible Light Rays	13
2.3.5	Ultraviolet Waves: Energetic Light	14
2.3.6	X-rays: Penetrating Radiation	14
2.3.7	Gamma Rays: Nuclear Energy	14
2.4	Sinusoidal Grating	14
2.5	Cold Plasma (Non-thermal Plasma)	14
2.6	Boundary Conditions	15
2.6.1	Natural or Dirichlet boundary condition	15
2.6.2	Normal or Neumann or Essential boundary condition	15
2.6.3	Mixed or Robins boundary condition	15

2.7	Fourier Transform	16
2.8	Gamma Function	17
2.9	Generalized Gamma Function	17
2.10	Asymptotic Expansions	18
2.11	Watson's Lemma:	19
2.12	Asymptotic Expansion of Certain Branch Cuts	21
2.13	Analytic Continuation	21
2.14	Asymptotic expansions	22
2.14.1	Method of Stationary Phase	22
2.14.2	Steepest Decent Method	23
2.15	Modeling of Helmholtz Equation	27
3	Non-thermal Plasma Effects on Diffraction of EM-Wave by a Finite Symmetric Plate with Dirichlet Conditions	29
3.1	Problem's Statement	29
3.2	Problem Transformation	31
3.3	Solution of the Wiener-Hopf Equation	33
3.4	Diffracted Field	35
3.5	Discussion and Numerical Results	37
3.6	Conclusions	43
4	Diffraction Affected by Cold Plasma with Neumann Conditions on Finite Plate	44
4.1	Problem Statement	44
4.2	Problem Transformation	46
4.3	Solution of the Wiener-Hopf Equation	48
4.4	Diffracted Field	50
4.5	Discussion and Numerical Results	52
4.6	Conclusions	58

5	Scattering of Electromagnetic Plane Wave Incident on a Finite Corrugated Grating in Non-thermal Plasma	59
5.1	Description Of The Model	60
5.2	Modeling of Wiener-Hopf Equations.	62
5.3	Exact and Asymptotic Results	66
5.4	Scattered Far Field	68
5.5	Numerical Results and Discussion	71
5.6	Conclusion	81
6	EM-Wave Incident on the Slit of Finite Width with Dirichlet Conditions in An-isotropy of Non-thermal Plasma	82
6.1	Problem Statement	82
6.2	Problem Transformation	84
6.3	Solution of the Wiener-Hopf Equation	86
6.4	Diffracted Field	88
6.5	Discussion and Numerical Results	90
6.6	Conclusions	96
7	EM-Wave Incident on Finite-Width Slit with Neumann Conditions in An-isotropy of Non-thermal Plasma	97
7.1	Problem Statement	97
7.2	Problem Transformation	99
7.3	Solution of the Wiener-Hopf Equation	101
7.4	Diffracted Field	103
7.5	Discussion and Numerical Results	105
7.6	Conclusions	111

Nomenclature

$\bar{\epsilon}$	dielectric permittivity tensor
$\epsilon_1, \epsilon_2, \epsilon_z$	dielectric permittivity parameters
ω	operating frequency
ω_p	plasma frequency
ω_c	cyclotron (gyro) frequency
e	electric charge
N_e	ion concentration
H_{dc}	magnitude of geo-magnetic field vector
H_z	magnetic field perpendicular to the plane
η_s	surface impedance
η_0	free surface impedance
ϵ_0	electric permittivity in vacuum
μ_0	magnetic permeability in vacuum
l	length parameter for strip and width parameter for slit
k_{eff}	propagation constant
k	wave-number
θ_0	incidence angle
θ	observation angle
EM	electromagnetic

Chapter 1

Introduction

1.1 Motivation

The literature survey made it clear that researchers were interested in analyzing the effects of cold plasma on scattering of EM-waves. Now a day's interest of researchers towards the scattering of EM-waves in the existence of non-plasma has made a very few investigations under the consideration of various aspects. Therefore, in our thesis we aim to explore the exact and asymptotic solutions for the scattered far field by considering different geometries. Also, to gain thorough insight towards the physics of the models proposed, the effects of the physical parameters will be presented and discussed briefly.

Analysis of diffraction and scattering of waves by planes, half-planes, finite planes and strips is a worthwhile subject matter regarding electromagnetic theory and modern optics. A lot of exact, asymptotic, analytical and numerical techniques are worked out and have been applied to evaluate the results for diffraction phenomena for different geometries. Wiener-Hopf method is one of the strongest techniques to tackle such a large class of problems modelled for diffraction of waves by different types of obstacles.

Electromagnetic waves propagate through an ionized gas and get affected due to interaction with ionized gas. This made the researchers curious. Particularly,

researchers started extensive study and investigation about the waves that radio waves got reflected from and got transmitted through the ionosphere containing cold plasma. This ionized gas is termed as plasma because it is electrically neutral as well as the electron and ion densities are substantially the same. The problem proposed to explore the antenna characteristics, journey of waves through plasma, and radars catching signals are worthwhile. Characteristics of Antenna and artificial satellites regarding wave propagation or communicating signals through ionosphere between vehicle and earth station are also worthwhile. The often existence of DC-magnetic field (geomagnetic field) in plasma makes it an-isotropic medium and named as magneto-plasma. For example, earth magnetic field is effective in ionosphere. Assuming the small effect of temperature and pressure variations in plasma reduces it to non-thermal plasma. The characteristics of an-isotropic medium due to plasma are examined by magneto-ionic theory. In the view of this theory, effects of finite temperature and pressure variations can be ignored, because their action is usually small that is why it is reasonable to deal with the plasma at low temperature. Hence, the magneto-ionic theory may be used as a tool to deal with a cold plasma. Methodology of solution is briefly discussed. The literature survey made it clear that researchers were interested in analyzing the non-plasma's effects on scattering of EM-waves. Now a day's interest of researchers towards the scattering of EM-waves in the existence of non-thermal plasma has made a very few investigations under the consideration of various aspects. Therefore, in our thesis we aim to explore the exact and asymptotic solutions for the scattered far field by considering different geometries.

1.2 Background

The study of scattering of EM-waves is a topic of great interest to the researchers due to wide-ranging application of solar photo-ionization, X-ray radiations of soft nature and communication of EM- signals from an artificial satellite. Poincare [1] and Sommerfeld [2] worked out for the half-plane problems which explored the new

ideas for deep analysis about electromagnetic waves and scattering of sound waves. The Wiener-Hopf method [3,4] used for the solution of different types of waves associated with canonical geometries was studied rigorously. Riemann- Hilbert method had been considered for the diffraction-propagation theory of electromagnetic waves [5]. For rigorous study of electromagnetic (EM) wave scattering, the mode-matching method is used [6]. Several problems on the analysis of line/source diffraction of electromagnetic (EM) waves had been investigated which presented a canonical problem corresponding to the model for GTD (geometrical theory diffraction). Kobayashi [7] studied and then investigated the diffracted wave by a strip in using Wiener-Hopf technique to evaluate the exact and asymptotic solutions. Kobayashi and Eizawa used Wiener-Hopf technique in order to study the diffraction of waves by considering sinusoidal grating [8]. We can look in historical aspects of Wiener-Hopf technique in [9]. Diffraction phenomena of the plane waves by a finite strip under the assumption of impedance on both sides of the surface of strip was investigated using Wiener-Hopf technique [10].

The models proposed to elaborate the diffraction phenomena of electromagnetic (EM) waves by slit with infinite width in the conductible screen have been brought under the rigorous investigation through mathematical analysis. Morse and Rubenstein [11] used the method of separation of variables for investigation of acoustic waves diffracted by slits and ribbon. Clemmow [12] proposed a mathematical model for diffraction by slit in which he derived a dual integral equation using spectrum description of electromagnetic (EM) fields. He assumed the width of slit much larger or greater than the wavelength giving the two complementary cases under the approximate analysis. Hongo [13] investigated the diffraction phenomena due to parallel slits in the conducting screen in which he used the Kobayashi potential technique. Imran et al. extended the Hongo's work to the slits in an impedance plane. He used the Kobayashi's potential technique to investigate the problem rigorously [14].

The EM-waves (electromagnetic waves) propagating across an ionized gas has got the significant attention of researchers for many years. The scientists have studied

extensively on the radio waves or signals reflected from and transmitted through the ionosphere [15-17]. It is known that plasma is such an ionized gas which is electrically neutral and consists of substantially the same electron and ion densities. The study of the problems modeled for the antenna characteristics, propagation of waves through the plasma and radar cross section are of great importance. The wave propagation and antenna characteristics of artificial satellites perform a vital function in transmitting the signals between the earth station and vehicles. A frequent existence of geomagnetic field in plasma allows it to behave as an an-isotropic, the best example is here that the earth magnetic field is effective in non-thermal plasma. The small as well as negligible effect of pressure variations and finite temperature make plasma to behave as a non-thermal plasma. Many researchers work out the effects of cold plasma during analyzing the diffraction waves. Keeping focus on that idea, scientists worked on the scattering of electromagnetic for different structures in the consideration of non-thermal plasma. The diffracted electromagnetic (EM) plane-wave embedded with impedance had been studied to inspect the effects of non-thermal plasma using Wiener-Hopf technique [18]. Khan et al. inspected the diffracted electrically-polarized plane wave by parallel plate wave-guide with imposition of impedance immersed in cold plasma, Wiener-Hopf technique along with mode matching analysis was used [19]. Ayub et al. investigated the affecting non-thermal plasma on the dominant TEM-wave radiated by parallel plate wave-guide with imposition of impedance, radiator behaving as a horn type launcher of surface wave and a horn with impedance loaded [20]. An EM-plane wave's diffraction caused by a finite strip under the effects of non-thermal plasma was inspected using Wiener-Hopf technique by assuming Dirichlet as well as Neumann conditions on the same strip [21, 22]. Later, Ayesha et al. extended the analysis made in [21] by considering the symmetric plate [23].

1.3 Dissertation Catalog

In this thesis our work is summarized as

In chapter 2, we discussed the some basic definitions and methodologies based on plane waves, electromagnetic waves, cold plasma , Fourier transform, boundary conditions, Modeling of Helmholtz Equation, asymptotic expansion, analytic continuation, Watson's lemma, Gamma function, Generalized Gamma function, decomposition theorem, factorization theorem, stationary phase method, decent steepest method, Wiener-Hopf technique.

In chapter 3, we have taken the incident wave in the existence of non-thermal plasma on a finite symmetric strip embedded with Dirichlet boundary conditions. By employing the Fourier transformation on Helmholtz equation we get the boundary value problem. The Wiener-Hopf technique is used to solve the proposed problem. To obtain high-frequency signal, we have assumed that $\omega \gg \omega_c$ leading to $\varepsilon_2 \rightarrow 0$ throughout the analysis. The separated field is evaluated and then effects of various physical parameters are discussed through graphical analysis in the existence of non-thermal plasma. Our research describes that symmetric length of plate has increased the amplitudes and the separated field's oscillations as compared to non symmetric length in the previous article [19]. On analyzing the results, it is observed that diffraction is affected by (a) different angles of incidence, (b) changing the k . (c) extending the $2l$, (d) permittivity of non-thermal plasma.

In chapter 4, we have taken the incident wave in the existence of non-thermal plasma on a finite symmetric strip embedded with Neumann boundary conditions. By the use of Fourier transform on Helmholtz equation, we get the boundary value problem. The Wiener-Hopf technique is used to solve the proposed problem. To obtain high-frequency signals, we have assumed condition $\omega \gg \omega_c$ leading to $\varepsilon_2 \rightarrow 0$ throughout the analysis. The separated field is evaluated and then effects of various physical parameters are discussed through graphical analysis in the existence of non-thermal plasma. Our research describes that symmetric length of plate has

increased the amplitudes and number of field's oscillations. On analyzing the results, it is observed that diffraction is affected by (a) different θ_0 , (b) changing the k , (c) extending the z , (d) permittivity of non-thermal plasma.

In chapter 5, we discussed the diffracted H-polarized plane wave incident at the sinusoidal-shaped grating of finite-length in the presence of nonthermal plasma is analyzed by Wiener-Hopf technique along with perturbation method. Helmholtz equation has been formulated by using Maxwell equations along with non-thermal plasma parameters to inspect the effects of non-thermal plasma on scattered far field intensity. The small corrugation amplitude as compared to wavelength is assumed and scattered field has been expanded in the terms of the perturbation series to lessen the problem to diffraction due to flat-strip embedded with mixed boundary condition. Wiener-Hopf equations of zero- and first-order are formulated with the aid of approximate boundary condition. The decomposition procedure is used to proceed these Wiener-Hopf equations which then yields the exact solutions with high-frequency.

Implementation of the inverse Fourier transformation along with the asymptotic method of saddle point, the scattered field function has been derived which shows validity for arbitrary angles of observation as well as incidence. We have accomplished graphical analysis of field intensity on the basis of results and investigated the diffraction by flat strip and sinusoidal grating in the existence and non-existence of non-thermal plasma in detail. On analyzing the plots, it is observed that the number of oscillations increase due to increasing the number of gratings. Also, non-thermal plasma is responsible in reduction of amplitude's oscillations.

In chapter 6 and 7, We discuss the diffraction of electromagnetic plane-waves due to a slit in the existence of non-thermal plasma. The slit is assumed to be of finite width with Dirichlet and Neumann boundary conditions. Using the Fourier transformation to the Helmholtz equation along with boundary condition, we get the Wiener-Hopf equations which are further solved via the stationary phase method. To obtain a frequency signal, we have assumed that $\omega \gg \omega_c$ leading to $\epsilon_2 \rightarrow 0$ throughout

the analysis. The separated field is calculated and then effects of various physical parameters are discussed through graphical analysis in the existence of non-thermal plasma. Observation describes that finite width of slit has increased the amplitudes and field's oscillations. On analyzing the results, it is observed that diffraction is affected by (a) different θ_0 , (b) changing the k , (c) extending the $2l$, (d) permittivity of non-thermal plasma.

Chapter 2

Mathematical Preliminaries

2.1 Plane Wave

The plane waves are represented by the function of following form

$$\psi(x, y, z, t) = \text{Re} \left\{ \psi_0 \exp(\pm i \vec{k} \cdot \vec{r} - i \omega t) \right\}$$

The sign of + indicates the outgoing waves propagating in the direction of $\vec{k} = [k_x, k_y, k_z]$ whereas the sign of minus represents the incoming waves propagating in the opposite direction of $\vec{k} = [k_x, k_y, k_z]$.

2.2 Electromagnetic Waves

Electromagnetic waves are created when electric field come in contact with magnetic field. These waves travelled with constant velocity in vaccum. These waves are tranverse i.e electric field is perpendicular to magnetic field and they are measured by their amplitude and wavelength.

2.3 Types of Electromagnetic Waves

Generally, there are seven types of electromagnetic waves:

2.3.1 Radio waves: Instant Communication

These are EM waves of low frequency. These waves are emitted by many natural and man made objects. For example radio, television, atara, planeta and other cosmic bodies emit radio waves.

2.3.2 Microwaves: Data and Heat

In the EM spectrum microwaves are the second-lowest frequency waves. These waves can measure from a few centimeters up to a foot. Due to their higher frequency, microwaves can penetrate obstacles that interfere with radio waves such as clouds, smoke and rain. Microwaves uaed for cooking food and carry radar, landline phone calls and computer data transmissions.

2.3.3 Infrared Waves: Invisible Heat

In the EM spectrum infrared waves are in the lower-middle range of frequencies, between microwaves and visible light. The size of infrared waves varies from a few millimeters down to microscopic lengths. The shorter-wavelength infrared rays do not produce much heat and are used in remote controls and imaging technologies, where as longer-wavelength infrared waves produce heat and include radiation emitted by fire, the sun and other heat-producing objects.

2.3.4 Visible Light Rays

The different frequencies of visible light are experienced by people as the colors of the rainbow. The frequencies move from the lower wavelengths, detected as reds, up to the higher visible wavelengths, detected as violet hues. The most noticeable natural source of visible light is, of course, the sun.

2.3.5 Ultraviolet Waves: Energetic Light

Ultraviolet waves has shorter wavelength then visible light. These are the cause of sunburn and can cause of cancer. These are emitted from television microwaves mobile phones etc.

2.3.6 X-rays: Penetrating Radiation

These rays are emitted by the sources which produces very high temperature like the sun's corona, which is much hotter then the surface of the sun. These are used in medical acience to view bone in the body.

2.3.7 Gamma Rays: Nuclear Energy

Gamma waves are the highest-frequency EM waves. These are emitted by only the most energetic comic objects such as neutron stars, supernova, pulsars, and black holes. Terrestrial sources include lightning, nuclear explosions and radioactive decay. The wavelengths of these waves are measured on the subatomic level and can actually pass through the empty space within an atom. These rays can destroy living cells; fortunately, the Earth's atmosphere absorbs any gamma rays that reach the planet.

2.4 Sinusoidal Grating

According to the sine curve $y = \sin x$ a grating having the luminance of the image surge along an axis, increasing and decreasing at a regular spatial frequency is called sinusoidal grating.

2.5 Cold Plasma (Non-thermal Plasma)

Plasma being a fourth or gaseous state of matter is an ionized gas which is electrically neutral medium and contains substantially the same densities of ions and electrons. If the effects of variations of the finite pressure force and temperature are

taken to be small and ignored then plasma is termed as cold plasma. For example, cold plasma can be found in the flow discharge in a fluorescent tube.

2.6 Boundary Conditions

The boundary conditions are linear if it is taken as a linear equation between ϕ and its derivative on the boundary. There are, generally, three types of boundary conditions; (1) : Natural or Dirichlet boundary condition

(2) : Normal or Neumann or Essential boundary condition. (3) : Mixed or Robins boundary condition.

2.6.1 Natural or Dirichlet boundary condition

The boundary condition that specifies the values of the unknown function ϕ on the boundary is called Natural or Dirichlet boundary condition, i.e:

$$\phi = p,$$

2.6.2 Normal or Neumann or Essential boundary condition

If the derivative of ϕ in the normal direction to the boundary is specified on the boundary, i.e;

$$\frac{\partial \phi}{\partial n} = q$$

2.6.3 Mixed or Robins boundary condition

A linear relation between ϕ and its normal derivative on the boundary is called Mixed or Robins boundary condition, i.e:

$$\frac{\partial \phi}{\partial n} + k\phi = r, \quad k > 0$$

2.7 Fourier Transform

This method of complex integral transformation is a mathematical tool which helps in solving the differential equations. This mathematical tool can be utilized for majority of the problems of finite and infinite domain. First suppose that a is real then usual Fourier integral transform of $f(x)$ for all $x \in R$ can be defined as

$$F(\alpha) = \int_{-\infty}^{\infty} f(x)e^{i\alpha x} dx$$

and inversion can be defined as

$$f(x) = \frac{1}{2\pi} \int_{-\infty}^{\infty} F(\alpha)e^{-i\omega x} d\alpha$$

Now suppose that $\alpha = \sigma + i\tau$ is a complex variable. We can define generalized Fourier transform under suitable conditions on f . By starting with half-range transform, $|f(x)| < A_1 e^{\tau-x}$ as $x \rightarrow \infty$ and $f(x) = 0$, for $x < 0$, where $A_1 > 0$ and τ_- are constanta, then we have following function

$$F_+(\alpha) = \int_0^{\infty} f(x)e^{i\alpha x} dx$$

of $F_+(\alpha)$ can found as

$$f(x) = \frac{1}{2\pi} \int_C F(\alpha)e^{-i\alpha x} d\alpha$$

where C is a path of integration lying in the region of analyticity on which varies from $-\infty$ to ∞

In the same way, if we assume that $f(x) = 0$ for $x > 0$, and $|f(x)| < A_2 e^{\tau+x}$ as $x \rightarrow -\infty$, where $A_2 > 0$ and τ_+ are constant, then

$$F_-(\alpha) = \int_{-\infty}^0 f(x)e^{i\alpha x} dx$$

which is analytic in the region $\tau < \tau_+$ of complex α -plane. Now the inverse Fourier

transform of $F_-(\alpha)$ can found as

$$f(x) = \frac{1}{2\pi} \int_C F_-(\alpha) e^{i\alpha x} ds,$$

where C is a path of integration lying in the region of analyticity on which varies from $-\infty$ to ∞ . Combining above results, we get

$$|f(x)| < \begin{cases} A_1 e^{\tau-x} & \text{as } x \rightarrow \infty \\ A_2 e^{\tau+x} & \text{as } x \rightarrow -\infty \end{cases}$$

with $\tau < \tau_+$, then Fourier transform given in (1.5) is the analytic function in the strip $\tau_- < \tau < \tau_+$ and inverse Fourier transform is defined by (1.6).

2.8 Gamma Function

The Gamma function $\Gamma(\eta)$ for a complex variable η is defined

$$\Gamma(\eta) = \int_0^{\infty} t^{\eta-1} e^{-t} dt$$

for $\text{Re } \eta > 0$, where $t^{\eta-1}$ is taken as principle value. The conditions $\text{Re } \eta > 0$ on right hand aide of $Eg(1.12)$ shows the convergence of the infinite integral. The Gamma function is very important special function used in many branches of mathematical physics and is investigated in detail in a number of literature.

2.9 Generalized Gamma Function

Let us consider the complex-variables η and ξ with $\text{Re } \eta > 0, |\xi| > 0$ and $|\arg \xi| < \pi$, and a new special function $\Gamma_m(\eta, \xi)$ as

$$\Gamma_m(\eta, \xi) = \int_0^{\infty} \frac{t^{\eta-1} e^{-t}}{(t + \xi)^m} dt$$

where m be a positive integer, where $t^{\eta-1}$ is again presented as principal value. The conditions $|\xi| > 0$ and $|\arg \xi| < \pi$ have been introduced in order to avoid the case where a pole of order m of the integrand in Eq_q.(1.10) at $t = -\xi$ lies on the integration path. The condition $\operatorname{Re} \eta > 0$ has the same meaning as that required for the definition of the Gamma function. Since the $\Gamma_m(\eta, \xi)$ reduces to $\Gamma(\eta)$ by taking $m = 0$ we shall call $\Gamma_m(\eta, \xi)$ as a generalized Gamma function.

Although analytical properties of $\Gamma_m(\eta, \xi)$ have not yet been sufficiently investigated so far. this function is of great importance in the wave scattering and diffraction theory as related to the Wiener-Hopf technique, since the multiple edge diffraction process can be defined explicitly in terms of this special function.

Kobayashi in his paper [25] worked on Generalized Gamma function in detail and investigated several important analytical properties such as regularity with respect to the variables η and ξ , asymptotic expansion for large $|\xi|$, analytic continuations in ξ –*plane*, generalized incomplete Gamma function and discuss fundamental properties briefly.

2.10 Asymptotic Expansions

Consider z with $\alpha \leq \arg(z) \leq \beta$ and

$$\sum_{n=0}^{\infty} \frac{a_n}{z^n} = \sum_{n=0}^{\infty} a_n z^{-n}$$

be a convergent or divergent series.

Definition: This series is called an asymptotic power series of $f(z)$ for $|z| \rightarrow \infty$ and $\alpha \leq \arg(z) \leq \beta$ if for each $n \in \{1, 2, 3, \dots\}$

$$f(z) = \sum_{k=0}^{n-1} a_k z^{-k} + R_n(z)$$

where

$$R_n(z) = O(z^{-n}) \text{ for } |z| \rightarrow \infty \text{ and } \alpha \leq \arg(z) \leq \beta$$

Theorem : A function f has an asymptotic expansion of the form () for $|z| \rightarrow \infty$ and $\alpha \leq \arg(z) \leq \beta$ if and only if for each $n \in \{1, 2, 3, \dots\}$

$$z^n \left[f(z) - \sum_{k=0}^{n-1} a_k z^{-k} \right] \rightarrow a_n \text{ for } |z| \rightarrow \infty \text{ and } \alpha \leq \arg(z) \leq \beta$$

Hence a function f has at most one asymptotic expansion of the form () for $\alpha \leq \arg(z) \leq \beta$. Asymptotic expansion might be different for distinct regions, however distinct functions will have same asymptotic expansion in some region. For example, if for some $\delta > 0$

$$f(z) \sim \sum_{n=0}^{\infty} a_n z^{-n} \text{ for } |z| \rightarrow \infty \text{ and } \arg(z) \leq \frac{\pi}{2} - \delta < \frac{\pi}{2}$$

and, $f(z) + e^{-z}$ have the same asymptotic expansions.

2.11 Watson's Lemma:

Let f be a complex valued function of a real variable t such that

(1). f is continuous on $(0, \infty)$, (2).

$$f(t) \sim \sum_{n=0}^{\infty} a_n t^{\lambda_n - 1} \text{ for } t \rightarrow 0$$

with

$$0 < \lambda_0 < \lambda_1 < \lambda_2 < \dots$$

and (3). for some $c > 0$

$$f(t) = O(e^{ct}) \quad \text{for } t \rightarrow \infty$$

Then we have

$$F(z) = \int_0^{\infty} e^{-zt} f(t) dt \sim \sum_{n=0}^{\infty} a_n \frac{\Gamma(\lambda_n)}{z^{\lambda_n}} \quad \text{for } |z| \rightarrow \infty \text{ and } \arg(z) \leq \frac{\pi}{2} - \delta < \frac{\pi}{2},$$

for some δ such that $0 < \delta < \frac{\pi}{2}$. Proof: We have

$$F(z) = \int_0^{\infty} e^{-zt} f(t) dt$$

the integral converges for $\operatorname{Re} z > c$.

$$\left| f(t) - \sum_{n=0}^{\infty} a_n t^{\lambda_n - 1} \right| \leq M t^{\lambda_{N-1}} \quad \text{for } t \rightarrow 0$$

where $M > 0$ is constant. Applying () we get

$$\left| f(t) - \sum_{n=0}^{\infty} a_n t^{\lambda_n - 1} \right| \leq K e^{ct} t^{\lambda_{N-1}} \quad \text{for } t > 0$$

where $K > 0$ is some constant. we have

$$\left| \int_0^{\infty} e^{-zt} f(t) dt - \sum_{n=0}^{N-1} a_n \int_0^{\infty} e^{-zt} t^{\lambda_n - 1} dt \right| \leq K \int_0^{\infty} e^{-(\operatorname{Re} z - c)t} t^{\lambda_{N-1}} dt$$

for $\operatorname{Re} z > 0$

$$\int_0^{\infty} e^{-zt} t^{\lambda_n - 1} dt = \frac{1}{z^{\lambda_n}} \int_0^{\infty} e^{-\tau} \tau^{\lambda_n - 1} d\tau = \frac{\Gamma(\lambda_n)}{z^{\lambda_n}}$$

we get

$$\left| F(z) - \sum_{n=0}^{N-1} a_n \frac{\Gamma(\lambda_n)}{z^{\lambda_n}} \right| \leq K \frac{\Gamma(\lambda_N)}{(\operatorname{Re} z - c)^{\lambda_N}} = K \frac{\Gamma(\lambda_N)}{z^{\lambda_N}} \left(\frac{|z|}{\operatorname{Re} z - c} \right)^{\lambda_N}$$

Since $|\arg(z)| \leq \frac{\pi}{2} - \delta < \frac{\pi}{2}$, we have $\operatorname{Re} z \geq |z| \sin \delta$ which implies that $\operatorname{Re} z - c \geq \frac{1}{2}|z| \sin \delta$ for $|z|$ large enough. Thus we have

$$F(z) - \sum_{n=0}^{N-1} a_n \frac{\Gamma(\lambda_n)}{z^{\lambda_n}} = O(z^{-\lambda_N})$$

which proves Watson's lemma.

2.12 Asymptotic Expansion of Certain Branch Cuts

Let $f(\beta)$ be a function with the following conditions: (i) $f(\beta)$ be the analytic function in $|\beta - k| < r_0 < \theta$ where k is complex number with both of its imaginary and real part are positive and $r_0 \neq 0$. (ii) $f(\beta)$ holds $f(\beta) = O[(\beta - k)^\delta]$ such that $|\beta - k| \geq R$ with $R < \infty$ and, δ is some real constant. (iii) $f(\beta)$ be a continuous function of β on any bounded part of the straight path from k to $k + i\infty$ in the β -plane.

Let us consider α in such a way that $|\alpha + k| > 0$ and $-\pi/2 < \arg(\alpha + k) < 3\pi/2$, and introduce $F_{\text{mov}}(l, \alpha)$ as

$$F_{mv}(l, \alpha) = \frac{1}{\pi i} \int_k^{k+i\infty} e^{i\beta l} \frac{(\beta - k)^v f(\beta)}{(\beta + \alpha)^m} d\beta$$

for $l > 0$, $\text{Re } v > -1$ and positive integer m , where $\arg(\beta - k) = \pi/2$ the condition $l > 0$, $\text{Re } v > -1$ ensures the indefinite integral's absolute convergence in Eq. (1.14) whereas $|\alpha + k| > 0$ and $-\pi/2 < \arg(\alpha + k) < 3\pi/2$, are required to ignore the case where a pole of order m of the integrand at $\beta = -\alpha$ lies on the contour. The condition $\arg(\beta - k) = \pi/2$ has also appeared in the definition of $F_{mv}(l, \alpha)$, which has been introduced in order that $(\beta - k)^v$ be a single-valued function of non integer v .

2.13 Analytic Continuation

If $f(z)$ is an analytic function in a domain D and $F(z)$ is analytic in a domain D' such that $F(z) = f(z)$ in $D \cap D'$, then F is said to be an analytic continuation of f .

Now we can say that analytic continuation is a process of extending an analytic function defined in a domain to a larger domain. For example, the geometric series at zero is given by

$$f(z) = 1 + z + z^2 + z^3 \dots$$

which is convergent in the open disk as $D = \{|z| < 1\}$. Multiplication of (1.1) by z and subtraction of result from (1.15) gives

$$(1 - z)f(z) = 1 \Rightarrow f(z) = \frac{1}{1 - z}$$

which is analytic in $D = C \setminus \{1\}$. Since $\{|z| < 1\} \subset C \setminus \{1\}$ i.e $D \subset D$ and $F(z) = f(z)$, therefore, $F(z)$ is analytic continuation of $f(z)$.

2.14 Asymptotic expansions

2.14.1 Method of Stationary Phase

Consider a function of the form

$$f(x) = \int_a^b e^{ixh(t)} g(t) dt$$

where $h(t)$ is a real function (known as phase function) and $g(t)$ can be complex or real function and integration is along the real axis over the interval (a, b) . The stationary phase method helps in finding an asymptotic representation of (1.25). Assume that there is one point $t_0 \in (a, b)$ such that $h'(t_0) = 0$ but $h''(t_0) \neq 0$. In accordance with the idea of the method of stationary phase, we assume that only the neighborhood of t_0 is of significance, and we write

$$ixh(t) \cong ix \left\{ h(t_0) + \frac{1}{2} h''(t_0) (t - t_0)^2 \right\}.$$

Then

$$f(x) \sim \int_{-\infty}^{\infty} g(t) \exp \left[ix \left\{ h(t_0) + \frac{1}{2} h''(t_0) (t - t_0)^2 \right\} \right] dt$$

This gives

$$f(x) \sim \left[\frac{2\pi}{x |h''(t_0)|} \right]^{1/2} g(t_0) \exp \left[ixh(t_0) \pm i \frac{\pi}{4} \right],$$

where the sign of $+$ or $-$ corresponds to $h''(t_0) > 0$ or $h''(t_0) < 0$, respectively. For detailed analysis about this method, see [23, 24]

2.14.2 Steepest Decent Method

To find the asymptotic behavior of the following integral

$$I(k) = \int_C f(z) e^{k\phi(z)} dz, \quad k \rightarrow \infty$$

where $f(z)$ and $\phi(z)$ are complex analytic functions. To reform the contour C to another contour \dot{C} (Cauchy theorem) in which the imaginary part of the exponent is constant, by taking the analytic character of the functions. As the integral take the form of a Laplace integral, we apply the rigorous Laplace method to get

$$\phi(z) = u(x, y) + iv(x, y), \quad z = x + iy$$

Taking, $\text{Im}\{\phi\} = v$ is constant in contour C then,

$$I(k) = \int_C f(z) e^{k\phi(z)} dz = \int_{\dot{C}} e^{ikv} f(z) e^{ku} dz$$

In order to choose the contour \dot{C} , we take the path of steepest decent passing through z_0 in which $\dot{\phi}(z_0) = 0$ (saddle point). We find where the major contributions comes from after choosing the path. The main contributions will happen at critical points $\dot{\phi}(z) = 0$, singular points and end points, then we analyze the Laplace integral at these points.

Steepest Path

Let $\phi(z) = u(x, y) + iv(x, y)$, with $z = x + iy$, then the paths passing through the points $z = z_0$ (where $v(x, y) = v(x_0, y_0)$) are the paths where the imaginary part of ϕ is constant. The direction of decent is from z_0 is along $Re(\phi(z))$ is decreasing; when this decrease is maximal, the path is called steepest decent. Similarly, the direction of ascent is a direction away from z_0 in which u is increasing; when this increase is

maximal, the path is called steepest ascent. We know that in calculus if $u(z_0)$ and $\nabla u \neq 0$, then $-\nabla u$ is the steepest path decreasing away from $u(z_0)$. It can easily be shown that the curves defined by $v(x, y) = v(x_0, y_0)$ are curves of steepest descent or ascent. Let $\delta\phi$ as the change of the function ϕ from the point z_0 , then

$$\delta\phi = \phi(z) - \phi(z_0) = \delta u + i\delta v \rightarrow |\delta u| \leq |\delta\phi|$$

Equality occurs when δu is maximal, so $\delta v = 0 \rightarrow v(x, y) = v(x_0, y_0)$. This, in fact, shows why we need the steepest path. The Saddle Point The point $z = z_0$ is a saddle point of order N for the function ϕ if:

$$\left. \frac{d^m \phi}{dz^m} \right|_{z=z_0} = 0, \quad m = 1, 2, \dots, N, \quad \left. \frac{d^{N+1} \phi}{dz^{N+1}} \right|_{z=z_0} \neq 0$$

How to Find Steepest Paths

If z_0 is a saddle point of order N , then we can write:

$$\phi(z) - \phi(z_0) \sim \left. \frac{(z - z_0)^{N+1} d^{N+1} \phi}{(N+1)! dz^{N+1}} \right|_{z=z_0}$$

Letting $\left. \frac{d^{N+1} \phi}{dz^{N+1}} \right|_{z=z_0} = ae^{i\alpha}$ and $z - z_0 = \rho e^{i\theta}$, then

$$\phi(z) - \phi(z_0) \sim \frac{\rho^{N+1} e^{i(N+1)\theta}}{(N+1)!} \times ae^{i(N+1)\alpha} = [\cos(\alpha + (N+1)\theta) + i \sin(\alpha + (N+1)\theta)] \times \frac{\rho^{N+1} a}{(N+1)!}$$

Steepest direction:

$$\text{Im} \left\{ \phi(z) - \phi(z_0) = 0 \rightarrow \sin(\alpha + (N+1)\theta) = 0 \rightarrow \alpha + (N+1)\theta = m\pi \rightarrow \theta = -\frac{\alpha}{N+1} + m\frac{\pi}{N+1}, m = 0, 1, \dots \right.$$

Steepest decent direction:

$$\text{Re} \left\{ \phi(z) - \phi(z_0) < 0 \rightarrow \cos(\alpha + (N+1)\theta) < 0 \rightarrow \theta_{sd} = -\frac{\alpha}{N+1} + (2m+1)\frac{\pi}{N+1} \right.$$

Steepest ascent direction:

$$\operatorname{Re} \left\{ \phi(z) - \phi(z_0) < 0 \rightarrow \cos(\alpha + (N+1)\theta) < 0 \rightarrow \theta_{sa} = -\frac{\alpha}{N+1} + m\frac{\pi}{N+1} \right.$$

Decomposition Theorem: Let $F(\alpha)$ be a regular function in the strip $\tau^- < \operatorname{Im}(\alpha) < \tau^+$ and $F(\alpha) \rightarrow 0$ as $\alpha \rightarrow \infty$ in the strip then $F(\alpha)$ can be decompose as

$$F(\alpha) = F_-(\alpha) + F_+(\alpha)$$

where

$$F_+(\alpha) = \frac{1}{2\pi i} \int_{-\infty+ic}^{\infty+ic} \frac{f(\xi)}{(\xi - \alpha)} d\xi \quad \tau^- < c < \tau < \tau^+,$$

is non zero and regular in the upper half plane ($\alpha > \tau^-$)

$$F_-(\alpha) = -\frac{1}{2\pi i} \int_{-\infty+id}^{\infty+id} \frac{f(\xi)}{(\xi - \alpha)} d\xi \quad \tau^- < d < \tau < \tau^+,$$

is non zero and regular in the lower half plane ($\alpha < \tau^+$). 2.0.19 Factorization theorem

Let $\Psi(\alpha)$ be a non zero and regular function in the strip $\tau^- < \operatorname{Im}(\alpha) < \tau^+$. If $|\Psi(\alpha)| \rightarrow 1$ as $\alpha \rightarrow \infty$ in the atrip then $\Psi(\alpha)$ can be factorize as

$$\Psi(\alpha) = \Psi_-(\alpha)\Psi_+(\alpha)$$

where

$$\Psi_+(\alpha) = \exp \left[\frac{1}{2\pi i} \int_{-\infty+ic}^{\infty+ic} \frac{f(\xi)}{(\xi - \alpha)} d\xi \right] \quad \tau^- < c < \tau < \tau^+$$

is analytic in the region defined by ($\alpha > \tau^-$)

$$\Psi_-(\alpha) = \exp \left[-\frac{1}{2\pi i} \int_{-\infty+id}^{\infty+id} \frac{f(\xi)}{(\xi - \alpha)} d\xi \right] \quad \tau^- < d < \tau < \tau^+$$

is analytic in the region defined by ($\alpha < T^+$). 2.0.20 Wiener-Hopf Technique This technique was initially utilized to solve the integral equation which presents most of

physical problema. An integral equation of that form is given by

$$\int_0^\theta K(x-y)f(y)dy = g(x), 0 < x < \infty$$

where the kernel difference $K(x-y)$ and $g(x)$ are known functions while the $f(x)$ is the function to be evaluated. The readera interested to know about this technique generally, can study the aalient points which are briefly outlined here. To proceed the method, domain of integral equation is extended to negative real values of x that is

$$\int_0^\theta K(x-y)f(y)dy = \begin{cases} g(x), & 0 < x < \infty \\ h(x), & -\infty < x < 0 \end{cases}$$

where $h(x)$ is an unknown function. Applying the Fourier transform on (1.46) we get the Wiener-Hopf functional equation

$$G_+(\alpha) + H_-(\alpha) = K(\alpha)F_+(\alpha)$$

in which $G_+(\alpha)$ and $K(\alpha)$ are half-range and full-range Fourier tranafom of known functions $g(x)$ and $K(x)$, reapectively whereas the quantities $H_-(\alpha)$ and $F(\alpha)$ are half-range Fourier transform of unknown functions $h(x)$ and $f(x)$, reapectively. The right side of (1.18) is product form which comes from integral operator being a convolution-type. The functions with subscript $+$ and $-$ are the analytic in their corresponding regions, respectively and they overlap to form a strip or band of analyticity. The Wiener-Hopf procedure depends on the product factorization of transformed kernel function, in $K(\alpha)$ the form

$$K(\alpha) = K_+(\alpha)K_-(\alpha)$$

Use of (1.48) enables to re-write (1.47) as

$$\frac{1}{K_-(\alpha)}[G_+(\alpha) + H_-(\alpha)] = K_+(\alpha)F_+(\alpha)$$

Note that R.H.S is analytic in its indicated region of analyticity. For left hand side, first term needs to be tackled, therefore, defining the sum-factorization for first term on the left hand side, in the form of

$$\frac{G_+(\alpha)}{K_-(\alpha)} = L_+(\alpha) + L_-(\alpha).$$

Inserting (1.50) in (1.49) and re-expressing the resulting equation as

$$L_-(\alpha) + \frac{H_-(\alpha)}{K_-(\alpha)} = K_+(\alpha)F_+(\alpha) + L_+(\alpha),$$

in which left hand side shows analytic behavior in the lower-half of complex α -plane and right hand side shows analytic behavior in the overlapping upper-half plane of complex α -plane. Analytic continuation allows to equate both sides of (1.51) to an entire function, say $J(\alpha)$. Now $J(\alpha)$ may be evaluated by assuming the behavior of functions $f(x), g(x), h(x)$ as $x \rightarrow 0$ and their corresponding transformed functions in (1.29) as $|\alpha| \rightarrow \infty$, and hence, $F_+(\alpha)$ and $H_-(\alpha)$ are distinctively evaluated. The inverse Fourier transform results the required unknown function $f(x)$.

2.15 Modeling of Helmholtz Equation

In the view of non-thermal plasma, the dielectric permittivity tensor is:

$$\bar{\varepsilon} = \begin{pmatrix} \varepsilon_1 & -\iota\varepsilon_2 & 0 \\ \iota\varepsilon_2 & \varepsilon_1 & 0 \\ 0 & 0 & \varepsilon_z \end{pmatrix},$$

where

$$\varepsilon_1 = \frac{1 - \left(\frac{\omega_p}{\omega}\right)^2}{1 - \left(\frac{\omega_c}{\omega}\right)^2}, \quad \varepsilon_2 = \left(\frac{\omega_p}{\omega}\right)^2 \left[\frac{\omega}{\omega_c} - \frac{\omega_c}{\omega} \right]^{-1}, \quad \varepsilon_z = 1 - \left(\frac{\omega_p}{\omega}\right)^2$$

with

$$\omega_p^2 = \frac{N_e e^2}{m \varepsilon_0}, \quad \omega_c = \frac{|e| \mu_0 H_{dc}}{m}.$$

For the formulation modeled here, the magnetic and electric fields vectors are $\vec{H} = H_z \hat{e}_z$ and be $\vec{E} = E_x \hat{e}_x + E_y \hat{e}_y$, respectively. $E_x(x, y)$ and $E_y(x, y)$ containing $H_z(x, y)$, embedded with $\bar{\varepsilon}$, can be derived from Maxwell's equations:

$$E_x = \frac{i\varepsilon_1}{\omega\varepsilon_0(\varepsilon_1^2 - \varepsilon_2^2)} \partial_y H_z(x, y) + \frac{\varepsilon_2}{\omega\varepsilon_0(\varepsilon_1^2 - \varepsilon_2^2)} \partial_x H_z(x, y)$$

$$E_y = \frac{\varepsilon_2}{\omega\varepsilon_0(\varepsilon_1^2 - \varepsilon_2^2)} \partial_y H_z(x, y) - \frac{i\varepsilon_1}{\omega\varepsilon_0(\varepsilon_1^2 - \varepsilon_2^2)} \partial_x H_z(x, y)$$

Also, from Maxwell's equation,

$$\vec{\nabla} \times \vec{E} = -\mu_0 \partial_t \vec{H}$$

Use of (1.20), (1.21) in (1.22) and following up the time as $\exp(-i\omega t)$, the Helmholtz's equation of H_z is as follows:

$$\partial_{xx} H_z + \partial_{yy} H_z + k_{eff}^2 H_z = 0$$

where

$$k_{eff} = k \sqrt{\frac{\varepsilon_1^2 - \varepsilon_2^2}{\varepsilon_1}}, \quad k = \omega \sqrt{\varepsilon_0 \mu_0}$$

Here, k_{eff} depends on k, ε_1 and ε_2 . Time dependence is taken as behaving harmonically as $\exp(-\omega t)$ and will be followed up throughout the study.

Chapter 3

Non-thermal Plasma Effects on Diffraction of EM-Wave by a Finite Symmetric Plate with Dirichlet Conditions

This chapter addresses the investigation of electromagnetic plane wave diffraction by a conducting plate of finite length in cold plasma. The boundary value problem along with Fourier transform for the corresponding is used to formulate Wiener-Hopf equation which is then solved by using Wiener-Hopf procedure in a standard way. The separated field is evaluated for an an-isotropic medium using asymptotic expansion and modified stationary phase method. The results for the isotropic medium can be achieved by taking $\varepsilon_1 \rightarrow 1$, $\varepsilon_2 \rightarrow 0$. Graphical results are discussed for separated field against observation angle for various physical parameters in isotropic and an-isotropic media.

3.1 Problem's Statement

We have investigated the diffraction pattern of plane electromagnetic waves due to a finite-length strip in non-thermal plasma, as illustrated in Fig. 3.1. Furthermore,

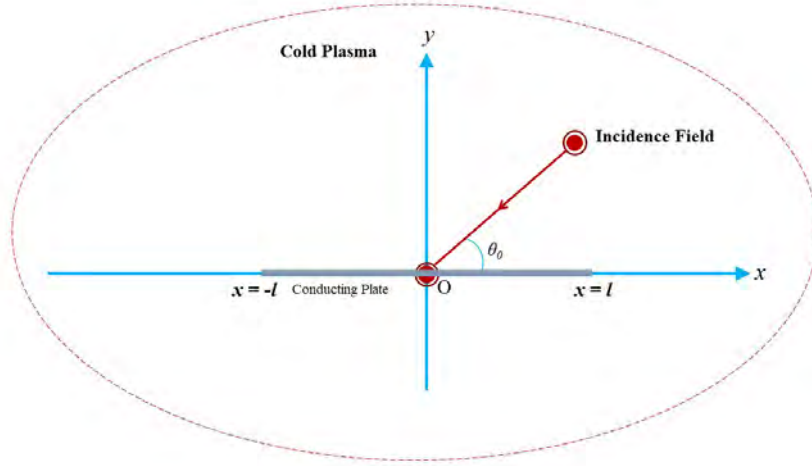


Figure 3.1: **Simplified figure of the problem.**

Dirichlet surfaces are assumed on the strip and angle of incidence is θ_0 . The total field can be represented in terms of incident, refracted and diffracted fields as:

$$H_z^{tot}(x, y) = H_z^{inc}(x, y) + H_z(x, y), \quad (3.1)$$

where the incident field is defined as

$$H_z^{inc}(x, y) = e^{-ik_{eff}(x \cos \theta_0 + y \sin \theta_0)}, \quad (3.2)$$

Suppose that medium is slightly lossy, and constant K_{eff} appearing in above equations is complex in such a way ($0 < \Im\{k_{eff}\} \ll \Re\{k_{eff}\}$). At the end, for real K_{eff} solution could be determine by taking its imaginary part to zero. The entire field $H_z^{tot}(x, y)$ meeting the Helmholtz equation is

$$[\partial_{xx} + \partial_{yy} + k_{eff}^2]H_z^{tot}(x, y) = 0, \quad (3.3)$$

Substituting the value of $H_z^{tot}(x, y)$ from (3.1), we get the equation for diffracted field as:

$$[\partial_{xx} + \partial_{yy} + k_{eff}^2]H_z(x, y) = 0, \quad (3.4)$$

To formulate the Wiener-Hopf equation, conditions at $x = \pm l$ in conjunction with continuity relations are used. Dirichlet boundary conditions on a finite-width slit are specified as

$$H_z^{tot} = 0, \text{ for } -l \geq x \geq l, \text{ at } y = 0^\pm, \quad (3.5)$$

along with

$$H_z^{tot}(x, 0^+) = H_z^{tot}(x, 0^-), \text{ for } |x| > l, \text{ at } y = 0, \quad (3.6)$$

$$\partial_y H_z^{tot}(x, 0^+) = \partial_y H_z^{tot}(x, 0^-), \text{ for } |x| > l, \text{ at } y = 0. \quad (3.7)$$

3.2 Problem Transformation

Following results can be obtained with the use of Fourier Transforms.

$$\begin{aligned} \mathcal{F}(\beta, y) &= \frac{1}{\sqrt{2\pi}} \int_{-\infty}^{\infty} e^{i\beta x} H_z(x, y) dx \\ &= e^{i\beta l} \mathcal{F}_+(\beta, y) + e^{-i\beta l} \mathcal{F}_-(\beta, y) + \mathcal{F}_l(\beta, y), \end{aligned} \quad (3.8)$$

where $\beta = \sigma + i\tau$.

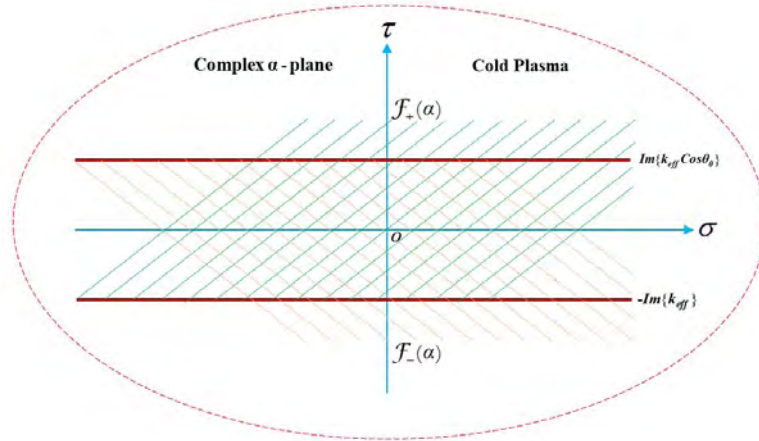


Figure 3.2: Illustration of Analytic-Continuation.

For high values of x , the diffracted field is interpreted as follows:

$$H_z(x, y) = \begin{cases} O(e^{-ik_{eff}x}), \\ O(e^{-k_{eff}x \cos \theta_0}). \end{cases} \quad (3.9)$$

The regions of regularity in the complex plane for $\mathcal{F}_+(\beta, y)$ and $\mathcal{F}_-(\beta, y)$ are $\Im\{\beta\} > -\Im\{k_{eff}\}$ and $\Im\{\beta\} < \Im\{k_{eff} \cos \theta_0\}$. From Fig ??, we can see the common region $-\Im\{k_{eff}\} < \Im\{\beta\} < \Im\{k_{eff} \cos \theta_0\}$ of analyticity, where the function $\mathcal{F}_l(\beta, y)$ is also holomorphic and hence, we can define

$$\mathcal{F}_\pm(\beta, y) = \pm \frac{1}{\sqrt{2\pi}} \int_{\pm l}^{\pm\infty} e^{i\beta(x \mp l)} H_z(x, y) dx \quad (3.10)$$

$$\mathcal{F}_l(\beta, y) = \frac{1}{\sqrt{2\pi}} \int_{-l}^l e^{i\beta x} H_z(x, y) dx \quad (3.11)$$

$$\mathcal{F}^{inc}(\beta, y) = \frac{\exp(-iyk_{eff} \sin \theta_0)}{\sqrt{2\pi}} \left(\frac{\exp[i\beta(\beta - k_{eff} \cos \theta_0)] - \exp[-i\beta(\beta - k_{eff} \cos \theta_0)]}{i(\beta - k_{eff} \cos \theta_0)} \right). \quad (3.12)$$

$$\mathcal{F}^{ref}(\beta, y) = \frac{\exp(iyk_{eff} \sin \theta_0)}{\sqrt{2\pi}} \left(\frac{\exp[i\beta(\beta - k_{eff} \cos \theta_0)] - \exp[-i\beta(\beta - k_{eff} \cos \theta_0)]}{(\beta - k_{eff} \cos \theta_0)} \right). \quad (3.13)$$

The following transformed boundary value problem could be obtained by applying the Fourier transformation to Eqs. (7.5 – 7.7) .

$$\left(\frac{d^2}{dy^2} + \gamma^2 \right) \mathcal{F} = 0 \quad (3.14)$$

where $\gamma(\beta) = \sqrt{k_{eff}^2 - \beta^2}$.

$$\begin{aligned} \mathcal{F}(\beta, 0^+) &= \mathcal{F}^{ref}(\beta, 0) - \mathcal{F}^{inc}(\beta, 0) \\ \mathcal{F}(\beta, 0^-) &= 0 \end{aligned}, \quad (3.15)$$

and

$$\mathcal{F}_\pm(\beta, 0^+) = 0 = \mathcal{F}_\pm(\beta, 0^-). \quad (3.16)$$

3.3 Solution of the Wiener-Hopf Equation

The solution of transformed boundary value problem (7.14), fulfilling the radiation conditions is,

$$\mathcal{F}(\beta, y) = \begin{cases} A_1(\beta) \exp(-i\gamma y) & y \geq 0, \\ A_2(\beta) \exp(i\gamma y) & y < 0. \end{cases} \quad (3.17)$$

Now using Eqs. (7.15 – 7.17), following Wiener-Hopf equation is obtained.

$$\exp(i\beta l)\mathcal{F}'_+(\beta, 0) + \exp(-i\beta l)\mathcal{F}'_-(\beta, 0) + \mathcal{K}(\beta)\tilde{\mathcal{F}}_l(\beta, 0) = -i\mathcal{G}(\beta), \quad (3.18)$$

where,

$$\mathcal{K}(\beta) = i\gamma, \quad (3.19)$$

$$\tilde{\mathcal{F}}_l(\beta, 0) = \frac{1}{2} (\mathcal{F}_l(\beta, 0^+) - \mathcal{F}_l(\beta, 0^-)) \quad (3.20)$$

$$\mathcal{G}(\beta) = \frac{\exp[i\beta(\beta - k_{eff} \cos \theta_0)] - \exp[-i\beta(\beta - k_{eff} \cos \theta_0)]}{\sqrt{2\pi(\beta - k_{eff} \cos \theta_0)}}, \quad (3.21)$$

The Kernel function defined in Eq. 7.19 can be written as:

$$\mathcal{K}(\beta) = \frac{1}{i\gamma(\beta)} = \mathcal{K}_\pm(\beta) \text{ with } \gamma(\beta) = \gamma_\pm(\beta), \quad (3.22)$$

where $\mathcal{K}_\pm(\beta)$ are,

$$\mathcal{K}_\pm(\beta) = \frac{\exp(-i\frac{\pi}{4})}{\gamma_\pm(\beta)} \text{ with } \gamma_\pm(\beta) = \sqrt{k_{eff} \pm \beta}. \quad (3.23)$$

It must be noted that the functions, $\mathcal{K}_\pm(\beta)$ have region of regularity are $\Im\{\beta\} > -\Im\{k_{eff}\}$ and $\Im\{\beta\} < \Im\{k_{eff} \cos \theta_0\}$ and similarly for $\gamma_\pm(\beta)$. From Eq. (7.18), equating the terms which are regular in their corresponding regions, creates a common region of analyticity. Hence, by analytic continuation, we get an entire function $\mathcal{P}(\beta)$ and by Liouville's theorem, $\mathcal{P}(\beta)$ must be equal to zero[12], yielding the following results.

$$\mathcal{F}_{\pm}(\beta, 0) = \frac{\mathcal{A}}{\sqrt{2\pi}} [\mathcal{K}_{\pm}(\beta)\mathcal{G}_{1,2}(\pm\beta) + \mathcal{K}_{\pm}(\beta)\mathcal{T}(\pm\beta)\mathcal{C}_{1,2}], \quad (3.24)$$

where

$$\mathcal{G}_{1,2}(\beta) = \frac{\exp(\mp ik_{eff}l \cos \theta_0)}{\alpha \mp k_{eff} \cos \theta_0} \left(\frac{1}{\mathcal{K}_{+}(\beta)} - \frac{1}{\mathcal{K}_{+}(\pm k_{eff} \cos \theta_0)} \right) - \exp(\pm ik_{eff}l \cos \theta_0) \mathcal{R}_{1,2}(\beta), \quad (3.25)$$

$$\mathcal{C}_{1,2} = \mathcal{K}_{+}(k_{eff}) \frac{\mathcal{G}_{2,1}(k_{eff}) + \mathcal{K}_{+}(k_{eff})\mathcal{G}_{1,2}(k_{eff})\mathcal{T}(k_{eff})}{1 - \mathcal{K}_{+}^2(k_{eff})\mathcal{T}^2(k_{eff})}, \quad (3.26)$$

$$\mathcal{R}_{1,2}(\beta) = \frac{E_{-1}}{2\pi i(\beta \mp k_{eff} \cos \theta_0)} [\mathcal{W}_{-1}(-i(k_{eff} \pm k_{eff} \cos \theta_0)) - \mathcal{W}_{-1}(-i(k_{eff} + \beta))], \quad (3.27)$$

$$\mathcal{T}(\beta) = \frac{E_{-1}}{2\pi} \mathcal{W}_{-1}[-i(k_{eff} + \beta)l], \quad E_{-1} = 2\sqrt{\frac{l}{i}} e^{ik_{eff}l + \beta}, \quad (3.28)$$

$$\mathcal{W}_{n-1/2}(q) = \int_0^{\infty} \frac{v^n e^{-v}}{v+q} dv = \Gamma(n+1) e^{(\frac{q}{2})} q^{(n-1)/2} \mathcal{W}_{-(n+1)/2, n/2}(q), \quad (3.29)$$

where $q = -i(k_{eff} + \beta)l$, $n = -\frac{1}{2}$ and \mathcal{W} is the Whittaker function. Solving Eqs. 7.17 and 7.18, diffracted field is,

$$\mathcal{F}(\beta, y) = -\frac{1}{\mathcal{K}(\beta)} [\exp(i\beta l)\mathcal{F}_{+}(\beta, 0) + \exp(-i\beta l)\mathcal{F}_{-}(\beta, 0) + \mathcal{F}_l(\beta, 0)] e^{-i\gamma|y|}, \quad (3.30)$$

where

$$\mathcal{F}_l(\beta, 0) = i\mathcal{G}(\beta), \quad (3.31)$$

Inverse Fourier transformation of Eq. (7.30), yields the diffracted field as:

$$H_z(x, y) = \frac{1}{\sqrt{2\pi}} \int_{-\infty}^{\infty} \mathcal{F}(\beta, y) e^{-i\beta x - i\gamma|y|} d\beta. \quad (3.32)$$

Inserting (7.30) in (7.32), we get

$$H_z(x, y) = -\frac{1}{\sqrt{2\pi}} \int_{-\infty}^{\infty} \frac{1}{\mathcal{K}(\beta)} \left\{ \begin{array}{l} e^{i\beta l}\mathcal{F}_{+}(\beta, 0) + e^{-i\beta l}\mathcal{F}_{-}(\beta, 0) + \\ + \tilde{\mathcal{F}}_l(\beta, 0) \end{array} \right\} e^{-i\beta x - i\gamma|y|} d\beta. \quad (3.33)$$

Diffracted field $H_z(x, y)$ further bifurcate in the separated and interaction fields $H_z^{sep}(x, y)$ and $H_z^{int}(x, y)$, respectively as,

$$H_z(x, y) = H_z^{sep}(x, y) + H_z^{int}(x, y), \quad (3.34)$$

where

$$H_z^{sep}(x, y) = \frac{1}{2\pi} \int_{-\infty}^{\infty} \frac{\mathcal{A}}{\mathcal{K}(\beta)} \left\{ \begin{array}{l} \frac{\mathcal{K}_+(\beta) \exp[i(\beta - k_{eff} \cos \theta_0)l]}{\mathcal{K}_+(k_{eff} \cos)(\beta - k_{eff} \cos \theta_0)} \\ - \frac{\mathcal{K}_+(-\beta) \exp[-i(\beta - k_{eff} \cos \theta_0)l]}{\mathcal{K}_+(-k_{eff} \cos)(\beta - k_{eff} \cos \theta_0)} \end{array} \right\} \exp(-i\beta x - i\gamma|y|) d\beta, \quad (3.35)$$

$$H_z^{int}(x, y) = \frac{1}{2\pi} \int_{-\infty}^{\infty} \frac{\mathcal{A}}{\mathcal{K}(\beta)} \left\{ \begin{array}{l} \exp(i\beta l) \mathcal{K}_+(\beta) \mathcal{T}(\beta) \mathcal{C}_1 \\ - \exp[i(\beta + k_{eff} \cos \theta_0)l] \mathcal{K}_+(\beta) \mathcal{R}_1(\beta) \\ + \exp(-i\beta l) \mathcal{K}_-(\beta) \mathcal{T}(-\beta) \mathcal{C}_2 \\ - \exp[-i(\beta + k_{eff} \cos \theta_0)l] \mathcal{K}_-(\beta) \mathcal{R}_2(-\beta) \end{array} \right\} \exp(-i\beta x - i\gamma|y|) d\beta. \quad (3.36)$$

The separated field given by (7.35) depicts diffraction separately at the edges. The $H_z^{inct}(x, y)$ represented by Eq. (7.36) explains the interaction of one end with the other.

3.4 Diffracted Field

The diffracted field due to slit of finite width for the far-field can be obtained by coping with the integral appearing in (7.32). Polar coordinates are introduced for the evaluation of Eq. 7.32 with the following transformation.

$$\beta = -k_{eff} \cos(\phi + i\eta), \quad 0 < \phi < \pi, \quad -\infty < \eta < \infty. \quad (3.37)$$

Now when the method of stationary phase [32] is used for (7.32), the following result are obtained:

$$H_z(r, \phi) = \frac{ik_{eff}}{\sqrt{k_{eff}r}} \mathcal{F}(-k_{eff} \cos \phi, \pm r \sin \phi) \sin \phi \exp\left(ik_{eff}r + i\frac{\pi}{4}\right). \quad (3.38)$$

Using the same polar coordinates, the transformation and subsequently the method of stationary phase are used to assess and yield the separated field and interaction fields as follows:

$$\{H_z^{sep}, H_z^{int}\}(r, \phi) = \frac{1}{\sqrt{2\pi}} \frac{ik_{eff}}{\sqrt{k_{eff}r}} \{f_{sep}, -f_{int}\}(-k_{eff} \cos \phi) \sin \phi \exp\left(ik_{eff}r + i\frac{\pi}{4}\right), \quad (3.39)$$

where

$$f_{sep}(-k_{eff} \cos \phi) = \frac{\mathcal{A}}{\mathcal{K}(-k_{eff} \cos \phi)} \left\{ \begin{array}{l} \frac{\mathcal{K}_+(-k_{eff} \cos \phi) \exp[-ik_{eff}l(\cos \phi + \cos \theta_0)]}{\mathcal{K}_+(k_{eff} \cos \theta_0)(-k_{eff} \cos \phi - k_{eff} \cos \theta_0)} \\ - \frac{\mathcal{K}_+(k_{eff} \cos \phi) \exp[ik_{eff}l(\cos \phi + \cos \theta_0)]}{\mathcal{K}_+(-k_{eff} \cos \theta_0)(-k_{eff} \cos \phi - k_{eff} \cos \theta_0)} \end{array} \right\} \quad (3.40)$$

$$f_{int}(-k_{eff} \cos \phi) = \frac{\mathcal{A}}{\mathcal{K}(-k_{eff} \cos \phi)} \left\{ \begin{array}{l} \exp(-ik_{eff}l \cos \phi) \mathcal{K}_+(-k_{eff} \cos \phi) \\ \quad \times \mathcal{T}(-k_{eff} \cos \phi) \mathcal{C}_1 \\ - \exp[il(-k_{eff} \cos \phi + k_{eff} \cos \theta_0)] \\ \quad \times \mathcal{K}_+(-k_{eff} \cos \phi) \mathcal{R}_1(-k_{eff} \cos \phi) \\ + \mathcal{K}_-(-k_{eff} \cos \phi) \exp(ik_{eff}l \cos \phi) \\ \quad \times \mathcal{T}(k_{eff} \cos \phi) \mathcal{C}_2 \\ - \exp[-il(-k_{eff} \cos \phi + k_{eff} \cos \theta_0)] \\ \quad \times \mathcal{K}_-(-k_{eff} \cos \phi) \mathcal{R}_2(k_{eff} \cos \phi) \end{array} \right\} \quad (3.41)$$

From Eq. (7.38), we can clearly see that the asymptotic expressions for far field can be obtained by letting $k_{eff}r \rightarrow \infty$ and the resulting expressions will be holds true for any observational angle. The separated field of an EM-wave is investigated in order to characterise both the field diffracted by the corners of a strip and the influence of the geometrical wave field. The separated field that results gives physical evidence for the

non-thermal plasma concept. Interacted-field, on the other hand, provides no physical information due to contact at edge to edge, which has formerly been enumerated by H^{sep} . As a result, we've only talked about the separated field because it conveys a full physical comprehension of EM-wave diffraction at the established boundaries. Additionally, we discovered that the interaction field is created by diffraction from the corners of strip at $x = \pm l$. Furthermore, when the strip width is increased to ∞ , the role due to interaction field terms disappears, leaving just the H^{sep} terms in the H . As a consequence, we merely examine the separated field, as illustrated visually in the next section.

3.5 Discussion and Numerical Results

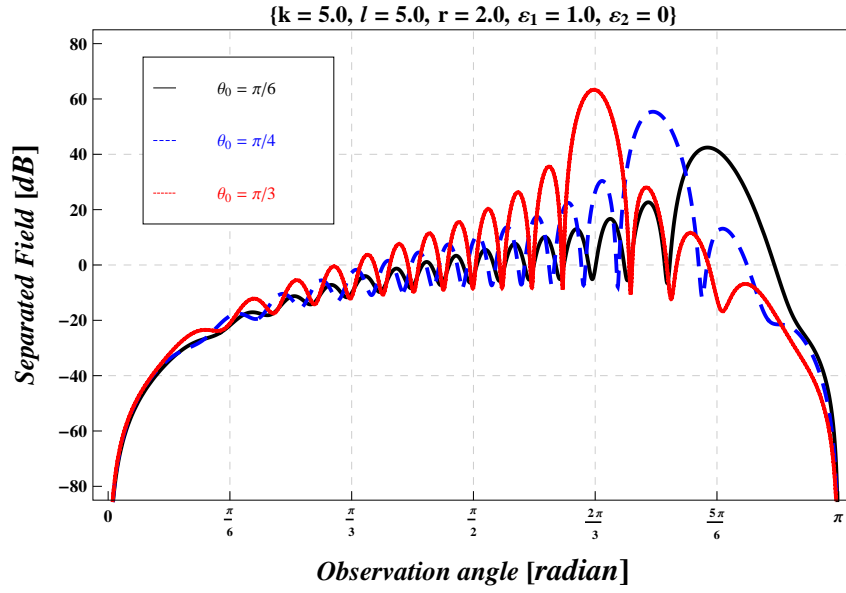
In this section, we examined the EM-waves by finite-length strip as graphically by the variation of physical parameters in an an-isotropic media with Dirichlet conditions versus the observational angle. For the ionosphere, we take the value of ω_p as $56.4MHz$ and ω_c as $8.78MHz$. Now, the values of ε_1 and ε_2 are computed numerically against ω to verify the considered model. Also, the values of ω are taken between $80MHz$ and $600MHz$ given in Table-3.1. It can be notice from Table-3.1, that the value of ε_2 is comparably very small from ε_1 with the boost up of ω in the frequency range. For isotropic medium, we can take $\varepsilon_1 = 1$ and $\varepsilon_2 = 0$, While the parameters ε_1 and ε_2 for the an-isotropic media (non-thermal plasma) can indeed be selected from Table-1.

ω (in MHz)	ε_1	ε_2
80.15	0.504834	0.054242
99.50	0.678699	0.028352
145.75	0.850259	0.009020
245.15	0.947071	0.001895
375.50	0.97744	0.000527
480.50	0.986222	0.000251
599.75	0.991157	0.000129

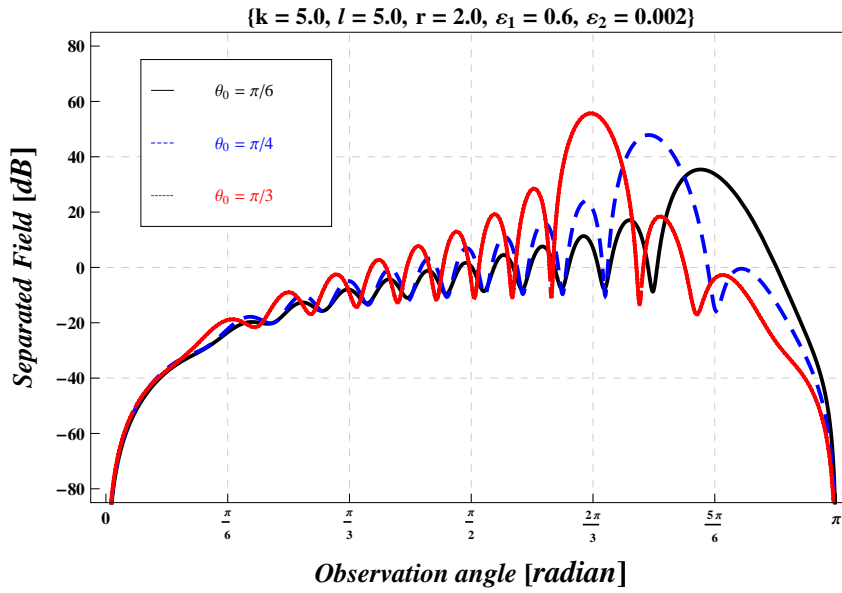
Table 3.1: Values of ε_1 and ε_2 for corresponding ω .

The graphical analysis is elaborated to explore the influence of physical param-

eters on diffracted field due to a finite-length strip lying in the ionosphere of non-thermal plasma. These physical parameters are θ_0 , k , $2l$ and ε_1 . Fig. 3.3 represents the pattern of the separated field for variation of θ_0 , and it gets maxima for $\theta_0 = \pi/3$, $\pi/4$, $\pi/6$ occurring at $\theta = 2\pi/3$, $3\pi/4$, $5\pi/6$, respectively. These maxima actually predict the shadow of reflected field. Fig. 3.4 reveals the separated field for k . It is notable that the field has a direct dependence upon k because the field gets amplified for k . Since the frequency is directly related to k , so it excites the frequency of wave towards the high range. As extension of the slit-width is actually the expansion of aperture which is responsible for the diffraction of electromagnetic radiations, and so, separated field gets amplified as well as more oscillated as can be seen in Fig. 3.5. This amplified amplitude could be controlled by introducing the ionosphere as can be observed through Fig. 3.5b. By comparing Figs. 3.3b, 3.4b and 3.5b of the separated field in the an-isotropic medium with their respective Figs. 3.3a, 3.4a and 3.5a in the isotropic medium. It is explained that an-isotropy of the medium caused by non-thermal plasma influenced the separation field, in both amplitude reduction and wavelength contraction. Fig. 3.6 explores the trend of the field for ε_1 , while its mathematical interpretation predicts its physical nature. It is expressed by Eq. (??) and can be described as ω_c has no big difference in the values in the different parts of Earth and ω_p has direct relation with the square root of N_e (ion concentration), which fluctuates massively with the variation of seasons and days to night. Therefore, without fluctuation on ω , ε_1 can be fluctuate. Since ε_1 has inverse relation with ω , so increase in N_e with fixed ω , ε_1 declines and wavelength will be increase. It means that the separated field with longer wavelength will occur for increasing N_e in the medium.

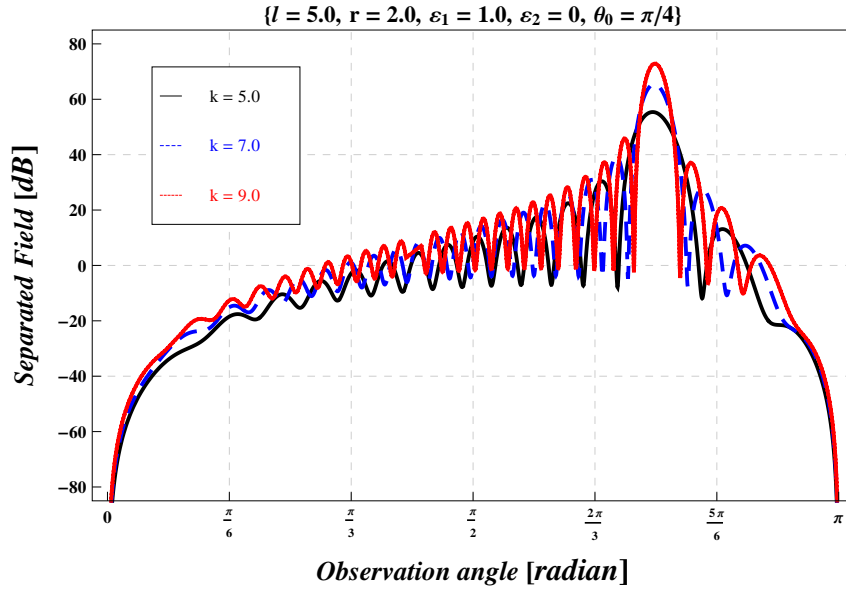


(a)

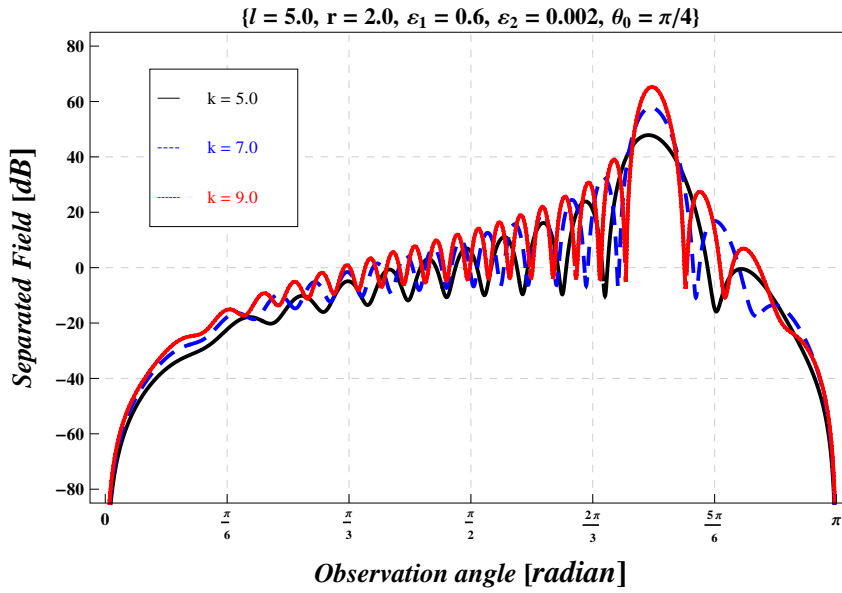


(b)

Figure 3.3: The separated field for θ_0 in the (a) isotropic and (b) an-isotropic medium.

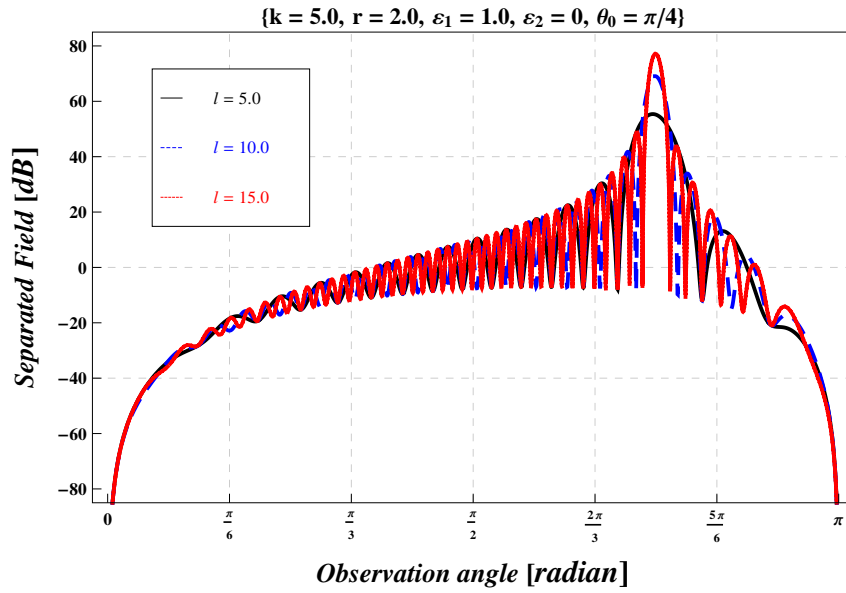


(a)

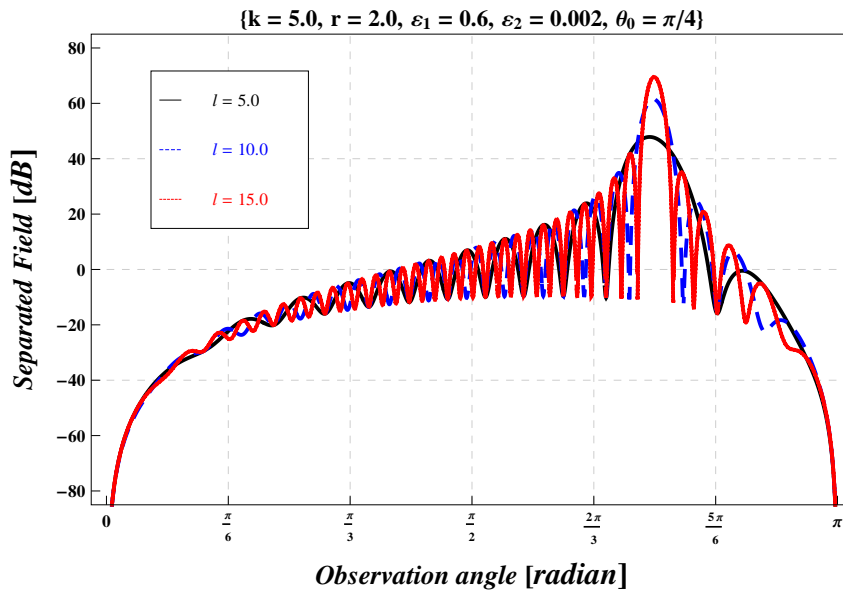


(b)

Figure 3.4: The separated field for k in the (a) isotropic and (b) an-isotropic medium.



(a)



(b)

Figure 3.5: The separated field for $2l$ in the (a) isotropic and (b) an-isotropic medium.

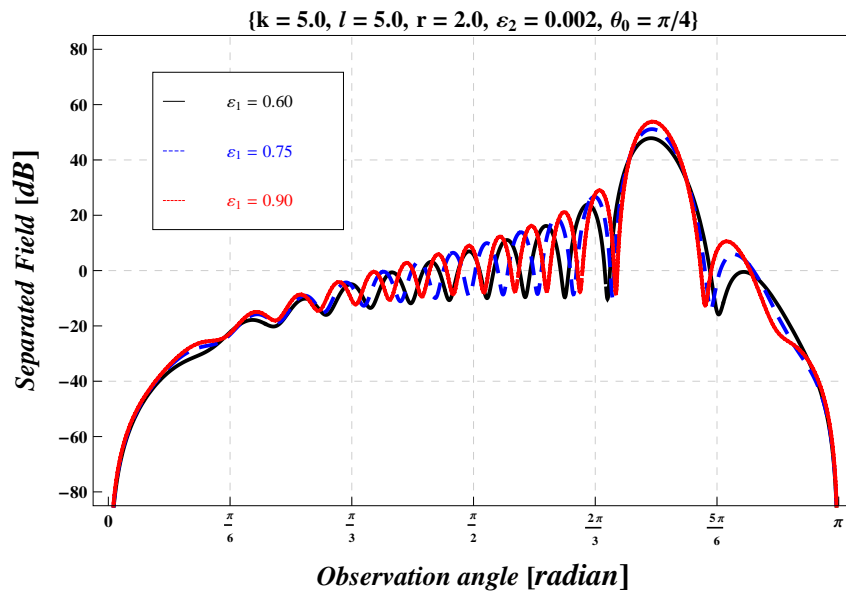


Figure 3.6: The separated field for ε_1 .

3.6 Conclusions

On the basis of above deep analysis, it is figured out that the diffraction behavior of EM-plane wave incident on finite-length strip under the assumptions of Dirichlet surface is affected rigorously by parameters controlling behavior in the existence of non-thermal plasma. It is deeply figured out that the function H^{sep} is amplified by different θ_0 , k , $2l$, ε_1 and reduced by ε_2 .

Chapter 4

Diffraction Affected by Cold Plasma with Neumann Conditions on Finite Plate

Present chapter elaborates the investigation of diffraction phenomenon of EM-plane wave by a non-symmetric plate of finite length in cold plasma. The Wiener-Hopf equation is formulated with the aid of boundary value problem along with Fourier transform for present model. The theory of Wiener-Hopf procedure is used to cope with resulting equation. Asymptotic expansion and method of stationary phase are used to obtain the result for diffracted field by finite plate (separated field) under the assumption of Neumann boundary conditions in the an-isotropic medium. The case of isotropic medium has been discussed by assigning the particular values to elements of permittivity tensor. Impact of physical parameters has been discussed graphically for the isotropic and an-isotropic medium.

4.1 Problem Statement

We have investigated the diffraction pattern of plane electromagnetic waves due to a finite-width slit in non-thermal plasma, as illustrated in Fig. 5.1. Furthermore, Neumann conditions are assumed on the slit and angle of incidence is θ_0 . The total

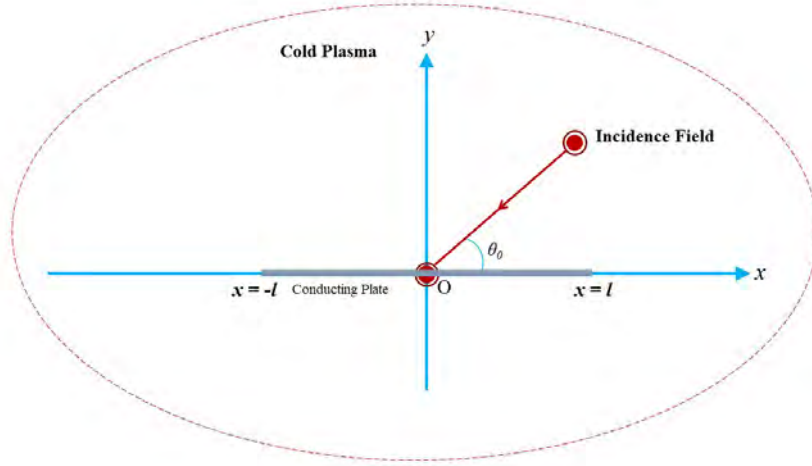


Figure 4.1: **Simplified figure of the problem.**

field could be expressed in terms of incident and diffracted fields,

$$H_z^{tot}(x, y) = H_z^{inc}(x, y) + H_z(x, y), \quad (4.1)$$

where the incident field is defined as

$$H_z^{inc}(x, y) = e^{-ik_{eff}(x \cos \theta_0 + y \sin \theta_0)}, \quad (4.2)$$

Suppose that medium is slightly lossy, and constant K_{eff} appearing in above equations is complex in such a way ($0 < \Im\{k_{eff}\} \ll \Re\{k_{eff}\}$). At the end, for real K_{eff} solution could be determine by taking its imaginary part to zero. The entire field $H_z^{tot}(x, y)$ meeting the Helmholtz equation is

$$[\partial_{xx} + \partial_{yy} + k_{eff}^2]H_z^{tot}(x, y) = 0, \quad (4.3)$$

Substituting the value of $H_z^{tot}(x, y)$ from (7.1), we get the equation for diffracted field as:

$$[\partial_{xx} + \partial_{yy} + k_{eff}^2]H_z(x, y) = 0, \quad (4.4)$$

To formulate the Wiener-Hopf equation, conditions at $x = \pm l$ in conjunction with continuity relations are used. Neumann boundary conditions on a finite-length strip are specified as

$$\partial_y H_z^{tot}(x, y) = 0, \quad |x| \leq l, \quad y = 0^\pm, \quad (13)$$

and

$$H_z^{tot}(x, 0^+) = H_z^{tot}(x, 0^-), \quad |x| > l, \quad y = 0, \quad (4.5)$$

$$\partial_y H_z^{tot}(x, 0^+) = \partial_y H_z^{tot}(x, 0^-), \quad |x| > l, \quad y = 0. \quad (4.6)$$

4.2 Problem Transformation

Following results can be obtained with the use of Fourier Transforms.

$$\begin{aligned} \mathcal{F}(\beta, y) &= \frac{1}{\sqrt{2\pi}} \int_{-\infty}^{\infty} e^{i\beta x} H_z(x, y) dx \\ &= e^{i\beta l} \mathcal{F}_+(\beta, y) + e^{-i\beta l} \mathcal{F}_-(\beta, y) + \mathcal{F}_l(\beta, y), \end{aligned} \quad (4.7)$$

where $\beta = \sigma + i\tau$.

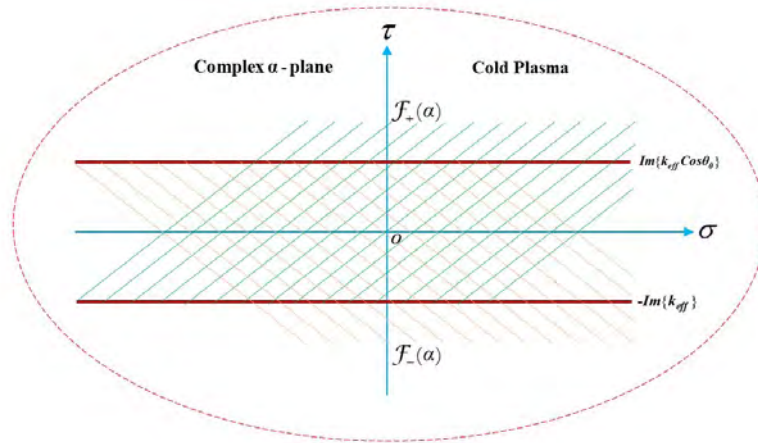


Figure 4.2: Illustration of Analytic-Continuation.

For high values of x , the diffracted field is interpreted as follows:

$$H_z(x, y) = \begin{cases} O(e^{-ik_{eff}x}), \\ O(e^{-k_{eff}x \cos \theta_0}). \end{cases} \quad (4.8)$$

The regions of regularity in the complex plane for $\mathcal{F}_+(\beta, y)$ and $\mathcal{F}_-(\beta, y)$ are $\Im\{\beta\} > -\Im\{k_{eff}\}$ and $\Im\{\beta\} < \Im\{k_{eff} \cos \theta_0\}$. From Fig 4.2, we can see the common region $-\Im\{k_{eff}\} < \Im\{\beta\} < \Im\{k_{eff} \cos \theta_0\}$ of analyticity, where the functions $\mathcal{F}_l(\beta, y)$ are also analytic and hence, we can define

$$\mathcal{F}_\pm(\beta, y) = \pm \frac{1}{\sqrt{2\pi}} \int_{\pm l}^{\pm\infty} e^{i\beta(x \mp l)} H_z(x, y) dx \quad (4.9)$$

$$\mathcal{F}_l(\beta, y) = \frac{1}{\sqrt{2\pi}} \int_{-l}^l e^{i\beta x} H_z(x, y) dx \quad (4.10)$$

$$\mathcal{F}^{inc}(\beta, y) = \frac{\exp(-iyk_{eff} \sin \theta_0)}{\sqrt{2\pi}} \left(\frac{\exp[i\beta(\beta - k_{eff} \cos \theta_0)] - \exp[-i\beta(\beta - k_{eff} \cos \theta_0)]}{i(\beta - k_{eff} \cos \theta_0)} \right). \quad (4.11)$$

$$\mathcal{F}^{ref}(\beta, y) = \frac{\exp(iyk_{eff} \sin \theta_0)}{\sqrt{2\pi}} \left(\frac{\exp[i\beta(\beta - k_{eff} \cos \theta_0)] - \exp[-i\beta(\beta - k_{eff} \cos \theta_0)]}{(\beta - k_{eff} \cos \theta_0)} \right). \quad (4.12)$$

The following transformed boundary value problem could be obtained by applying the Fourier transformation to Eqs. (7.5 – 7.7) .

$$\left(\frac{d^2}{dy^2} + \gamma^2 \right) \mathcal{F} = 0 \quad (4.13)$$

where $\gamma(\beta) = \sqrt{k_{eff}^2 - \beta^2}$.

$$\begin{aligned} \mathcal{F}(\beta, 0^+) &= \mathcal{F}^{ref}(\beta, 0) - \mathcal{F}^{inc}(\beta, 0) \\ \mathcal{F}(\beta, 0^-) &= 0 \end{aligned}, \quad (4.14)$$

and

$$\mathcal{F}_\pm(\beta, 0^+) = 0 = \mathcal{F}_\pm(\beta, 0^-). \quad (4.15)$$

4.3 Solution of the Wiener-Hopf Equation

The solution of transformed boundary value problem (7.14), fulfilling the radiation conditions is,

$$\mathcal{F}(\beta, y) = \begin{cases} A_1(\beta) \exp(-i\gamma y) & y \geq 0, \\ A_2(\beta) \exp(i\gamma y) & y < 0. \end{cases} \quad (4.16)$$

Now using Eqs. (7.15 – 7.17), following Wiener-Hopf equation is obtained.

$$e^{i\beta l} \mathcal{F}'_+(\beta, 0) + e^{-i\beta l} \mathcal{F}'_-(\beta, 0) + \mathcal{K}(\beta) \tilde{\mathcal{F}}_l(\beta, 0) = -i\mathcal{G}(\beta), \quad (4.17)$$

where,

$$\mathcal{K}(\beta) = i\gamma, \quad (4.18)$$

$$\tilde{\mathcal{F}}_l(\beta, 0) = \frac{1}{2} (\mathcal{F}_l(\beta, 0^+) - \mathcal{F}_l(\beta, 0^-)) \quad (4.19)$$

$$\mathcal{G}(\beta) = \frac{\exp[i l(\beta - k_{eff} \cos \theta_0)] - \exp[-i l(\beta - k_{eff} \cos \theta_0)]}{\sqrt{2\pi}(\beta - k_{eff} \cos \theta_0)}, \quad (4.20)$$

The Kernel function defined in Eq. 7.19 can be written as:

$$\mathcal{K}(\beta) = \frac{1}{i\gamma(\beta)} = \mathcal{K}_\pm(\beta) \text{ with } \gamma(\beta) = \gamma_\pm(\beta), \quad (4.21)$$

where $\mathcal{K}_\pm(\beta)$ are,

$$\mathcal{K}_\pm(\beta) = \frac{\exp(-i\frac{\pi}{4})}{\gamma_\pm(\beta)} \text{ with } \gamma_\pm(\beta) = \sqrt{k_{eff} \pm \beta}. \quad (4.22)$$

It must be noted that the functions, $\mathcal{K}_\pm(\beta)$ have region of regularity are $\Im\mathbf{m}\{\beta\} > -\Im\mathbf{m}\{k_{eff}\}$ and $\Im\mathbf{m}\{\beta\} < \Im\mathbf{m}\{k_{eff} \cos \theta_0\}$ and similarly for $\gamma_\pm(\beta)$. From Eq. (7.18), equating the terms which are regular in their corresponding regions, creates a common region of analyticity. Hence, by analytic continuation, we get an entire function $\mathcal{P}(\beta)$ and by Liouville's theorem, $\mathcal{P}(\beta)$ must be equal to zero[12], yielding the following results.

$$\mathcal{F}_{\pm}(\beta, 0) = \frac{\mathcal{A}}{\sqrt{2\pi}} [\mathcal{K}_{\pm}(\beta)\mathcal{G}_{1,2}(\pm\beta) + \mathcal{K}_{\pm}(\beta)\mathcal{T}(\pm\beta)\mathcal{C}_{1,2}], \quad (4.23)$$

where

$$\mathcal{G}_{1,2}(\beta) = \frac{\exp(\mp ik_{eff}l \cos \theta_0)}{\alpha \mp k_{eff} \cos \theta_0} \left(\frac{1}{\mathcal{K}_{+}(\beta)} - \frac{1}{\mathcal{K}_{+}(\pm k_{eff} \cos \theta_0)} \right) - \exp(\pm ik_{eff}l \cos \theta_0) \mathcal{R}_{1,2}(\beta), \quad (4.24)$$

$$\mathcal{C}_{1,2} = \mathcal{K}_{+}(k_{eff}) \frac{\mathcal{G}_{2,1}(k_{eff}) + \mathcal{K}_{+}(k_{eff})\mathcal{G}_{1,2}(k_{eff})\mathcal{T}(k_{eff})}{1 - \mathcal{K}_{+}^2(k_{eff})\mathcal{T}^2(k_{eff})}, \quad (4.25)$$

$$\mathcal{R}_{1,2}(\beta) = \frac{E_{-1}}{2\pi i(\beta \mp k_{eff} \cos \theta_0)} [\mathcal{W}_{-1}(-i(k_{eff} \pm k_{eff} \cos \theta_0)) - \mathcal{W}_{-1}(-i(k_{eff} + \beta))], \quad (4.26)$$

$$\mathcal{T}(\beta) = \frac{E_{-1}}{2\pi} \mathcal{W}_{-1}[-i(k_{eff} + \beta)l], \quad E_{-1} = 2\sqrt{\frac{l}{i}} e^{ik_{eff}l + \beta}, \quad (4.27)$$

$$\mathcal{W}_{n-1/2}(q) = \int_0^{\infty} \frac{v^n e^{-v}}{v+q} dv = \Gamma(n+1) e^{(\frac{q}{2})} q^{(n-1)/2} \mathcal{W}_{-(n+1)/2, n/2}(q), \quad (4.28)$$

where $q = -i(k_{eff} + \beta)l$, $n = -\frac{1}{2}$ and \mathcal{W} is the Whittaker function. Solving Eqs. 7.17 and 7.18, diffracted field is,

$$\mathcal{F}(\beta, y) = -\frac{1}{\mathcal{K}(\beta)} [\exp(i\beta l)\mathcal{F}_{+}(\beta, 0) + \exp(-i\beta l)\mathcal{F}_{-}(\beta, 0) + \mathcal{F}_l(\beta, 0)] e^{-i\gamma|y|}, \quad (4.29)$$

where

$$\mathcal{F}_l(\beta, 0) = i\mathcal{G}(\beta), \quad (4.30)$$

Inverse Fourier transformation of Eq. (7.30), yeilds the diffracted field as:

$$H_z(x, y) = \frac{1}{\sqrt{2\pi}} \int_{-\infty}^{\infty} \mathcal{F}(\beta, y) \exp(-i\beta x - i\gamma|y|) d\beta. \quad (4.31)$$

Inserting (7.30) in (7.32), we get

$$H_z(x, y) = -\frac{1}{\sqrt{2\pi}} \int_{-\infty}^{\infty} \frac{1}{\mathcal{K}(\beta)} \left\{ \begin{array}{l} e^{i\beta l}\mathcal{F}_{+}(\beta, 0) + e^{-i\beta l}\mathcal{F}_{-}(\beta, 0) + \\ + \tilde{\mathcal{F}}_l(\beta, 0) \end{array} \right\} e^{-i\beta x - i\gamma|y|} d\beta. \quad (4.32)$$

Diffracted field $H_z(x, y)$ further bifurcate in the separated and interaction fields $H_z^{sep}(x, y)$ and $H_z^{int}(x, y)$, respectively as,

$$H_z(x, y) = H_z^{sep}(x, y) + H_z^{int}(x, y), \quad (4.33)$$

where

$$H_z^{sep}(x, y) = \frac{1}{2\pi} \int_{-\infty}^{\infty} \frac{\mathcal{A}}{\mathcal{K}(\beta)} \left\{ \begin{array}{l} \frac{\mathcal{K}_+(\beta) \exp[i(\beta - k_{eff} \cos \theta_0)l]}{\mathcal{K}_+(k_{eff} \cos)(\beta - k_{eff} \cos \theta_0)} \\ - \frac{\mathcal{K}_+(-\beta) \exp[-i(\beta - k_{eff} \cos \theta_0)l]}{\mathcal{K}_+(-k_{eff} \cos)(\beta - k_{eff} \cos \theta_0)} \end{array} \right\} \exp(-i\beta x - i\gamma|y|) d\beta, \quad (4.34)$$

$$H_z^{int}(x, y) = \frac{1}{2\pi} \int_{-\infty}^{\infty} \frac{\mathcal{A}}{\mathcal{K}(\beta)} \left\{ \begin{array}{l} \exp(i\beta l) \mathcal{K}_+(\beta) \mathcal{T}(\beta) \mathcal{C}_1 \\ - \exp[i(\beta + k_{eff} \cos \theta_0)l] \mathcal{K}_+(\beta) \mathcal{R}_1(\beta) \\ + \exp(-i\beta l) \mathcal{K}_-(\beta) \mathcal{T}(-\beta) \mathcal{C}_2 \\ - \exp[-i(\beta + k_{eff} \cos \theta_0)l] \mathcal{K}_-(\beta) \mathcal{R}_2(-\beta) \end{array} \right\} \exp(-i\beta x - i\gamma|y|) d\beta. \quad (4.35)$$

The separated field given by (7.35) depicts diffraction separately at the edges. The $H_z^{inct}(x, y)$ represented by Eq. (7.36) explains the interaction of one end with the other.

4.4 Diffracted Field

The diffracted field due to finite-length strip for the far-field can be obtained by coping with the integral appearing in (7.32). Polar coordinates are introduced for the evaluation of Eq. 7.32 with the following transformation.

$$\beta = -k_{eff} \cos(\phi + i\eta), \quad 0 < \phi < \pi, \quad -\infty < \eta < \infty. \quad (4.36)$$

Now when the method of stationary phase [32] is used for (7.32), the following result are obtained:

$$H_z(r, \phi) = \frac{ik_{eff}}{\sqrt{k_{eff}r}} \mathcal{F}(-k_{eff} \cos \phi, \pm r \sin \phi) \sin \phi \exp\left(ik_{eff}r + i\frac{\pi}{4}\right). \quad (4.37)$$

Using the same polar coordinates, the transformation and subsequently the method of stationary phase are used to assess and yield the separated field and interaction fields as follows:

$$\{H_z^{sep}, H_z^{int}\}(r, \phi) = \frac{1}{\sqrt{2\pi}} \frac{ik_{eff}}{\sqrt{k_{eff}r}} \{f_{sep}, -f_{int}\}(-k_{eff} \cos \phi) \sin \phi \exp\left(ik_{eff}r + i\frac{\pi}{4}\right), \quad (4.38)$$

where

$$f_{sep}(-k_{eff} \cos \phi) = \frac{\mathcal{A}}{\mathcal{K}(-k_{eff} \cos \phi)} \left\{ \begin{array}{l} \frac{\mathcal{K}_+(-k_{eff} \cos \phi) \exp[-ik_{eff}l(\cos \phi + \cos \theta_0)]}{\mathcal{K}_+(k_{eff} \cos \theta_0)(-k_{eff} \cos \phi - k_{eff} \cos \theta_0)} \\ - \frac{\mathcal{K}_+(k_{eff} \cos \phi) \exp[ik_{eff}l(\cos \phi + \cos \theta_0)]}{\mathcal{K}_+(-k_{eff} \cos \theta_0)(-k_{eff} \cos \phi - k_{eff} \cos \theta_0)} \end{array} \right\} \quad (4.39)$$

$$f_{int}(-k_{eff} \cos \phi) = \frac{\mathcal{A}}{\mathcal{K}(-k_{eff} \cos \phi)} \left\{ \begin{array}{l} \exp(-ik_{eff}l \cos \phi) \mathcal{K}_+(-k_{eff} \cos \phi) \\ \quad \times \mathcal{T}(-k_{eff} \cos \phi) \mathcal{C}_1 \\ - \exp[il(-k_{eff} \cos \phi + k_{eff} \cos \theta_0)] \\ \quad \times \mathcal{K}_+(-k_{eff} \cos \phi) \mathcal{R}_1(-k_{eff} \cos \phi) \\ + \mathcal{K}_-(-k_{eff} \cos \phi) \exp(ik_{eff}l \cos \phi) \\ \quad \times \mathcal{T}(k_{eff} \cos \phi) \mathcal{C}_2 \\ - \exp[-il(-k_{eff} \cos \phi + k_{eff} \cos \theta_0)] \\ \quad \times \mathcal{K}_-(-k_{eff} \cos \phi) \mathcal{R}_2(k_{eff} \cos \phi) \end{array} \right\} \quad (4.40)$$

From Eq. (7.38), we can clearly see that the asymptotic expressions for far field can be obtained by letting $k_{eff}r \rightarrow \infty$ and the resulting expressions will be holds true for any observational angle. The separated field of an EM-wave is investigated in order to characterise both the field diffracted by the corners of a strip and the influence of the geometrical wave field. The separated field that results gives physical evidence for the

non-thermal plasma concept. Interacted-field, on the other hand, provides no physical information due to contact at edge to edge, which has formerly been enumerated by H^{sep} . As a result, we've only talked about the separated field because it conveys a full physical comprehension of EM-wave diffraction at the established boundaries. Additionally, we discovered that the interaction field is created by diffraction from the corners of strip at $x = \pm l$. Furthermore, when the strip width is increased to ∞ , the role due to interaction field terms disappears, leaving just the H^{sep} terms in the H . As a consequence, we merely examine the separated field, as illustrated visually in the next section.

4.5 Discussion and Numerical Results

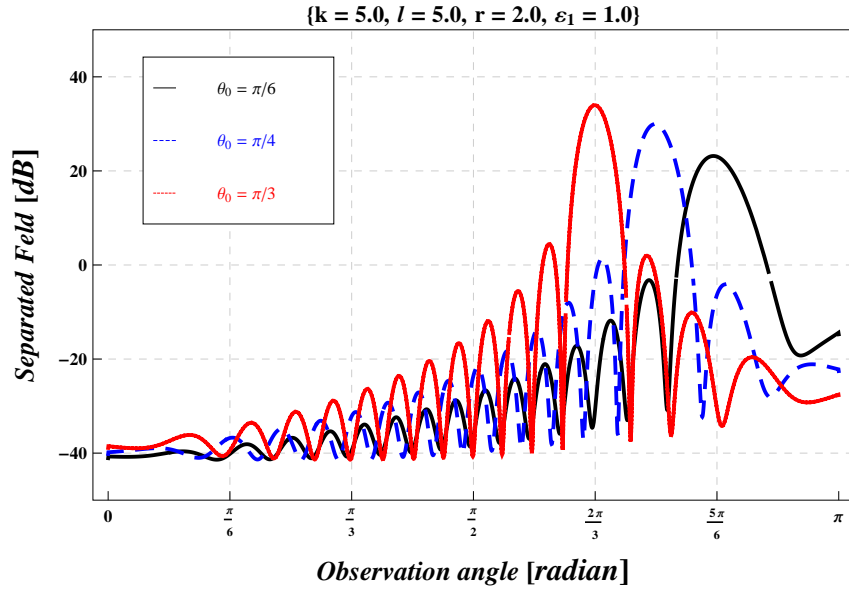
In this section, we examined the EM-waves by finite-length strip as graphically by the variation of physical parameters in an an-isotropic media with Neumann conditions versus the observational angle. For the ionosphere, we take the value of ω_p as $56.4MHz$ and ω_c as $8.78 MHz$. Now, the values of ε_1 and ε_2 are computed numerically against ω to verify the considered model. Also, the values of ω are taken between $80MHz$ and $600MHz$ given in Table-4.1. It can be notice from Table-4.1, that the value of ε_2 is comparably very small from ε_1 with the boost up of ω in the frequency range. For isotropic medium, we can take $\varepsilon_1 = 1$ and $\varepsilon_2 = 0$, While the parameters ε_1 and ε_2 for the an-isotropic media (non-thermal plasma) can indeed be selected from Table-1.

ω (in MHz)	ε_1	ε_2
80.15	0.504834	0.054242
99.50	0.678699	0.028352
145.75	0.850259	0.009020
245.15	0.947071	0.001895
375.50	0.97744	0.000527
480.50	0.986222	0.000251
599.75	0.991157	0.000129

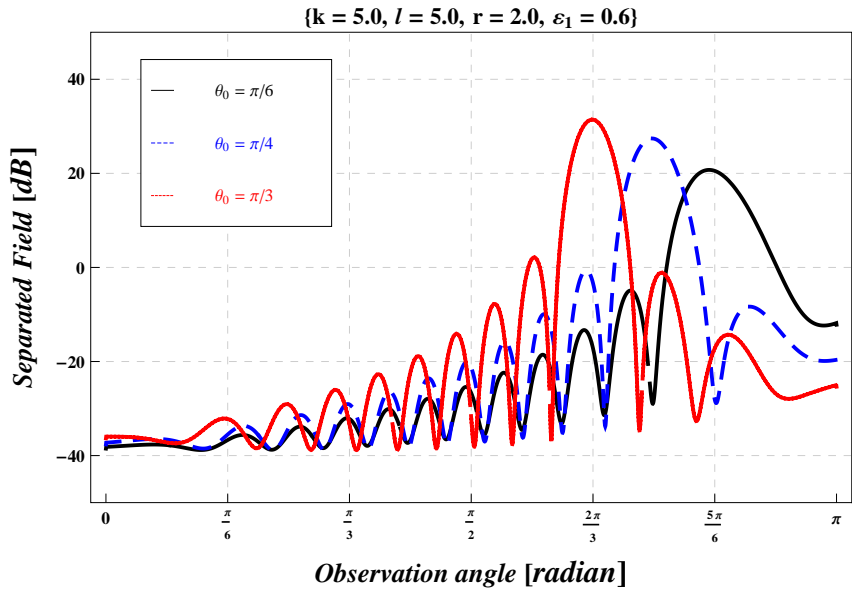
Table 4.1: Values of ε_1 and ε_2 for corresponding ω .

The graphical analysis is elaborated to explore the influence of physical parame-

ters on diffracted field due to a finite-width slit lying in the ionosphere of non-thermal plasma. These physical parameters are θ_0 , k , $2l$ and ε_1 . Fig. 4.3 represents the pattern of the separated field for variation of θ_0 , and it gets maxima for $\theta_0 = \pi/3, \pi/4, \pi/6$ occurring at $\theta = 2\pi/3, 3\pi/4, 5\pi/6$, respectively. These maxima actually predict the shadow of reflected field. Fig. 4.4 reveals the separated field for k . It is notable that the field has a direct dependence upon k because the field gets amplified for k . Since the frequency is directly related to k , so it excites the frequency of wave towards the high range. As extension of the slit-width is actually the expansion of aperture which is responsible for the diffraction of electromagnetic radiations, and so, separated field gets amplified as well as more oscillated as can be seen in Fig. ???. This amplified amplitude could be controlled by introducing the ionosphere as can be observed through Fig. 4.5b. By comparing Figs. 4.3b, 4.4b and 4.5b of the separated field in the an-isotropic medium with their respective Figs. 4.3a, 4.4a and 4.5a in the isotropic medium. It is explained that an-isotropy of the medium caused by non-thermal plasma influenced the separation field, in both amplitude reduction and wavelength contraction. Fig. 4.6 explores the trend of the field for ε_1 , while its mathematical interpretation predicts its physical nature. It is expressed by Eq. (??) and can be described as ω_c has no big difference in the values in the different parts of Earth and ω_p has direct relation with the square root of N_e (ion concentration), which fluctuates massively with the variation of seasons and days to night. Therefore, without fluctuation on ω , ε_1 can be fluctuate. Since ε_1 has inverse relation with ω , so increase in N_e with fixed ω , ε_1 declines and wavelength will be increase. It means that the separated field with longer wavelength will occur for increasing number of free charges in the medium.

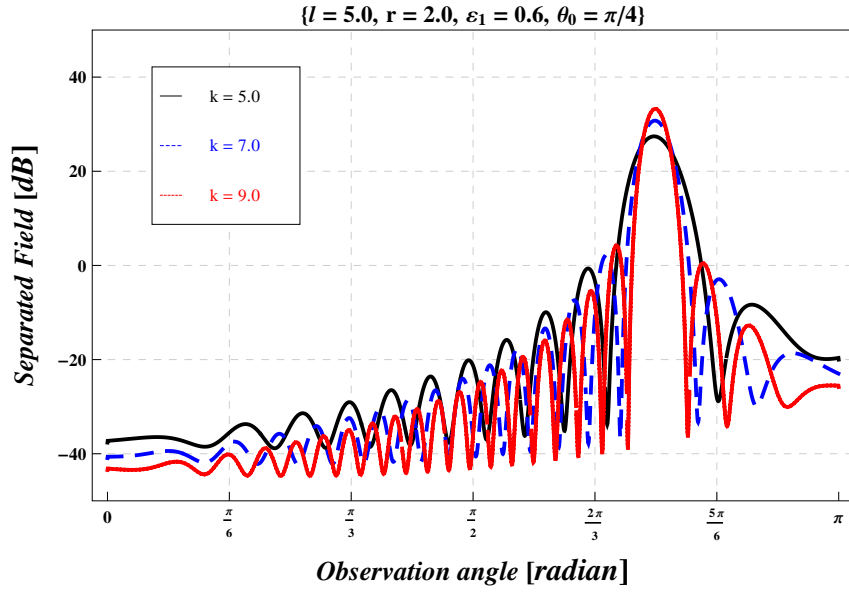


(a)

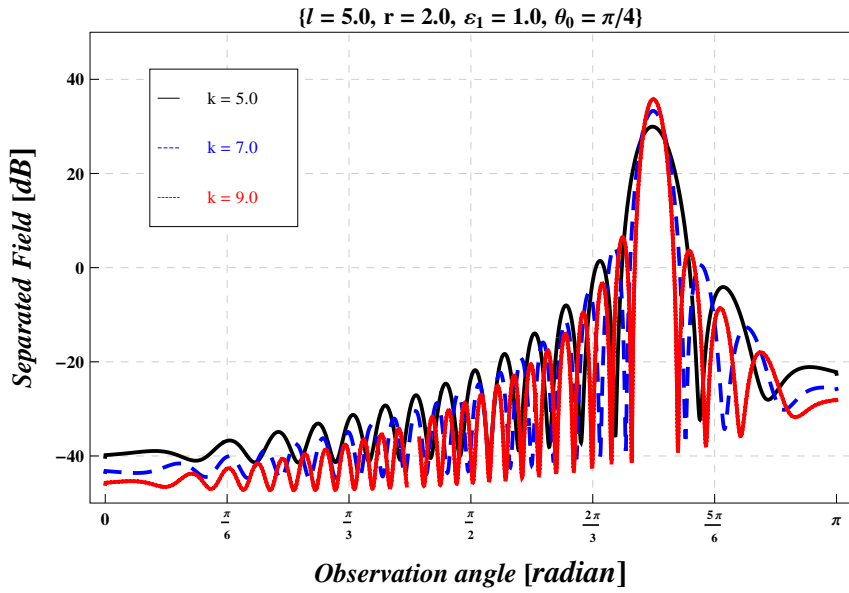


(b)

Figure 4.3: The separated field for θ_0 in the (a) isotropic and (b) an-isotropic medium.

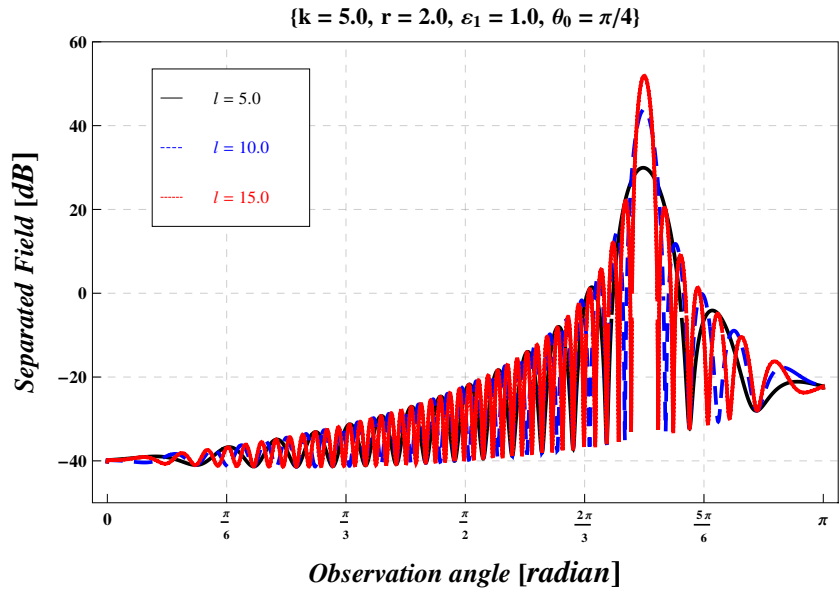


(a)

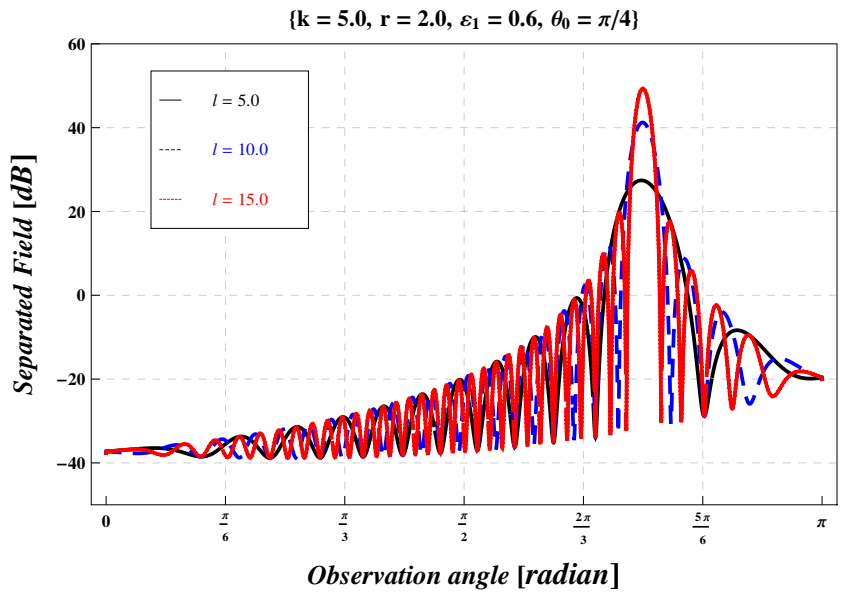


(b)

Figure 4.4: The separated field for k in the (a) isotropic and (b) an-isotropic medium.



(a)



(b)

Figure 4.5: The separated field for $2l$ in the (a) isotropic and (b) an-isotropic medium.

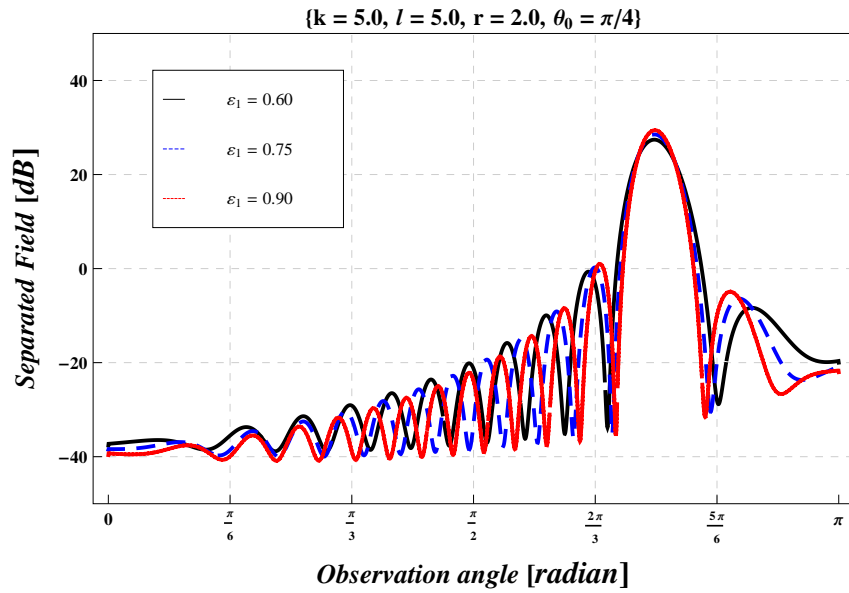


Figure 4.6: The separated field for ϵ_1 .

4.6 Conclusions

From above rigorous analysis, it is wrapped-up that the diffraction behavior of H^{inc} incident finite-symmetric strip embedded with Neumann surface is affected rigorously by behavior changing parameters in the existence of non-thermal plasma. It is deeply explored that the function H^{sep} is amplified by different θ_0 , k , $2l$, ε_1 and reduced by ε_2 .

Chapter 5

Scattering of Electromagnetic Plane Wave Incident on a Finite Corrugated Grating in Non-thermal Plasma

In the present chapter, the scattering of magnetically polarized waves due to sinusoidal grating is investigated in the context of non-thermal plasma under the consideration of high frequency signal. Assumption of small depth of grating as compared to the wavelength and approximation of boundary conditions on the grating surface leads to the reduction of model for diffraction problem of flat-strip embedded with mixed boundary conditions. Applying the Fourier transform and approximating the boundary conditions along with perturbation series expansion, the Wiener-Hopf equations of zero-order and first-order are formulated. Wiener-Hopf technique along with perturbation method is used to tackle this model. The scattered field is explicitly derived by applying the inverse Fourier transformation and then using the saddle point method. For high frequency signals, operating frequency is considered to be very large as compared to cyclotron frequency, at the same order with plasma frequency. Numerical values for permittivity elements controlling cold plasma are

computed for corresponding operating frequency. The characteristics of scattering in the existence and non-existence of non-thermal plasma by grating are graphically discussed.

5.1 Description Of The Model

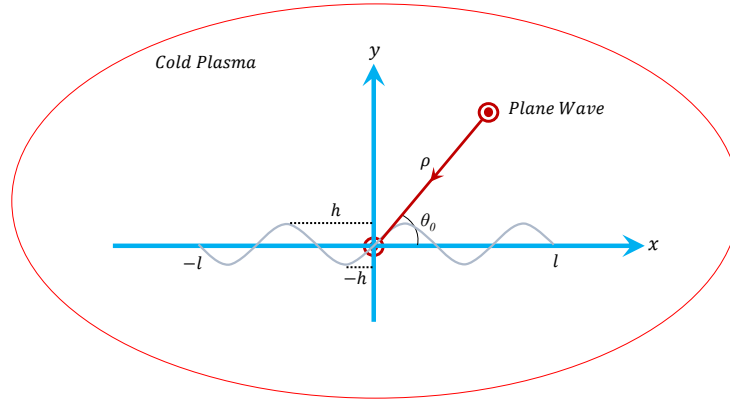


Figure 5.1: **Simplified figure of the problem.**

H-Polarized plane-waves are being incident on the surface as shown in Fig. 1. In present scenario, the surface is taken as perfectly conducting, uniform and infinitely thin lying along the x -direction, which is defined by

$$y = h \sin mx, \quad |x| \leq l \quad (5.1)$$

with $2h$ ($h > 0$) being the distance between crest and trough or grating depth, and $m > 0$ being the periodicity measurement parameter. The magnetic field is taken to be parallel to z -axis with consideration of grating geometry. This leads to the two-dimensional scattering problem regarding.

Let the total magnetic field $H_z^{tot}(x, y)$ be defined by

$$H_z^{tot}(x, y) = H_z^{inc}(x, y) + H_z^{scat}(x, y), \quad (5.2)$$

where H_z^{inc} is the incident field satisfying the Helmholtz equation, is given by

$$H_z^{inc}(x, y) = e^{-ik_{eff}(x \sin \theta_0 + y \cos \theta_0)}, \quad 0 < \theta_0 < \pi/2 \quad (5.3)$$

where k_{eff} is given by (8). The two-dimensional Helmholtz equation of scattered field $H_z(x, y)$ is given by

$$(\partial_x^2 + \partial_y^2 + k_{eff}^2) H_z^{scat}(x, y) = 0 \quad (5.4)$$

The total electric field E_{tan}^{tot} having tangential components satisfies, the boundary conditions.

$$E_{tan}^{tot} = \partial_n H_z^{tot}(x, h \sin mx) = 0, \quad |x| < l \quad (5.5)$$

Here ∂_n denotes the normal derivative. Assume that the grating depth $2h$ is tiny in comparison to the wavelength and extend the (6) in terms of the Taylor series. Then, in the Taylor series, omitting the terms of order $O(h^2)$, we get

$$\partial_y H_z^{tot}(x, 0) + h [\sin mx \partial_y^2 H_z^{tot}(x, 0) - m \cos mx \partial_x H_z^{tot}(x, 0)] + O(h^2) = 0, \quad |x| < l \quad (5.6)$$

where (14) depicts the boundary condition and will be utilized to proceed the remaining part of analysis.

Let us expand the unknown scattered field $H_z(x, y)$ through the perturbation technique as:

$$H_z(x, y) = H_z^{(0)}(x, y) + h H_z^{(1)}(x, y) + O(h^2), \quad (5.7)$$

where $H_z^{(0)}(x, y)$ is the zero-order and $H_z^{(1)}(x, y)$ is the first-order unknown terms in the scattered field.

$H_z^{(n)}$ for $n = 0, 1$ appearing (15) satisfy

$$(\partial_x^2 + \partial_y^2 + k_{eff}^2) H_z^{(n)}(x, y) = 0, \quad (5.8)$$

with continuity relations

$$H_z^{(0)}(x, +0) = H_z^{(0)}(x, -0) [\equiv H_z^{(0)}(x, 0)], \quad (5.9)$$

$$\partial_y H_z^{(0)}(x, +0) = \partial_y H_z^{(0)}(x, -0) [\equiv \partial_y H_z^{(0)}(x, 0)], \quad (5.10)$$

$$H_z^{(1)}(x, +0) = H_z^{(1)}(x, -0) [\equiv H_z^{(1)}(x, 0)], \quad (5.11)$$

$$\partial_y H_z^{(1)}(x, +0) = \partial_y H_z^{(1)}(x, -0) [\equiv \partial_y H_z^{(1)}(x, 0)], \quad (5.12)$$

for $|x| > l$, and

$$H_z^{(0)}(x, +0) - H_z^{(0)}(x, -0) = j^{(0)}(x, 0), \quad (5.13)$$

$$\partial_y H_z^{(0)}(x, 0) = ik_{eff} \sin \theta_0 e^{-ik_{eff}x \cos \theta_0}, \quad (5.14)$$

$$H_z^{(1)}(x, +0) - H_z^{(1)}(x, -0) = j^{(1)}(x, 0), \quad (5.15)$$

$$\begin{aligned} & \partial_y H_z^{(1)}(x, 0) + \sin mx \partial_y^2 H_z^{(0)}(x, 0) - m \cos mx \partial_x H_z^{(0)}(x, 0) \\ &= \frac{ik_{eff}}{2} [k_{eff} \sin^2 \theta_0 \sum_{n=1}^2 (-1)^n e^{-ik_{eff}x \cos \theta_n} - m \cos \theta_0 \sum_{n=1}^2 e^{-ik_{eff}x \cos \theta_n}] \end{aligned} \quad (5.16)$$

for $|x| < l$

$$\cos \theta_1 = \cos \theta_0 - m/k, \quad \cos \theta_2 = \cos \theta_0 + m/k. \quad (5.17)$$

The terms $j^{(0)}(x, 0)$ and $j^{(1)}(x, 0)$ in their respective equations (21) and (23), presenting the unknown currents at the surface, respectively. As it can be visualized from above argument that zero-order function leads to the diffraction problem by flat-strip whereas the first-order corresponds to the problem of wave diffracted by sinusoidal corrugation of finite length.

5.2 Modeling of Wiener-Hopf Equations.

For ease of analysis, the medium is assumed to be slightly lossy as in $k_{eff} = \Re\{k_{eff}\} + i\Im\{k_{eff}\}$ with $0 < \Im\{k_{eff}\} \ll \Re\{k_{eff}\}$. The solution of present model for real value of k_{eff} is achieved by taking $\Im\{k_{eff}\} \rightarrow +0$ at the end of analysis. For Eq. (15) considering the radiation condition, the asymptotic behavior

of the $H^{(n)}(x, y)$ for $n = 0, 1$ is given by

$$H_z^{(n)}(x, y) = O\left(e^{-\Im\{k_{eff}\}|x|\cos\theta_0}\right), \quad |x| \longrightarrow \infty \quad (5.18)$$

Employing the Fourier transformation on $H_z^{(n)}(x, y)$, we have

$$\mathcal{F}^{(n)}(\alpha, y) = (2\pi)^{-1/2} \int_{-\infty}^{\infty} H_z^{(n)}(x, y) e^{i\alpha x} dx, \quad (5.19)$$

where α is taken as complex. Eqs. (26) and (27) show that $H_z^{(n)}(\alpha, y)$ for $n = 0, 1$ behave as regular functions for α in the strip $|\tau| < \Im\{k_{eff}\} \cos\theta_0$ of the complex α -plane. Let us introduce the Fourier integrals as

$$\mathcal{F}_{\pm}^{(n)}(\alpha, y) = \pm (2\pi)^{-1/2} \int_{\pm l}^{\pm\infty} H_z^{(n)}(x, y) e^{i\alpha(x\mp a)} dx, \quad (5.20)$$

$$\mathcal{F}_l^{(n)}(\alpha, y) = (2\pi)^{-1/2} \int_{-l}^l H_z^{(n)}(x, y) e^{i\alpha x} dx, \quad (5.21)$$

$$\mathcal{F}_S^{(n)}(\alpha, 0) = (2\pi)^{-1/2} \int_{-l}^l H_z^{(n)}(x, 0) e^{i\alpha x} dx \quad (5.22)$$

As $\mathcal{F}_{\pm}^{(n)}(\alpha, y)$ are regular in $\tau \gtrless \mp \Im\{k_{eff}\} \cos\theta_0$ where as $\mathcal{F}_l^{(n)}(\alpha, y)$ and $\mathcal{F}_S^{(n)}(\alpha, 0)$ are entire functions. From Eqs. (27) – (29), we get

$$\mathcal{F}^{(n)}(\alpha, y) = e^{-i\alpha l} \mathcal{F}_-^{(n)}(\alpha, y) + \mathcal{F}_l^{(n)}(\alpha, y) + e^{i\alpha l} \mathcal{F}_+^{(n)}(\alpha, y) \quad (5.23)$$

Using Fourier transformation of Eq. (16) along Eq. (26), we get

$$[d^2/dy^2 - \gamma^2(\alpha)] \mathcal{F}^{(n)}(\alpha, y) = 0, \quad (5.24)$$

where $\gamma(\alpha) = (\alpha^2 - k_{eff}^2)^{1/2}$ with $\Re\{\gamma(\alpha)\} > 0$. $\gamma(\alpha)$ is a double-valued function of α such that $\gamma(\alpha) = -ik_{eff}$ for $\alpha = 0$ so we can have proper choice of branch. The

solution of (32) is presented as

$$\mathcal{F}^{(n)}(\alpha, y) = \begin{cases} \mathcal{U}^{(n)}(\alpha) e^{-\gamma(\alpha)y}, & y > 0 \\ \mathcal{V}^{(n)}(\alpha) e^{\gamma(\alpha)y}, & y < 0, \end{cases} \quad (5.25)$$

where the arbitrary functions appearing in the Eq (33) $\mathcal{U}^{(n)}(\alpha)$ and $\mathcal{V}^{(n)}(\alpha)$ for $n = 0, 1$ will be evaluated. Using Eqs. (17) – (24), we have

$$\left. \begin{array}{l} \mathcal{U}^{(0)}(\alpha) \\ \mathcal{V}^{(0)}(\alpha) \end{array} \right\} = \pm \frac{\mathcal{F}_S^{(0)}(\alpha)}{2} \quad (5.26)$$

$$\left. \begin{array}{l} \mathcal{U}^{(1)}(\alpha) \\ \mathcal{V}^{(1)}(\alpha) \end{array} \right\} = \pm \frac{\mathcal{F}_S^{(1)}(\alpha)}{2} + \frac{1}{4i\gamma(\alpha)} \left\{ \begin{array}{l} [\gamma^2(\alpha + m) - m(\alpha + m)] \mathcal{F}_S^{(0)}(\alpha + m) \\ - [\gamma^2(\alpha - m) + m(\alpha - m)] \mathcal{F}_S^{(0)}(\alpha - m) \end{array} \right\}, \quad (5.27)$$

where

$$\mathcal{F}_S^{(0)}(\alpha) = \mathcal{F}_l^{(n)}(\alpha, +0) - \mathcal{F}_l^{(n)}(\alpha, -0) \quad (5.28)$$

for $n = 0, 1$. Putting Eq. (34) and Eq. (35) into Eq. (33), we get the following for $y \gtrless 0$:

$$\mathcal{F}^{(0)}(\alpha, y) = \pm \frac{\mathcal{F}_S^{(0)}(\alpha)}{2} e^{\mp\gamma(\alpha)y}, \quad (5.29)$$

$$\begin{aligned} & \mathcal{F}^{(1)}(\alpha, y) = \pm \frac{\mathcal{F}_S^{(1)}(\alpha)}{2} e^{\mp\gamma(\alpha)y} \\ & + \frac{1}{4i\gamma(\alpha)} \left\{ \begin{array}{l} [\gamma^2(\alpha + m) - m(\alpha + m)] \mathcal{F}_S^{(0)}(\alpha + m) \\ - [\gamma^2(\alpha - m) + m(\alpha - m)] \mathcal{F}_S^{(0)}(\alpha - m) \end{array} \right\} e^{\mp\gamma(\alpha)y}. \end{aligned} \quad (5.30)$$

Equations (37) and (38) express the transformed scattered fields of the zero- and first-order, respectively. Plugging $y = \pm 0$ in (29) and (30) and using the boundary conditions, we have

$$e^{-i\alpha l} \mathcal{S}_-(\alpha) + \mathcal{K}(\alpha) \mathcal{F}_S^{(0)}(\alpha) + e^{i\alpha l} \mathcal{S}_{(+)}(\alpha) = 0, \quad (5.31)$$

$$e^{-i\alpha l} \mathcal{D}_-(\alpha) + \mathcal{K}(\alpha) \mathcal{F}_S^{(1)}(\alpha) + e^{i\alpha l} \mathcal{D}_{(+)}(\alpha) = 0, \quad (5.32)$$

for $|\tau| < \Im\{k_{eff}\} \cos \theta_0$, where

$$\mathcal{S}_-(\alpha) = \mathcal{F}_-^{(0)'}(\alpha, 0) + \frac{\mathcal{U}_0}{\alpha - k_{eff} \cos \theta_0}, \quad (5.33)$$

$$\mathcal{S}_{(+)}(\alpha) = \mathcal{F}_+^{(0)'}(\alpha, 0) - \frac{\mathcal{V}_0}{\alpha - k_{eff} \cos \theta_0}, \quad (5.34)$$

$$\mathcal{D}_-(\alpha) = \mathcal{F}_-(\alpha) - \sum_{n=1}^2 (-1)^n \frac{\mathcal{U}_n \mathcal{C}_n}{\alpha - k_{eff} \cos \theta_n}, \quad (5.35)$$

$$\mathcal{D}_{(+)}(\alpha) = \mathcal{F}_+(\alpha) + \sum_{n=1}^2 (-1)^n \frac{\mathcal{V}_n \mathcal{C}_n}{\alpha - k_{eff} \cos \theta_n}, \quad (5.36)$$

$$\mathcal{K}(\alpha) = \frac{\gamma(\alpha)}{2}, \quad (5.37)$$

$$\mathcal{F}_\pm(\alpha) = \mathcal{F}_\pm^{(1)'}(0, \alpha) + \frac{1}{2i} \left\{ \begin{array}{l} [\gamma^2(\alpha + m) - m(\alpha + m)] e^{\pm iml} \mathcal{F}_\pm^{(0)}(\alpha + m, 0) \\ - [\gamma^2(\alpha - m) - m(\alpha - m)] e^{\mp iml} \mathcal{F}_\pm^{(0)}(\alpha - m, 0) \\ \pm (2\pi)^{-1/2} m \cos ml H_z^{(0)}(0, l) \end{array} \right\} \quad (5.38)$$

$$\left. \begin{array}{l} \mathcal{U}_0 \\ \mathcal{V}_0 \end{array} \right\} = \frac{-k_{eff} \sin \theta_0 e^{\pm i k_{eff} l \cos \theta_0}}{\sqrt{2\pi}}, \quad (5.39)$$

$$\left. \begin{array}{l} \mathcal{U}_n \\ \mathcal{V}_n \end{array} \right\} = \frac{e^{\pm i k_{eff} l \cos \theta_n}}{\sqrt{2\pi}}, \quad n = 1, 2 \quad (5.40)$$

$$\mathcal{C}_n = (k_{eff}/2) [k_{eff} \sin^2 \theta_0 - (-1)^n m \cos \theta_0], \quad n = 1, 2 \quad (5.41)$$

where the prime represent the derivative with respect to y . Eqs. (39) and (40) are Wiener-Hopf equations of zero- and first-order, respectively.

5.3 Exact and Asymptotic Results

For exact and asymptotic solutions, we solve the Wiener-Hopf equations of the zero- and first-order. The product decomposition of $\mathcal{K}(\alpha)$ given in (45) presented as

$$\mathcal{K}(\alpha) = \mathcal{K}_+(\alpha) \mathcal{K}_-(\alpha). \quad (5.42)$$

The factors appearing in (50) are evaluated as

$$\mathcal{K}_\pm(\alpha) = \frac{e^{-i\pi/4} (k_{eff} \pm \alpha)^{1/2}}{\sqrt{2}}. \quad (5.43)$$

Multiplying $e^{\pm i\alpha l} / \mathcal{K}_\pm(\alpha)$ on both sides of (39) and using the decomposition method, we get

$$\mathcal{S}_{(+)}(\alpha) = \mathcal{K}_+(\alpha) \left(-\frac{\mathcal{U}_0}{\mathcal{K}_+(k_{eff} \cos \theta_0) (\alpha - k_{eff} \cos \theta_0)} + \frac{1}{2} [u_s(\alpha) - u_d(\alpha)] \right), \quad (5.44)$$

$$\mathcal{S}_-(\alpha) = \mathcal{K}_-(\alpha) \left(\frac{\mathcal{V}_0}{\mathcal{K}_-(k_{eff} \cos \theta_0) (\alpha - k_{eff} \cos \theta_0)} + \frac{1}{2} [u_s(-\alpha) + u_d(-\alpha)] \right), \quad (5.45)$$

where

$$u_{s,d}(\alpha) = \frac{1}{\pi i} \int_{k_{eff}}^{k_{eff} + i\infty} \frac{e^{2i\beta a} \mathcal{S}_{(+)}^{s,d}(\beta)}{(\beta + \alpha) K_-(\beta)} d\beta, \quad (5.46)$$

$$\mathcal{S}_{(+)}^{s,d}(\alpha) = \mathcal{S}_{(+)}(\alpha) \pm \mathcal{S}_-(-\alpha). \quad (5.47)$$

Eqs. (52) and (53) comprise of branch-cut integrals involving unknown functions $\mathcal{S}_{(+)}^{s,d}(\beta)$ as the integrands. Using an asymptotic method, we explicitly find a high-frequency solution as

$$\mathcal{S}_-(\alpha) \sim -\frac{\mathcal{U}_0 (\alpha - k_{eff})^{1/2}}{(k_{eff} \cos \theta_0 - k_{eff})^{1/2} (\alpha - k_{eff} \cos \theta_0)} + \mathcal{K}_-(\alpha) [\mathcal{C}_1^u \xi(-\alpha) + \mathcal{V}_0 \eta_0^b(-\alpha)], \quad (5.48)$$

$$\mathcal{S}_{(+)}(\alpha) \sim \frac{\mathcal{V}_0 (\alpha + k_{eff})^{1/2}}{(k_{eff} \cos \theta_0 + k_{eff})^{1/2} (\alpha - k_{eff} \cos \theta_0)} + \mathcal{K}_+(\alpha) [\mathcal{C}_2^u \xi(\alpha) + \mathcal{U}_0 \eta_0^a(\alpha)], \quad (5.49)$$

for $k_{eff}l \rightarrow \infty$, where

$$\mathcal{C}_{1,2}^u = \frac{\mathcal{K}_+(k_{eff}) \left[\chi_0^{a,b}(k_{eff}) + \mathcal{K}_+(k_{eff}) \xi(k_{eff}) \chi_0^{b,a}(k_{eff}) \right]}{1 - \mathcal{K}_+^2(k_{eff}) \xi^2(k_{eff})}, \quad (5.50)$$

$$\xi(\alpha) = -\frac{2a^{1/2} e^{2ik_{eff}l}}{\pi} \Gamma_1(1/2, -2i(\alpha + k_{eff})l), \quad (5.51)$$

$$\eta_0^{a,b}(\alpha) = \frac{\xi(\alpha) - \xi(\pm k_{eff} \cos \theta_0)}{\alpha \mp k_{eff} \cos \theta_0}, \quad (5.52)$$

with

$$\chi_0^a(\alpha) = \mathcal{U}_0 \eta_0^a(\alpha) + \mathcal{V}_0 L_0^b(\alpha), \quad (5.53)$$

$$\chi_0^b(\alpha) = \mathcal{V}_0 \eta_0^b(\alpha) + \mathcal{U}_0 L_0^a(\alpha), \quad (5.54)$$

$$\mathcal{L}_0^{a,b}(\alpha) = \frac{1}{\alpha \pm k_{eff} \cos \theta_0} \left[\frac{1}{\mathcal{K}_+(\alpha)} - \frac{1}{\mathcal{K}_\mp(k_{eff} \cos \theta_0)} \right]. \quad (5.55)$$

In (51), $\Gamma_1(.,.)$ is the gamma function in generalized form calculated by Kobayashi [21] and is defined

$$\Gamma_s(u, v) = \int_0^\infty \frac{t^{u-1} e^{-t}}{(t+v)^p} dt. \quad (5.56)$$

with p being the positive integer, and $\Re\{u\} > 0$, $|v| > 0$, $|\arg v| < \pi$. This is the complete solution for Wiener-Hopf zero-order (39). Similarly, for the first-order Wiener-Hopf equation (40), same procedure may be used. The procedure of decomposition and factorization yields the solution of first-order Wiener-Hopf equation (40) with following result:

$$\mathcal{D}_-(\alpha) = -\mathcal{K}_-(\alpha) \left\{ \sum_{n=1}^2 (-1)^n \frac{\mathcal{U}_n \mathcal{C}_n}{\mathcal{K}_-(k_{eff} \cos \theta_n) (\alpha - k_{eff} \cos \theta_n)} + \frac{1}{2} [v_s(-\alpha) + v_d(-\alpha)] \right\}, \quad (5.57)$$

$$\mathcal{D}_{(+)}(\alpha) = \mathcal{K}_+(\alpha) \left\{ \sum_{n=1}^2 (-1)^n \frac{\mathcal{V}_n \mathcal{C}_n}{\mathcal{K}_+(k_{eff} \cos \theta_n) (\alpha - k_{eff} \cos \theta_n)} + \frac{1}{2} [v_s(\alpha) - v_d(\alpha)] \right\}, \quad (5.58)$$

where

$$v_{s,d}(\alpha) = \frac{1}{\pi i} \int_{k_{eff}}^{k_{eff}+i\infty} \frac{e^{2i\beta l} \mathcal{D}_{(+)}^{s,d}(\beta)}{(\beta + \alpha) \mathcal{K}_-(\beta)} d\beta, \quad (5.59)$$

with

$$\mathcal{D}_{(+)}^{s,d}(\alpha) = \mathcal{D}_{(+)}(\alpha) \pm \mathcal{D}_{-}(-\alpha). \quad (5.60)$$

Evaluating (67) asymptotically and then arranging the results, we obtain

$$\begin{aligned} \mathcal{D}_{-}(\alpha) \sim & -\sum_{n=1}^2 (-1)^n \frac{\mathcal{C}_n e^{ik_{eff}l \cos \theta_n} (\alpha - k_{eff})^{1/2}}{(2\pi)^{1/2} (k_{eff} \cos \theta_n - k_{eff})^{1/2} (\alpha - k_{eff} \cos \theta_n)} \\ & + \mathcal{K}_{-}(\alpha) [\mathcal{P}_1^v \xi(-\alpha) + \mathcal{V}_1 \eta_1^b(-\alpha) + \mathcal{V}_2 \eta_2^b(-\alpha)], \end{aligned} \quad (5.61)$$

$$\begin{aligned} \mathcal{D}_{(+)}(\alpha) \sim & -\sum_{n=1}^2 (-1)^n \frac{\mathcal{C}_n e^{-ik_{eff}l \cos \theta_n} (\alpha + k)^{1/2}}{(2\pi)^{1/2} (k_{eff} \cos \theta_n + k_{eff})^{1/2} (\alpha - k_{eff} \cos \theta_n)} \\ & + \mathcal{K}_{+}(\alpha) [\mathcal{P}_2^v \xi(\alpha) + \mathcal{U}_1 \eta_1^b(\alpha) + \mathcal{U}_2 \eta_2^b(\alpha)], \end{aligned} \quad (5.62)$$

as $k_{eff}l \rightarrow \infty$, where

$$\mathcal{P}_{1,2}^v = \frac{\mathcal{K}_{+}(k_{eff})}{1 - \mathcal{K}_{+}^2(k_{eff}) \xi^2(k_{eff})} \sum_{n=1}^2 [\chi_n^{a,b}(k_{eff}) + \mathcal{K}_{+}(k_{eff}) \xi(k_{eff}) \chi_n^{b,a}(k_{eff})], \quad (5.63)$$

$$\eta_n^{a,b}(\alpha) = -(-1)^n \mathcal{C}_n \frac{\xi(\alpha) - \xi(\pm k_{eff} \cos \theta_n)}{\alpha \mp k_{eff} \cos \theta_n}, \quad (5.64)$$

$$\chi_n^a(\alpha) = \mathcal{U}_n \eta_n^a(\alpha) - (-1)^n \mathcal{V}_n \mathcal{C}_n \mathcal{L}_n^b(\alpha), \quad (5.65)$$

$$\chi_n^b(\alpha) = \mathcal{V}_n \eta_n^b(\alpha) - (-1)^n \mathcal{U}_n \mathcal{C}_n \mathcal{L}_n^a(\alpha), \quad (5.66)$$

$$\mathcal{L}_n^{a,b}(\alpha) = \frac{1}{\alpha \pm k_{eff} \cos \theta_n} \left[\frac{1}{\mathcal{K}_{+}(\alpha)} - \frac{1}{\mathcal{K}_{\mp}(k_{eff} \cos \theta_n)} \right]. \quad (5.67)$$

for $n = 1, 2$. Eqs. (56), (57) and (69), (70) give the asymptotic solutions of equations (39) and (40) for high-frequency, respectively.

5.4 Scattered Far Field

With the aid of results evaluated in above section, we drive the analytical expressions for scattered field. The inverse Fourier transform is applied on $\mathcal{F}^{(n)}(\alpha, y)$ to obtain the result for scattered field $H_z^n(x, y)$ with $n = 0, 1$ which is defined as

$$H_z^{(n)}(x, y) = \frac{1}{\sqrt{2\pi}} \int_{-\infty+id}^{\infty+id} e^{-i\alpha x} \mathcal{F}^{(n)}(\alpha, y) d\alpha, \quad (5.68)$$

where d is a constant such that $|d| < \Im\{k_{eff} \cos \theta_0\}$. Now we shall derive the explicit asymptotic expressions for the scattered far fields of the zero- and first-order.

For scattered far field of zero-order, we express $\mathcal{F}_S^{(0)}(\alpha)$ explicitly from (39) that is

$$\mathcal{F}_S^{(0)}(\alpha) = \frac{-e^{-i\alpha l} \mathcal{S}_-(\alpha) - e^{i\alpha l} \mathcal{S}_+(\alpha)}{\mathcal{K}(\alpha)}. \quad (5.69)$$

Substituting (77) into (37) we obtain

$$\mathcal{F}^{(0)}(\alpha, y) = \pm \left(\frac{-e^{-i\alpha l} \mathcal{S}_-(\alpha) - e^{i\alpha l} \mathcal{S}_+(\alpha)}{2\mathcal{K}(\alpha)} \right) e^{\mp\gamma(\alpha)y}, \quad (5.70)$$

Substitution of (78) in (76) with $n = 0$ leads to an integral expression for the scattered field of the zero-order $H_z^{(0)}(x, y)$ is presented as

$$H_z^{(0)}(x, y) = \mp (2\pi)^{-1/2} \int_{-\infty+id}^{\infty+id} \frac{e^{-i\alpha x} \mathcal{S}_-(\alpha) + e^{i\alpha x} \mathcal{S}_+(\alpha)}{\gamma} e^{\mp\gamma(\alpha)y} d\alpha, \quad (5.71)$$

for $y \geq 0$, where d is a constant such that $|d| < \Im\{k_{eff} \cos \theta_0\}$ and $\gamma = 2\mathcal{K}(\alpha)$. Since the integral presented by (79) includes branch points at $\alpha = \pm k_{eff}$, therefore, in general, it is difficult to get solution in closed form. However, we may tackle (79) utilizing the saddle point method to get an asymptotic expression. Now we introduce the polar coordinates as:

$$x = \rho \cos \theta, \quad y = \rho \sin \theta, \quad -\pi < \theta < \pi \quad (5.72)$$

The expression of $H_z^{(0)}(x, y)$ can be derived by using Saddle point method as:

$$H_z^{(0)}(\rho, \theta) \sim \mp \frac{e^{ik_{eff}l \cos \theta} \mathcal{S}_-(-k_{eff} \cos \theta) + e^{-ik_{eff}l \cos \theta} \mathcal{S}_+(-k_{eff} \cos \theta)}{2\mathcal{K}(-k_{eff} \cos \theta)} \times k_{eff} \sin |\theta| \frac{e^{i(k_{eff}\rho - \pi/4)}}{\sqrt{k_{eff}\rho}} \quad (5.73)$$

for $y \geq 0$ as $k_{eff}\rho \rightarrow \infty$. Substituting the (56) and (57) in (81), the results will be achieved for scattered far field with high-frequency for large $|k_{eff}|l$.

In the similar manner, an integral form of $H_z^{(1)}(x, z)$ can be derived by substituting

(38) in (76) and utilizing (39) and (40), we get

$$H_z^{(1)}(x, y) = H_{z,v}^{(1)}(x, y) + H_{z,u}^{(1)}(x, y), \quad (5.74)$$

where

$$H_{z,v}^{(1)}(x, y) = \mp (2\pi)^{-1/2} \int_{-\infty+id}^{\infty+id} \frac{e^{-i\alpha l} \mathcal{D}_-(\alpha) + e^{i\alpha l} \mathcal{D}_+(\alpha)}{2\mathcal{K}(\alpha)} e^{\mp \gamma(\alpha)y - i\alpha x} d\alpha, \quad (5.75)$$

$$H_{z,u}^{(1)}(x, y) = -(2\pi)^{-1/2} \int_{-\infty+id}^{\infty+id} \frac{1}{8i\pi\mathcal{K}(\alpha)} \left\{ \begin{array}{l} [\gamma^2(\alpha+m) - m(\alpha+m)] \\ \times \frac{e^{-i(\alpha+m)l} \mathcal{S}_-(\alpha+m) + e^{i(\alpha+m)l} \mathcal{S}_+(\alpha+m)}{\mathcal{K}(\alpha+m)} \\ - [\gamma^2(\alpha-m) - m(\alpha-m)] \\ \times \frac{e^{-i(\alpha-m)l} \mathcal{S}_-(\alpha-m) + e^{i(\alpha-m)l} \mathcal{S}_+(\alpha-m)}{\mathcal{K}(\alpha-m)} \end{array} \right\} \\ \times e^{\mp \gamma(\alpha)y - i\alpha x} d\alpha. \quad (5.76)$$

Now with the aid of saddle point method along with polar coordinates defined by (80), the $H_{z,v}^{(1)}(x, y)$ is evaluated asymptotically as

$$H_{z,v}^{(1)}(\rho, \theta) \sim \mp \frac{e^{ik_{eff}l \cos \theta} \mathcal{D}_-(-k_{eff} \cos \theta) + e^{-ik_{eff}l \cos \theta} \mathcal{D}_+(-k_{eff} \cos \theta)}{2\mathcal{K}(k_{eff} \cos \theta)} \\ \times k_{eff} \sin |\theta| \frac{e^{i(k_{eff}\rho - \pi/4)}}{(k_{eff}\rho)^{1/2}}, \quad (5.77)$$

for $y \geq 0$ as $k_{eff}\rho \rightarrow \infty$.

For $H_{z,u}^{(1)}(x, y)$ given by (84), in general it is difficult to evaluate asymptotic expression, because $\alpha = \pm k_{eff} + m$, $\pm k_{eff} - m$ and $\alpha = \pm k_{eff}$ are the branch points occurring in (84). To proceed further, we consider $|m/k_{eff}| \ll 1$ which leads to larger period of grating than the wavelength and can be evaluated asymptotically by the saddle point method. It's asymptotic expression is as follows:

$$\begin{aligned}
H_{z,u}^{(1)}(\rho, \theta) &\sim \frac{1}{8i\mathcal{K}(k_{eff} \cos \theta)} \sum_{n=1}^2 (-1)^n [4\mathcal{K}^2(k_{eff} \cos \theta^{(n)}) - (-1)^n m k_{eff} \cos \theta^{(n)}] \\
&\times \frac{e^{ik_{eff}l \cos \theta^{(n)}} \mathcal{S}_-(-k_{eff} \cos \theta^{(n)}) + e^{-ik_{eff}l \cos \theta^{(n)}} \mathcal{S}_+(-k_{eff} \cos \theta^{(n)})}{\mathcal{K}(k_{eff} \cos \theta^{(n)})} k_{eff} \sin |\theta| \frac{e^{i(k_{eff}\rho - \pi/4)}}{\sqrt{k_{eff}\rho}}
\end{aligned} \tag{5.78}$$

for $y \geq 0$ as $k_{eff}\rho \rightarrow \infty$, where

$$\theta^{(1,2)} = \cos^{-1}(\cos \theta \mp m/k_{eff}). \tag{5.79}$$

Introducing Eqs (85) and (86) into (82), the asymptotic expression of first-order field is,

$$\begin{aligned}
H_z^{(1)}(\rho, \theta) &\sim \mp \frac{e^{ik_{eff}l \cos \theta} \mathcal{D}_-(-k_{eff} \cos \theta) + e^{-ik_{eff}l \cos \theta} \mathcal{D}_+(-k_{eff} \cos \theta)}{2\mathcal{K}(k_{eff} \cos \theta)} \times k_{eff} \sin |\theta| \frac{e^{i(k_{eff}\rho - \pi/4)}}{\sqrt{k_{eff}\rho}} \\
&+ \frac{1}{8i\mathcal{K}(k_{eff} \cos \theta)} \sum_{n=1}^2 (-1)^n \left(\begin{aligned} &[4\mathcal{K}^2(k_{eff} \cos \theta^{(n)}) - (-1)^n m k_{eff} \cos \theta^{(n)}] \\ &\times \frac{e^{ik_{eff}l \cos \theta^{(n)}} \mathcal{S}_-(-k_{eff} \cos \theta^{(n)}) + e^{-ik_{eff}l \cos \theta^{(n)}} \mathcal{S}_+(-k_{eff} \cos \theta^{(n)})}{\mathcal{K}(k_{eff} \cos \theta^{(n)})} \\ &\times k_{eff} \sin |\theta| \frac{e^{i(k_{eff}\rho - \pi/4)}}{\sqrt{k_{eff}\rho}}, \end{aligned} \right)
\end{aligned} \tag{5.80}$$

for $y \geq 0$ as $k_{eff}\rho \rightarrow \infty$. With careful observation, that (88) expresses the uniform asymptotic expression for $H_z^{(1)}(\rho, \theta)$

5.5 Numerical Results and Discussion

In this section, the intensity of far field and characteristics of scattering by grating is elaborated mathematically and numerically as well. For ease, the normalized

function of far field intensity is introduced as in

$$|H_z(\rho, \theta)|[dB] = 20 \log_{10} \left[\frac{\lim_{\rho \rightarrow \infty} |(k_{eff}\rho)^{1/2} H_z(\rho, \theta)|}{\max_{|\theta| < \pi} \lim_{\rho \rightarrow \infty} |(k_{eff}\rho)^{1/2} H_z(\rho, \theta)|} \right], \quad (5.81)$$

where

$$H_z(\rho, \theta) = H_z^{(0)}(\rho, \theta) + hH_z^{(1)}(\rho, \theta). \quad (5.82)$$

Scattered field given by (81) is computed using the expressions given by (73) and (79). Under the assumption of small-depth approximations of Leontovich type boundary conditions, original model for grating is reduced to diffraction phenomena of a flat strip. The boundary condition expressed in (7) may be utilized to simulate corrugated surface by taking the grating depth $2h$ which satisfies for $2h \leq 0.1\lambda$. In this paper, we have taken depth (of grating) $2h = 0.1\lambda$ to consider the sinusoidal surface. On the other hand, the ratio $\frac{m}{k_{eff}}$ has been chosen as $\frac{m}{k_{eff}} \leq 0.2$ for validity of the asymptotic expression of $H_{z,u}^{(1)}(x, y)$ given in (77). Under this condition, the process of asymptotic evaluation of (77) gives rise to the branch point's appearance at $\alpha = \pm k + m$, $\alpha = \pm k - m$ leading to the contributions of branch-cut integrals which play a little role but not greater than the saddle point involvement and therefore, (77) may be employed with suitable accuracy. The characteristic values of ω_p and ω_c can be computed as $\omega_p = 56.4\text{MHz}$ and $\omega_c = 8.78\text{MHz}$. Further, result for high frequency signal is obtained by setting $\omega \gg \omega_c$ and following the same order for ω_p . This yields $\varepsilon_1 \approx 1 - (\omega_p/\omega)^2$ and $\varepsilon_2 \rightarrow 0$ in the limiting case. For numerical analysis, ω is chosen between 80MHz and 600MHz . For verification of this assumption, the values of ε_1 and ε_2 computed for corresponding ω are given in Table 1.

Presence of cold plasma is considered by taking $\varepsilon_1 = 0.6$ and $\varepsilon_2 = 0.001$ whereas for the absence of cold plasma we have chosen particular values as $\varepsilon_1 = 1.0$ and $\varepsilon_2 = 0$. Figs. 2 and 5, 3 and 6, 4 and 7 show the plots for scattered far field intensity versus θ for respective grating length $2l = 10\lambda, 25\lambda, 45\lambda$ with $N = \frac{2l/\lambda}{m/k_{eff}}$ being the number of periods of grating and θ_0 being the incidence angle fixed as 60 . In Figs.

ω (in MHz)	ε_1	ε_2
80.50	0.50913	0.05353
95.75	0.65303	0.03181
130.15	0.81221	0.01266
210.25	0.92804	0.003005
300.60	0.96479	0.001028
440.50	0.98360	0.000326
595.50	0.99103	0.000132

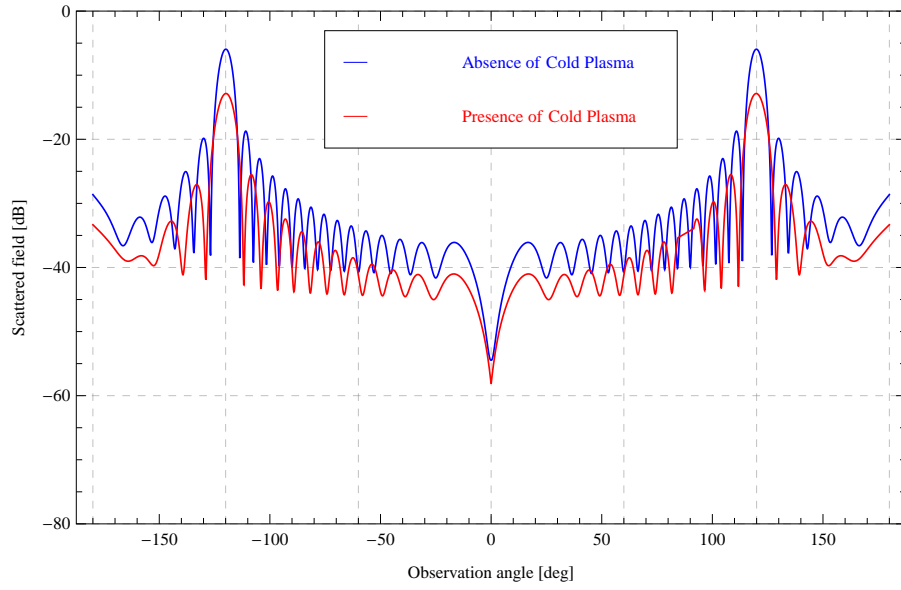
Table 5.1: Values of ε_1 and ε_2 for corresponding operating frequency.

(2 – 4), blue and red lines show the scattered field in the existence and non-existence of non-thermal plasma, respectively, on the other hand, in Figs. (5 – 7), blue and red lines show the scattered far field for flat as well as corrugated grating, respectively. The depth (of grating) has been taken as $2h = 0.1\lambda$ to investigate the effects due to sinusoidal structure of grating in Figs. 2(b), 3(b), 4(b), 5, 6 and 7. Another important parameter is the periodicity parameter $\frac{m}{k_{eff}}$ which is taken as 0.1 in Figs. 2, 5 and as 0.2 in Figs. 3, 4, 6, 7. The comparative study of scattering features between flat strip and sinusoidal grating is of significance. Figs. 2(a), 3(a), 4(a) are displayed to study the comparison between effects due to absence and presence of cold plasma for flat strip, on the other hand Figs. 2(b), 3(b), 4(b) are plotted to investigate the existence and non-existence of non-thermal plasma for sinusoidal grating. Figs. 5(a), 6(a), 7(a) show the comparative analysis of scattered field due to flat strip and sinusoidal grating in absence of cold plasma whereas Figs. 5(b), 6(b), 7(b) show the analysis for presence of cold plasma.

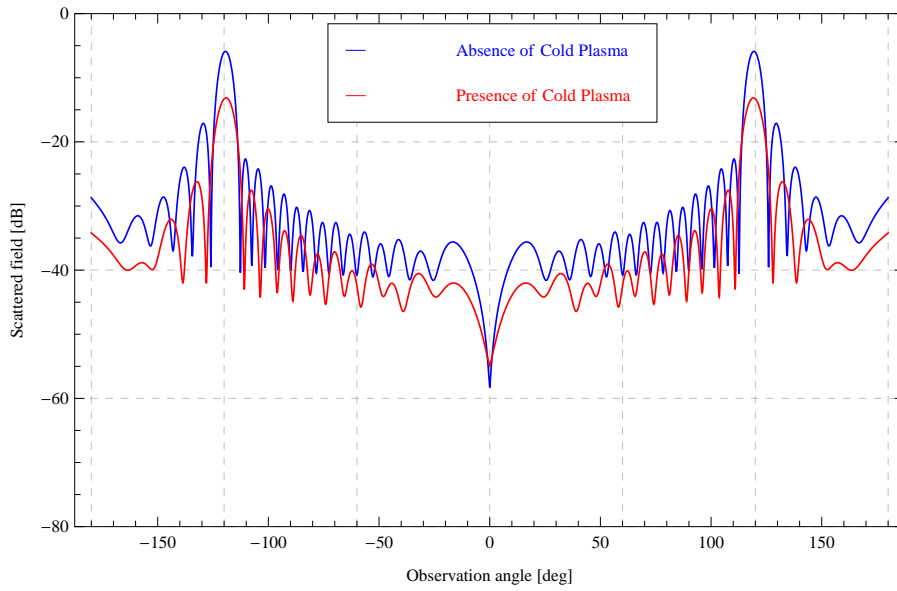
From all the figures, it can be seen that far field show maximum peaks at two distinct angles $\theta = -120$, and 120 corresponding to the shadow boundaries of incident and reflected fields, respectively. Now we discuss the comparison of sinusoidal-shaped grating in Figs. 2(b), 3(b), 4(b) with flat strip in Figs. 2(b), 3(b), 4(b). It can be seen that in case of finite sinusoidal grating, nullity of far field intensity is lesser than those of flat strip. Also, behavior of oscillations for sinusoidal grating is different from those for the flat strip. Most noticeable behavior in Figs. 2 – 4 is the effects of cold plasma. It can be observed that presence of non-thermal plasma (red lines) has lessen

the sharp peaks occurring at $\theta = -120$, and 120 , and number of oscillations too. This means that presence of non-thermal plasma avoids the waves from dispersion.

Now we briefly explain the plots of intensity far field shown in Figs. 5 – 7 for flat strip versus sinusoidal grating in the existence and nonexistence of non-thermal plasma. On comparing Fig. 5(b), 6(b) with that of 5(a), 6(a), respectively, we see that existence of non-thermal plasma has reduced the amplitude, number of oscillations and nullity at $\theta = 0$ of far field intensity. Also, the sharp peaks occurring in the neighborhood of maximum peaks at $\theta = -120$, and 120 shown in Fig. 6(a) are reduced by inclusion of non-thermal plasma in Fig. 6(b). A particular oscillating behavior for sinusoidal grating (red lines) at $\theta = 0$ is shown by subplot in Fig. 7(b), which is an opposite behavior of far field intensity for sinusoidal grating at $\theta = 0$ in Fig. 7(a). If we analyze the Figs. 2, 5 for $N = 1$, and Figs. 3, 6 for $N = 5$ and Figs. 4, 7 for $N = 9$, we find that for larger values of N numbers of oscillations are increased. This happens because of the structure approaching an infinite sinusoidal grating for enhancement of N and hence, waves are strongly excited along the directions of propagation.

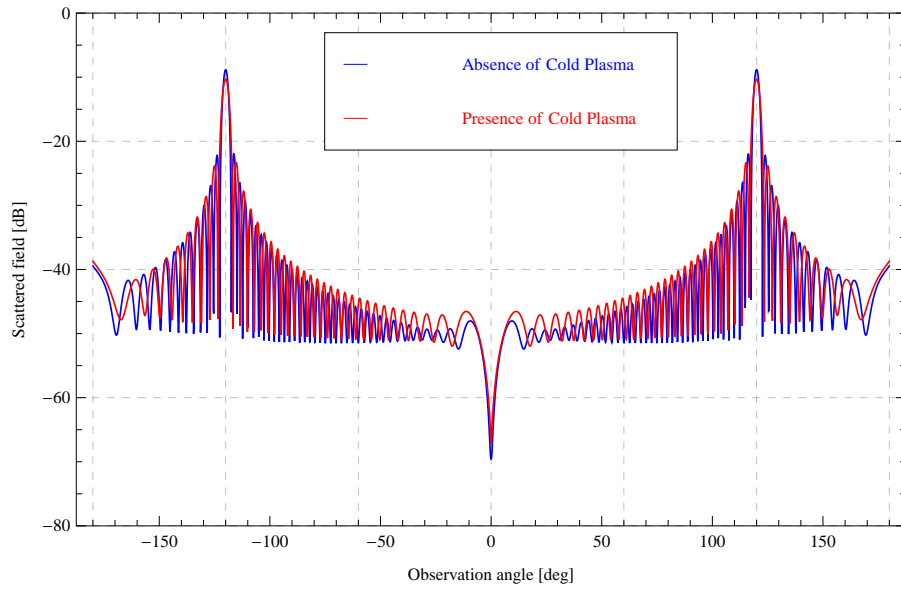


(a)

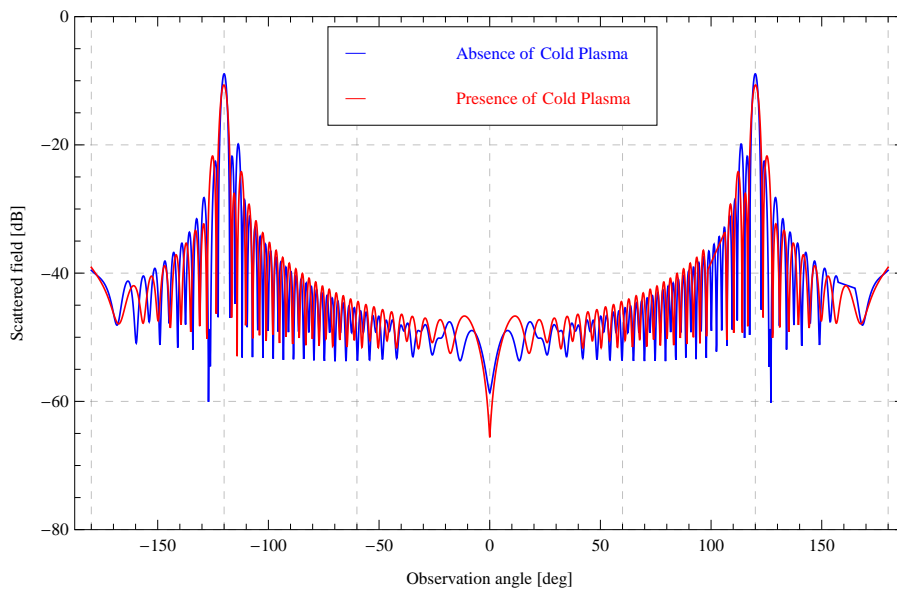


(b)

Figure 5.2: Behavior of $H(x, y)$ for $\theta_0 = 60$, $N = 1$, $2l = 10\lambda$, $m/k_{eff} = 0.1$ (a) $h = 0$ (b) $2h = 0.1\lambda$.

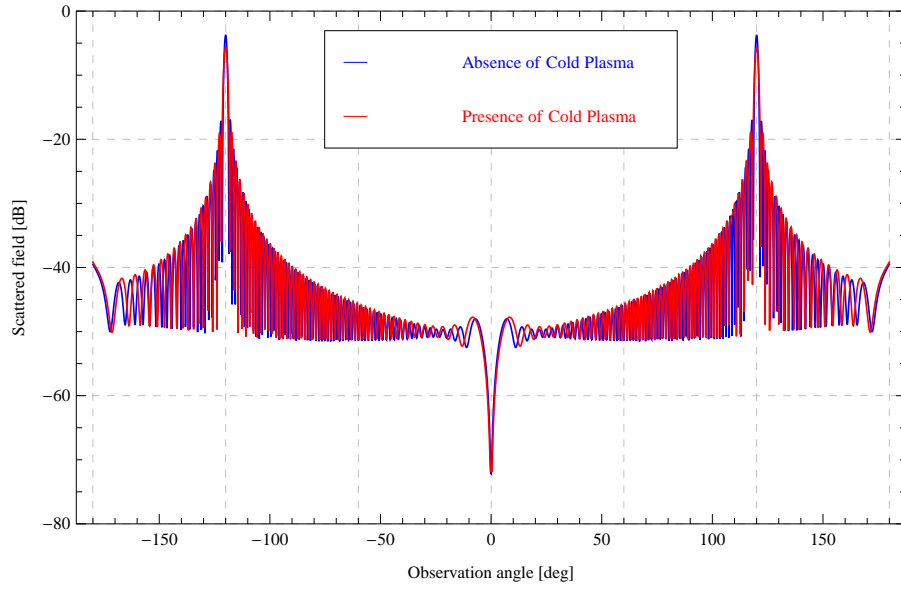


(a)

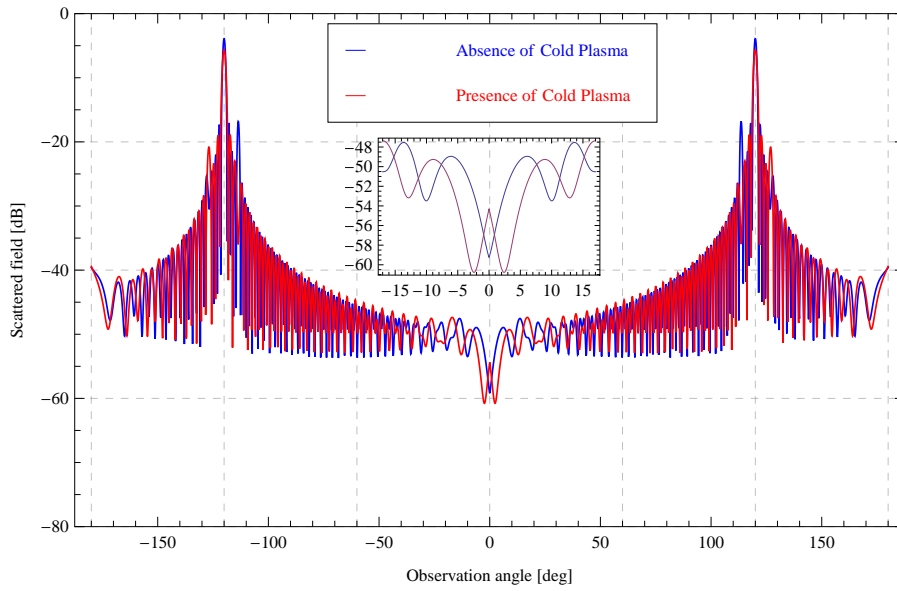


(b)

Figure 5.3: Behavior of $H(x, y)$ for $\theta_0 = 60$, $N = 5$, $2l = 25\lambda$, $m/k_{eff} = 0.2$ (a) $h = 0$ (b) $2h = 0.1\lambda$.

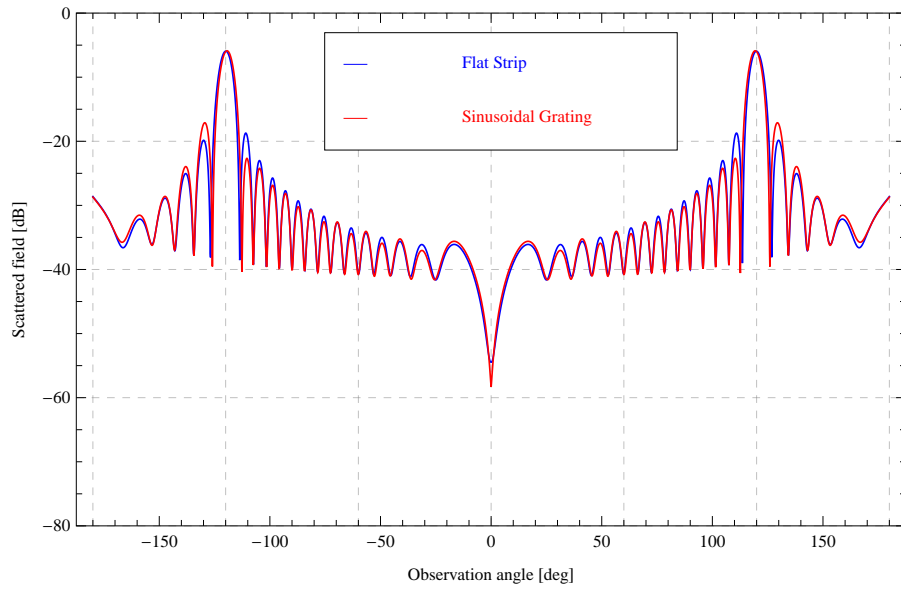


(a)

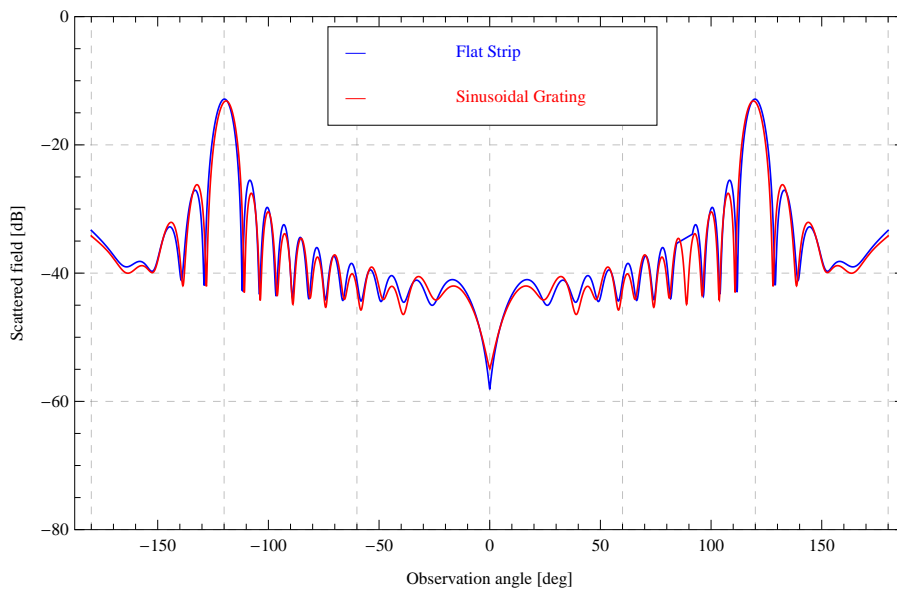


(b)

Figure 5.4: Behavior of $H(x, y)$ for $\theta_0 = 60$, $N = 9$, $2l = 45\lambda$, $m/k_{eff} = 0.2$ (a) $h = 0$ (b) $2h = 0.1\lambda$.

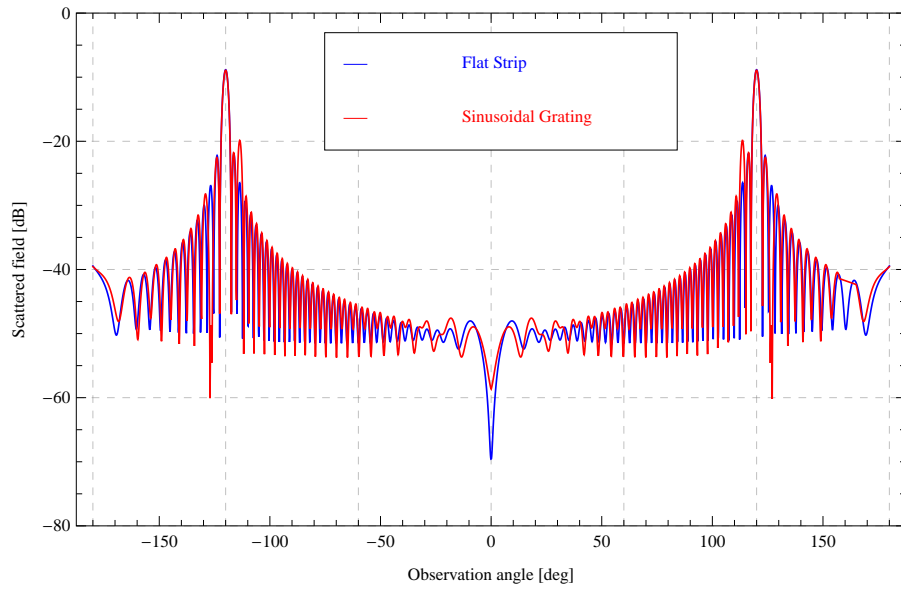


(a)

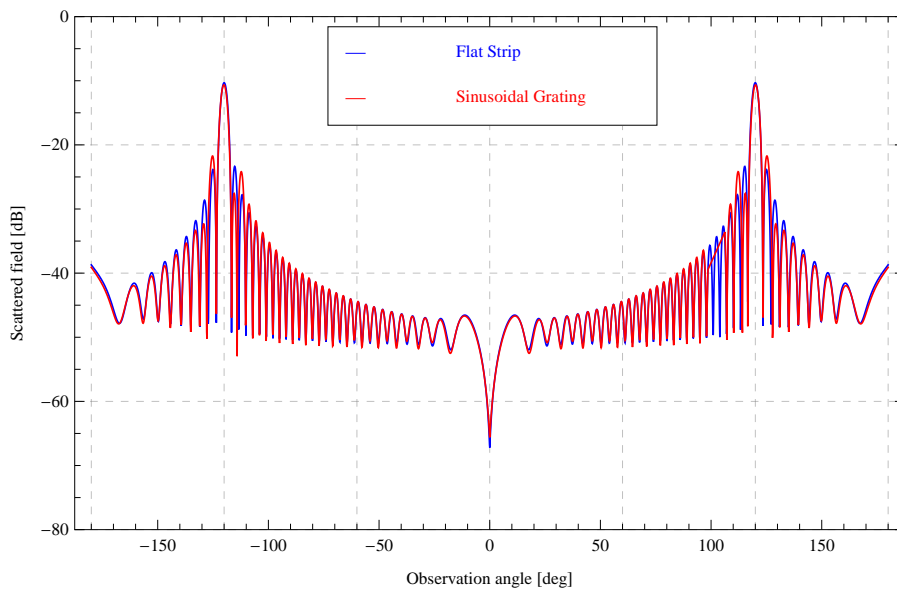


(b)

Figure 5.5: Behavior of $H(x, y)$ for $\theta_0 = 60$, $N = 1$, $2l = 10\lambda$, $m/k = 0.1$ (a) absence of cold plasma (b) presence of cold plasma.

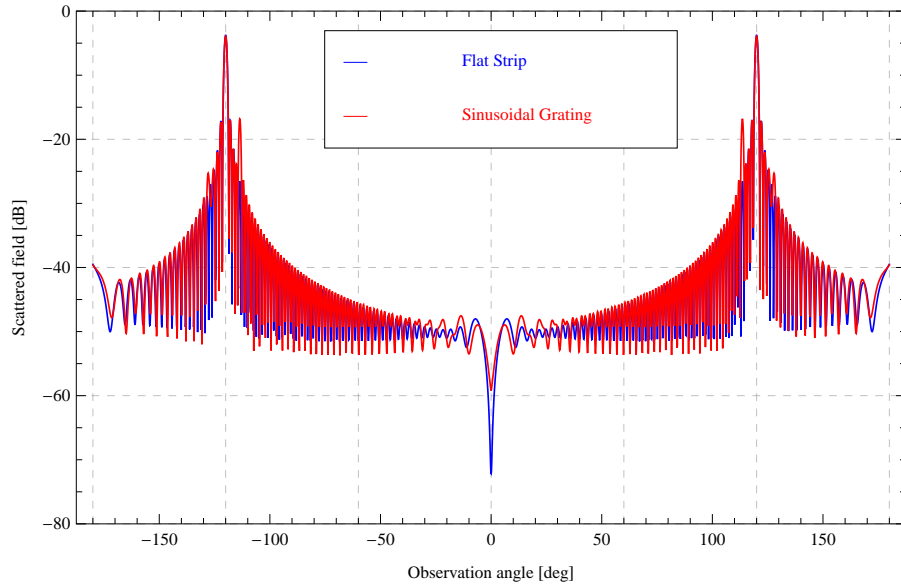


(a)

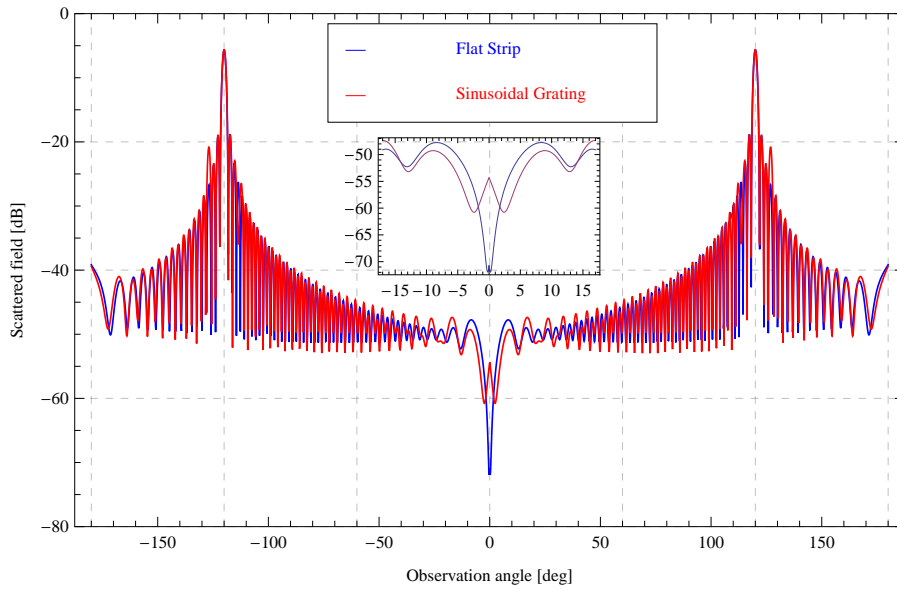


(b)

Figure 5.6: Behavior of $H(x, y)$ for $\theta_0 = 60$, $N = 5$, $2l = 25\lambda$, $m/k_{eff} = 0.2$ (a) absence of cold plasma (b) presence of cold plasma.



(a)



(b)

Figure 5.7: Behavior of $H(x, y)$ for $\theta_0 = 60$, $N = 9$, $2l = 45\lambda$, $m/k_{eff} = 0.2$ (a) absence of cold plasma (b) presence of cold plasma.

5.6 Conclusion

In this article, diffracted H-polarized plane wave incident at the sinusoidal-shaped grating of finite length in the presence of cold plasma is analyzed by Wiener-Hopf technique along with perturbation method. Helmholtz equation has been formulated by using Maxwell equations along with non-thermal plasma tensor to analyze the effects of non-thermal plasma on scattered far field intensity. The small corrugation amplitude as compared to wavelength is assumed and scattered field has been expanded via perturbation series to reduce the problem to diffraction behavior for flat strip embedded the surface with mixed conditions. Wiener-Hopf equations of zero- and first-order are formulated with the aid of approximate boundary condition. The decomposition procedure is used to proceed these Wiener-Hopf equations which then yields the exact solutions with high-frequency.

Implementation of the inverse Fourier transformation along with the asymptotic method of saddle point, the scattered field is devised which shows validity for arbitrary angles of observation as well as incidence. We have accomplished graphical analysis of field intensity on the basis of results and investigated the diffraction by flat strip and sinusoidal grating in existing and non-existing non-thermal plasma in detail. On analyzing the plots, it is observed that the number of oscillations increase due to increasing the number of gratings. Also, the existence of non-thermal plasma has reduced the peaks of the field oscillations. Model can be thought of an artificial satellite in the space or a screen with sinusoidal shape.

Chapter 6

EM-Wave Incident on the Slit of Finite Width with Dirichlet Conditions in An-isotropy of Non-thermal Plasma

This chapter thoroughly investigate the interaction of wave field due to a finite-width slit with Dirichlet boundary conditions in the context of non-thermal plasma. After applying the Fourier transform to the Helmholtz equation, the boundary value problem is established. To solve the challenge stated for this model, the Wiener-Hopf analysis is used. At the completion of the analysis, the separated field computed along with its numerical findings are elaborated to further investigate the impacts of variation in physical parameters in an an-isotropic medium.

6.1 Problem Statement

We have investigated the diffraction pattern of plane electromagnetic waves due to a finite-width slit in non-thermal plasma, as illustrated in Fig. 6.1. Furthermore, Dirichlet conditions are assumed on the slit and angle of incidence is θ_0 . The total

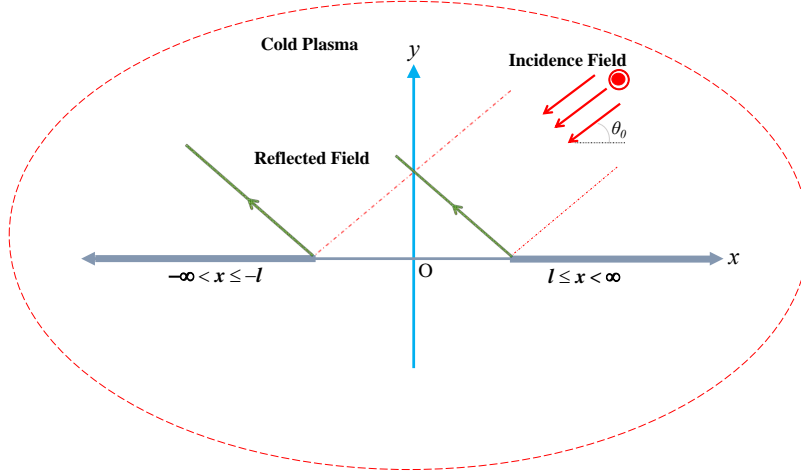


Figure 6.1: **Simplified figure of the problem.**

field can be represented in terms of incident, refracted and diffracted fields as:

$$H_z^{tot}(x, y) = H_z^{inc}(x, y) + H_z^{ref}(x, y) + H_z(x, y), \quad (6.1)$$

where the incident and refracted fields are defined as

$$H_z^{inc}(x, y) = e^{-ik_{eff}(x \cos \theta_0 + y \sin \theta_0)}, \quad (6.2)$$

$$H_z^{ref}(x, y) = e^{-ik_{eff}(x \cos \theta_0 - y \sin \theta_0)}. \quad (6.3)$$

Suppose that medium is slightly lossy, and constant K_{eff} appearing in above equations is complex in such a way ($0 < \Im\{k_{eff}\} \ll \Re\{k_{eff}\}$). At the end, for real K_{eff} solution could be determine by taking its imaginary part to zero. The entire field $H_z^{tot}(x, y)$ meeting the Helmholtz equation is

$$[\partial_{xx} + \partial_{yy} + k_{eff}^2]H_z^{tot}(x, y) = 0, \quad (6.4)$$

Substituting the value of $H_z^{tot}(x, y)$ from (7.1), we get the equation for diffracted field as:

$$[\partial_{xx} + \partial_{yy} + k_{eff}^2]H_z(x, y) = 0, \quad (6.5)$$

In order to establish the Wiener-Hopf equation, conditions at $x = \pm l$ in conjunction with continuity relations are used. Neumann boundary conditions on a finite-width slit are specified as

$$H_z^{tot} = 0, \text{ for } -l \geq x \geq l, \text{ and } y = 0^\pm, \quad (6.6)$$

along with

$$H_z^{tot}(x, 0^+) = H_z^{tot}(x, 0^-) = 0, \quad \text{at } |x| < l, \quad y = 0, \quad (6.7)$$

6.2 Problem Transformation

Following results can be obtained with the use of Fourier Transforms.

$$\begin{aligned} \mathcal{F}(\beta, y) &= \frac{1}{\sqrt{2\pi}} \int_{-\infty}^{\infty} e^{i\beta x} H_z(x, y) dx \\ &= e^{i\beta l} \mathcal{F}_+(\beta, y) + e^{-i\beta l} \mathcal{F}_-(\beta, y) + \mathcal{F}_l(\beta, y), \end{aligned} \quad (6.8)$$

where $\beta = \sigma + i\tau$.

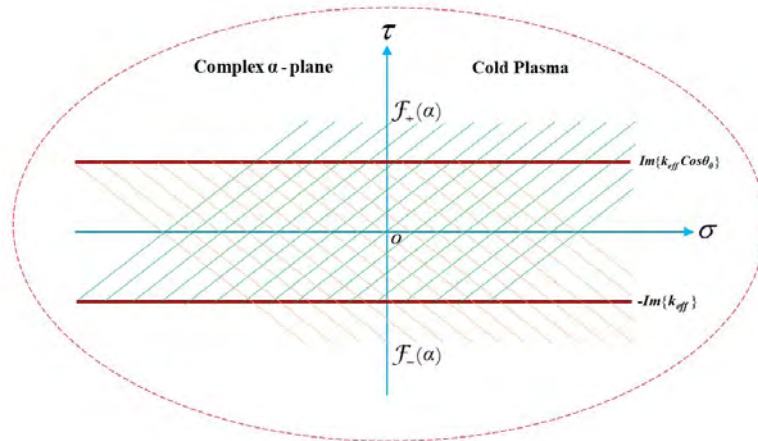


Figure 6.2: Illustration of Analytic-Continuation.

For high values of x , the diffracted field is interpreted as follows:

$$H_z(x, y) = \begin{cases} O(e^{-ik_{eff}x}), \\ O(e^{-k_{eff}x \cos \theta_0}). \end{cases} \quad (6.9)$$

The regions of regularity in the complex plane for $\mathcal{F}_+(\beta, y)$ and $\mathcal{F}_-(\beta, y)$ are $\Im\{\beta\} > -\Im\{k_{eff}\}$ and $\Im\{\beta\} < \Im\{k_{eff} \cos \theta_0\}$. From Fig 6.2, we can see the common region $-\Im\{k_{eff}\} < \Im\{\beta\} < \Im\{k_{eff} \cos \theta_0\}$ of analyticity, where the functions $\mathcal{F}_l(\beta, y)$ are also analytic and hence, we can define

$$\mathcal{F}_\pm(\beta, y) = \pm \frac{1}{\sqrt{2\pi}} \int_{\pm l}^{\pm\infty} e^{i\beta(x \mp l)} H_z(x, y) dx \quad (6.10)$$

$$\mathcal{F}_l(\beta, y) = \frac{1}{\sqrt{2\pi}} \int_{-l}^l e^{i\beta x} H_z(x, y) dx \quad (6.11)$$

$$\mathcal{F}^{inc}(\beta, y) = \frac{\exp(-iyk_{eff} \sin \theta_0)}{\sqrt{2\pi}} \left(\frac{\exp[i\beta(\beta - k_{eff} \cos \theta_0)] - \exp[-i\beta(\beta - k_{eff} \cos \theta_0)]}{i(\beta - k_{eff} \cos \theta_0)} \right). \quad (6.12)$$

$$\mathcal{F}^{ref}(\beta, y) = \frac{\exp(iyk_{eff} \sin \theta_0)}{\sqrt{2\pi}} \left(\frac{\exp[i\beta(\beta - k_{eff} \cos \theta_0)] - \exp[-i\beta(\beta - k_{eff} \cos \theta_0)]}{(\beta - k_{eff} \cos \theta_0)} \right). \quad (6.13)$$

The following transformed boundary value problem could be obtained by applying the Fourier transformation to Eqs. (7.5 – 7.7) .

$$\left(\frac{d^2}{dy^2} + \gamma^2 \right) \mathcal{F} = 0 \quad (6.14)$$

where $\gamma(\beta) = \sqrt{k_{eff}^2 - \beta^2}$.

$$\begin{aligned} \mathcal{F}(\beta, 0^+) &= \mathcal{F}^{ref}(\beta, 0) - \mathcal{F}^{inc}(\beta, 0), \\ \mathcal{F}(\beta, 0^-) &= 0 \end{aligned}, \quad (6.15)$$

and

$$\mathcal{F}_\pm(\beta, 0^+) = 0 = \mathcal{F}_\pm(\beta, 0^-). \quad (6.16)$$

6.3 Solution of the Wiener-Hopf Equation

The solution of transformed boundary value problem (7.14), fulfilling the radiation conditions is,

$$\mathcal{F}(\beta, y) = \begin{cases} A_1(\beta) \exp(-i\gamma y) & y \geq 0, \\ A_2(\beta) \exp(i\gamma y) & y < 0. \end{cases} \quad (6.17)$$

Now using Eqs. (7.15 – 7.17), following Wiener-Hopf equation is obtained.

$$\exp(i\beta l)\mathcal{F}'_+(\beta, 0) + \exp(-i\beta l)\mathcal{F}'_-(\beta, 0) + \mathcal{K}(\beta)\tilde{\mathcal{F}}_i(\beta, 0) = -k_{eff} \sin \theta_0 \mathcal{G}(\beta), \quad (6.18)$$

where,

$$\mathcal{K}(\beta) = i\gamma, \quad (6.19)$$

$$\tilde{\mathcal{F}}_i(\beta, 0) = \frac{1}{2} (\mathcal{F}_i(\beta, 0^+) - \mathcal{F}_i(\beta, 0^-)) \quad (6.20)$$

$$\mathcal{G}(\beta) = \frac{\exp[i\beta(\beta - k_{eff} \cos \theta_0)] - \exp[-i\beta(\beta - k_{eff} \cos \theta_0)]}{\sqrt{2\pi(\beta - k_{eff} \cos \theta_0)}}, \quad (6.21)$$

The Kernel function defined in Eq. 7.19 can be written as:

$$\mathcal{K}(\beta) = \frac{1}{i\gamma(\beta)} = \mathcal{K}_\pm(\beta) \text{ with } \gamma(\beta) = \gamma_\pm(\beta), \quad (6.22)$$

where $\mathcal{K}_\pm(\beta)$ are,

$$\mathcal{K}_\pm(\beta) = \frac{\exp(-i\frac{\pi}{4})}{\gamma_\pm(\beta)} \text{ with } \gamma_\pm(\beta) = \sqrt{k_{eff} \pm \beta}. \quad (6.23)$$

It must be noted that the functions, $\mathcal{K}_\pm(\beta)$ have region of regularity are $\Im\{\beta\} > -\Im\{k_{eff}\}$ and $\Im\{\beta\} < \Im\{k_{eff} \cos \theta_0\}$ and similarly for $\gamma_\pm(\beta)$. From Eq. (7.18), equating the terms which are regular in their corresponding regions, creates a common region of analyticity. Hence, by analytic continuation, we get an entire function $\mathcal{P}(\beta)$ and by Liouville's theorem, $\mathcal{P}(\beta)$ must be equal to zero[12], yielding the following results.

$$\mathcal{F}_{\pm}(\beta, 0) = \frac{\mathcal{A}}{\sqrt{2\pi}} [\mathcal{K}_{\pm}(\beta)\mathcal{G}_{1,2}(\pm\beta) + \mathcal{K}_{\pm}(\beta)\mathcal{T}(\pm\beta)\mathcal{C}_{1,2}], \quad (6.24)$$

where

$$\mathcal{G}_{1,2}(\beta) = \frac{\exp(\mp ik_{eff}l \cos \theta_0)}{\alpha \mp k_{eff} \cos \theta_0} \left(\frac{1}{\mathcal{K}_{+}(\beta)} - \frac{1}{\mathcal{K}_{+}(\pm k_{eff} \cos \theta_0)} \right) - \exp(\pm ik_{eff}l \cos \theta_0) \mathcal{R}_{1,2}(\beta), \quad (6.25)$$

$$\mathcal{C}_{1,2} = \mathcal{K}_{+}(k_{eff}) \frac{\mathcal{G}_{2,1}(k_{eff}) + \mathcal{K}_{+}(k_{eff})\mathcal{G}_{1,2}(k_{eff})\mathcal{T}(k_{eff})}{1 - \mathcal{K}_{+}^2(k_{eff})\mathcal{T}^2(k_{eff})}, \quad (6.26)$$

$$\mathcal{R}_{1,2}(\beta) = \frac{E_{-1}}{2\pi i(\beta \mp k_{eff} \cos \theta_0)} [\mathcal{W}_{-1}(-i(k_{eff} \pm k_{eff} \cos \theta_0)) - \mathcal{W}_{-1}(-i(k_{eff} + \beta))], \quad (6.27)$$

$$\mathcal{T}(\beta) = \frac{E_{-1}}{2\pi} \mathcal{W}_{-1}[-i(k_{eff} + \beta)l], \quad E_{-1} = 2\sqrt{\frac{l}{i}} e^{ik_{eff}l + \beta}, \quad (6.28)$$

$$\mathcal{W}_{n-1/2}(q) = \int_0^{\infty} \frac{v^n e^{-v}}{v+q} dv = \Gamma(n+1) e^{(\frac{q}{2})} q^{(n-1)/2} \mathcal{W}_{-(n+1)/2, n/2}(q), \quad (6.29)$$

where $q = -i(k_{eff} + \beta)l$, $n = -\frac{1}{2}$ and \mathcal{W} is the Whittaker function. Solving Eqs. 7.17 and 7.18, diffracted field is,

$$\mathcal{F}(\beta, y) = -\frac{1}{\mathcal{K}(\beta)} [\exp(i\beta l)\mathcal{F}_{+}(\beta, 0) + \exp(-i\beta l)\mathcal{F}_{-}(\beta, 0) + \mathcal{F}_l(\beta, 0)] e^{-i\gamma|y|}, \quad (6.30)$$

where

$$\mathcal{F}_l(\beta, 0) = -\mathcal{A}\mathcal{G}(\beta), \quad \text{and} \quad \mathcal{A} = -k_{eff} \sin \theta_0 \quad (6.31)$$

Inverse Fourier transformation of Eq. (7.30), yields the diffracted field as:

$$H_z(x, y) = \frac{1}{\sqrt{2\pi}} \int_{-\infty}^{\infty} \mathcal{F}(\beta, y) \exp(-i\beta x - i\gamma|y|) d\beta. \quad (6.32)$$

Inserting (7.30) in (7.32), we get

$$H_z(x, y) = -\frac{1}{\sqrt{2\pi}} \int_{-\infty}^{\infty} \frac{1}{\mathcal{K}(\beta)} \left\{ \begin{array}{l} \exp(i\beta l)\mathcal{F}_{+}(\beta, 0) + \exp(-i\beta l)\mathcal{F}_{-}(\beta, 0) + \\ + \tilde{\mathcal{F}}_l(\beta, 0) \end{array} \right\} \exp(-i\beta x - i\gamma|y|) d\beta. \quad (6.33)$$

Diffracted field $H_z(x, y)$ further bifurcate in the separated and interaction fields $H_z^{sep}(x, y)$ and $H_z^{int}(x, y)$, respectively as,

$$H_z(x, y) = H_z^{sep}(x, y) + H_z^{int}(x, y), \quad (6.34)$$

where

$$H_z^{sep}(x, y) = \frac{1}{2\pi} \int_{-\infty}^{\infty} \frac{\mathcal{A}}{\mathcal{K}(\beta)} \left\{ \begin{array}{l} \frac{\mathcal{K}_+(\beta) \exp[i(\beta - k_{eff} \cos \theta_0)l]}{\mathcal{K}_+(k_{eff} \cos)(\beta - k_{eff} \cos \theta_0)} \\ - \frac{\mathcal{K}_+(-\beta) \exp[-i(\beta - k_{eff} \cos \theta_0)l]}{\mathcal{K}_+(-k_{eff} \cos)(\beta - k_{eff} \cos \theta_0)} \end{array} \right\} \exp(-i\beta x - i\gamma|y|) d\beta, \quad (6.35)$$

$$H_z^{int}(x, y) = \frac{1}{2\pi} \int_{-\infty}^{\infty} \frac{\mathcal{A}}{\mathcal{K}(\beta)} \left\{ \begin{array}{l} \exp(i\beta l) \mathcal{K}_+(\beta) \mathcal{T}(\beta) \mathcal{C}_1 \\ - \exp[i(\beta + k_{eff} \cos \theta_0)l] \mathcal{K}_+(\beta) \mathcal{R}_1(\beta) \\ + \exp(-i\beta l) \mathcal{K}_-(\beta) \mathcal{T}(-\beta) \mathcal{C}_2 \\ - \exp[-i(\beta + k_{eff} \cos \theta_0)l] \mathcal{K}_-(\beta) \mathcal{R}_2(-\beta) \end{array} \right\} \exp(-i\beta x - i\gamma|y|) d\beta. \quad (6.36)$$

The separated field given by (7.35) depicts diffraction separately at the edges. The $H_z^{inct}(x, y)$ represented by Eq. (7.36) explains the interaction of one end with the other.

6.4 Diffracted Field

The diffracted field due to slit of finite width for the far field can be obtained asymptotically by coping with the integral appearing in (7.32). Polar coordinates are introduced for the evaluation of Eq. 7.32 with the following transformation.

$$\beta = -k_{eff} \cos(\phi + i\eta), \quad 0 < \phi < \pi, \quad -\infty < \eta < \infty. \quad (6.37)$$

Now when the method of stationary phase [32] is used for (7.32), the following result are obtained:

$$H_z(r, \phi) = \frac{ik_{eff}}{\sqrt{k_{eff}r}} \mathcal{F}(-k_{eff} \cos \phi, \pm r \sin \phi) \sin \phi \exp\left(ik_{eff}r + i\frac{\pi}{4}\right). \quad (6.38)$$

Using the same polar coordinates, the transformation and subsequently the method of stationary phase are used to assess and yield the separated field and interaction fields as follows:

$$\{H_z^{sep}, H_z^{int}\}(r, \phi) = \frac{1}{\sqrt{2\pi}} \frac{ik_{eff}}{\sqrt{k_{eff}r}} \{f_{sep}, -f_{int}\}(-k_{eff} \cos \phi) \sin \phi \exp\left(ik_{eff}r + i\frac{\pi}{4}\right), \quad (6.39)$$

where

$$f_{sep}(-k_{eff} \cos \phi) = \frac{\mathcal{A}}{\mathcal{K}(-k_{eff} \cos \phi)} \left\{ \begin{array}{l} \frac{\mathcal{K}_+(-k_{eff} \cos \phi) \exp[-ik_{eff}l(\cos \phi + \cos \theta_0)]}{\mathcal{K}_+(k_{eff} \cos \theta_0)(-k_{eff} \cos \phi - k_{eff} \cos \theta_0)} \\ - \frac{\mathcal{K}_+(k_{eff} \cos \phi) \exp[ik_{eff}l(\cos \phi + \cos \theta_0)]}{\mathcal{K}_+(-k_{eff} \cos \theta_0)(-k_{eff} \cos \phi - k_{eff} \cos \theta_0)} \end{array} \right\} \quad (6.40)$$

$$f_{int}(-k_{eff} \cos \phi) = \frac{\mathcal{A}}{\mathcal{K}(-k_{eff} \cos \phi)} \left\{ \begin{array}{l} \exp(-ik_{eff}l \cos \phi) \mathcal{K}_+(-k_{eff} \cos \phi) \\ \times \mathcal{T}(-k_{eff} \cos \phi) \mathcal{C}_1 \\ - \exp[i l(-k_{eff} \cos \phi + k_{eff} \cos \theta_0)] \\ \times \mathcal{K}_+(-k_{eff} \cos \phi) \mathcal{R}_1(-k_{eff} \cos \phi) \\ + \mathcal{K}_-(-k_{eff} \cos \phi) \exp(ik_{eff}l \cos \phi) \\ \times \mathcal{T}(k_{eff} \cos \phi) \mathcal{C}_2 \\ - \exp[-i l(-k_{eff} \cos \phi + k_{eff} \cos \theta_0)] \\ \times \mathcal{K}_-(-k_{eff} \cos \phi) \mathcal{R}_2(k_{eff} \cos \phi) \end{array} \right\} \quad (6.41)$$

From Eq. (7.38), we can clearly see that the asymptotic expressions for far field can be obtained by letting $k_{eff}r \rightarrow \infty$ and the resulting expressions will be holds true for any observational angle. The separated field of an EM-wave is investigated in order to characterise both the field diffracted by the corners of a slit and the influence of the geometrical wave field. The separated field that results gives physical evidence

for the non-thermal plasma concept. Separated-field, on the other hand, provides no physical information due to contact at one edge with the other, which has already been enumerated by separated-field. As a result, we've only talked about the separated field because it conveys a full physical comprehension of EM-wave diffraction at the established boundaries. Additionally, we discovered that the interaction field is created by diffraction from the corners of slit at $x = \pm l$. Furthermore, when the slit width is increased to ∞ , the contribution due to H_z^{inct} terms disappears, leaving just the separated field terms in the diffracted field. As a consequence, we merely examine the separated field, as illustrated visually in the next section.

6.5 Discussion and Numerical Results

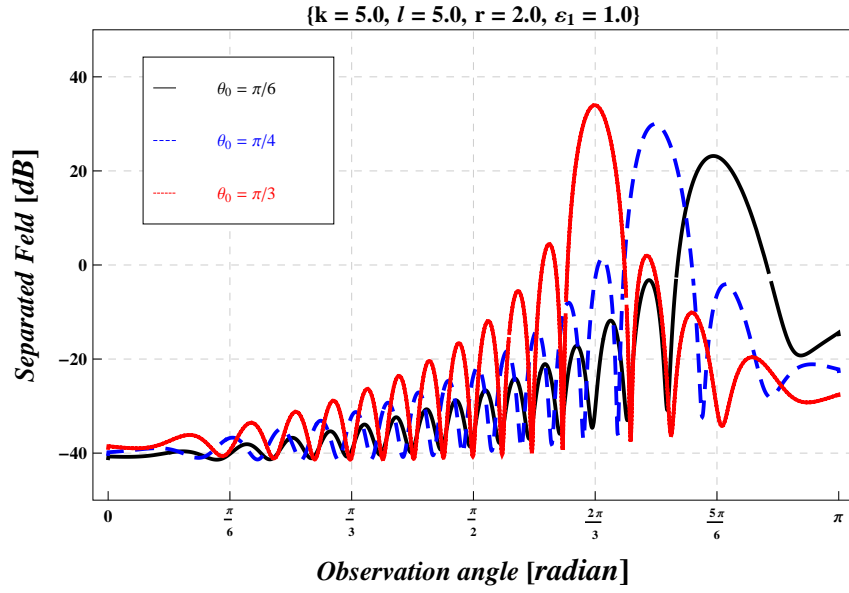
In this section, we examined the EM-waves by finite-width slit as graphically by the variation of physical parameters in an an-isotropic media with Neumann conditions versus the observational angle. For the ionosphere, we take the value of ω_p as $56.4MHz$ and ω_c as $8.78 MHz$. Now, the values of ε_1 and ε_2 are computed numerically against ω to verify the considered model. Also, the values of ω are taken between $80MHz$ and $600MHz$ given in Tab 6.1. It can be notice from Table-6.1, that the value of ε_2 is comparably very small from ε_1 with the boost up of ω in the frequency range. For isotropic medium, we can take $\varepsilon_1 = 1$ and $\varepsilon_2 = 0$, While the parameters ε_1 and ε_2 for the an-isotropic media (non-thermal plasma) can indeed be selected from Table-1.

ω (in MHz)	ε_1	ε_2
80.15	0.504834	0.054242
99.50	0.678699	0.028352
145.75	0.850259	0.009020
245.15	0.947071	0.001895
375.50	0.97744	0.000527
480.50	0.986222	0.000251
599.75	0.991157	0.000129

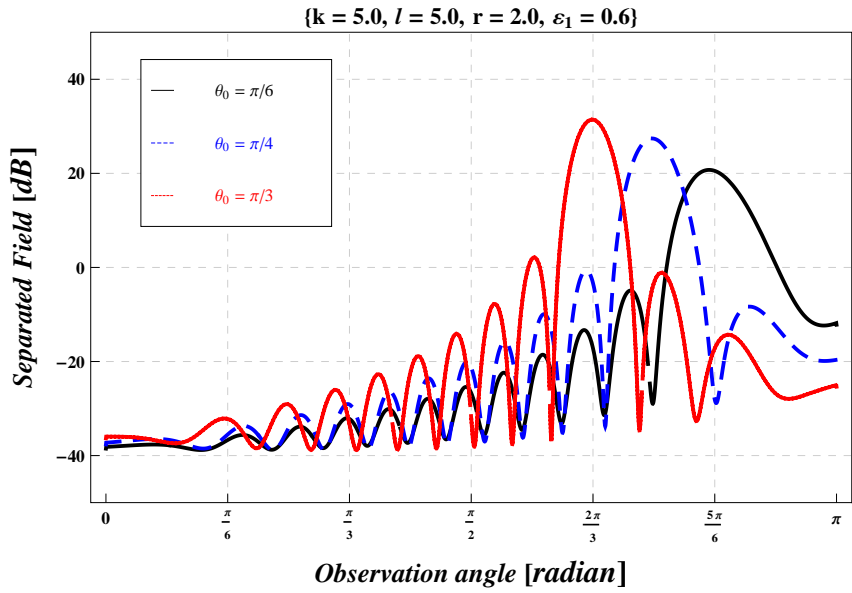
Table 6.1: Values of ε_1 and ε_2 for corresponding ω .

The graphical analysis is elaborated to explore the influence of physical parame-

ters on diffracted field due to a finite-width slit lying in the ionosphere of non-thermal plasma. These physical parameters are θ_0 , k , $2l$ and ε_1 . Fig. 6.3 represents the pattern of the separated field for variation of θ_0 , and it gets maxima for $\theta_0 = \pi/3, \pi/4, \pi/6$ occurring at $\theta = 2\pi/3, 3\pi/4, 5\pi/6$, respectively. These maxima actually predict the shadow of reflected field. Fig. 6.4 reveals the separated field for k . It is notable that the field has a direct dependence upon k because the field gets amplified for k . Since the frequency is directly related to k , so it excites the frequency of wave towards the high range. As extension of the slit-width is actually the expansion of aperture which is responsible for the diffraction of electromagnetic radiations, and so, separated field gets amplified as well as more oscillated as can be seen in Fig. 6.5. This amplified amplitude could be controlled by introducing the ionosphere as can be observed through Fig. 6.5b. By comparing Figs. 6.3b, 6.4b and 6.5b of the separated field in the an-isotropic medium with their respective Figs. 6.3a, 6.4a and ?? in the isotropic medium. It is explained that an-isotropy of the medium caused by non-thermal plasma influenced the separation field, in both amplitude reduction and wavelength contraction. Fig. 6.6 explores the trend of the field for ε_1 , while its mathematical interpretation predicts its physical nature. It is expressed by Eq. (??) and can be described as ω_c has no big difference in the values in the different parts of Earth and ω_p has direct relation with the square root of N_e (ion concentration), which fluctuates massively with the variation of seasons and days to night. Therefore, without fluctuation on ω , ε_1 can be fluctuate. Since ε_1 has inverse relation with ω , so increase in N_e with fixed ω , ε_1 declines and wavelength will be increase. It means that the separated field with longer wavelength will occur for increasing number of free charges in the medium.

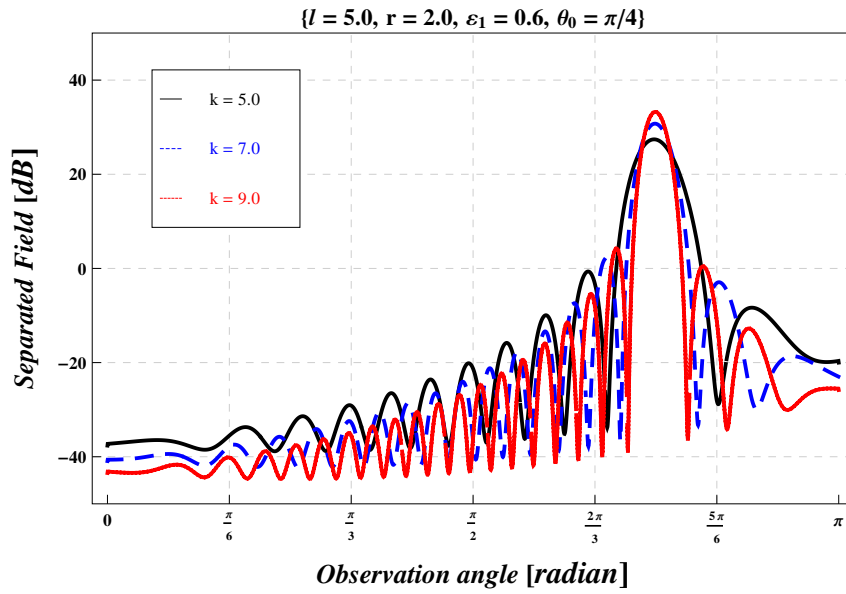


(a)

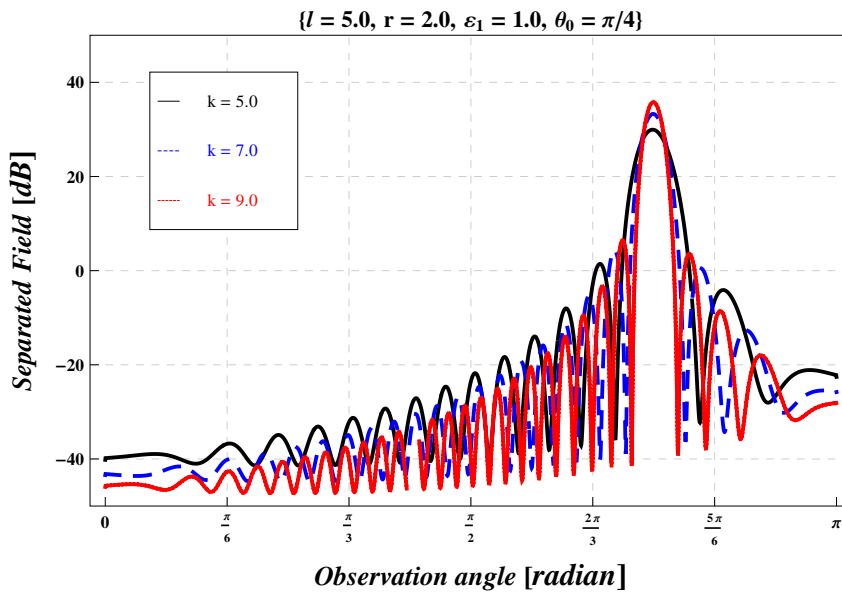


(b)

Figure 6.3: The separated field for θ_0 in the (a) isotropic and (b) an-isotropic medium.

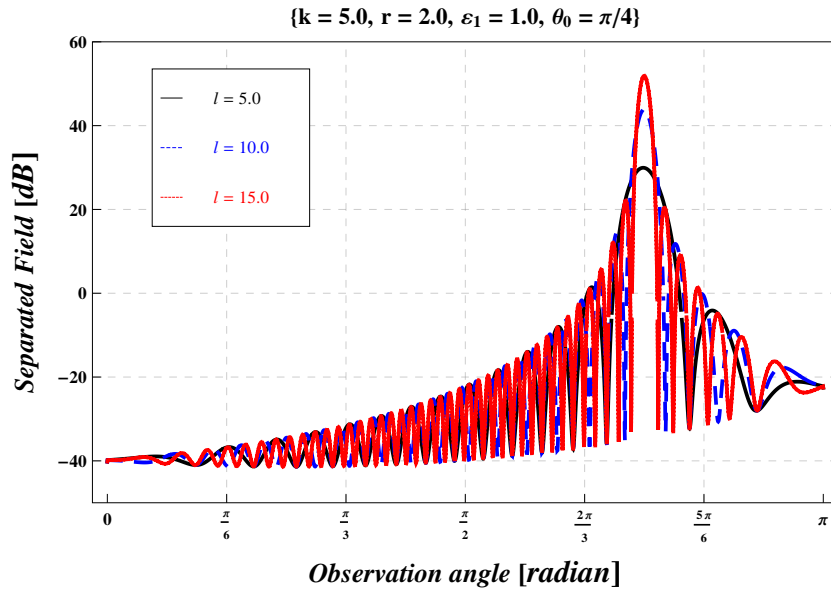


(a)

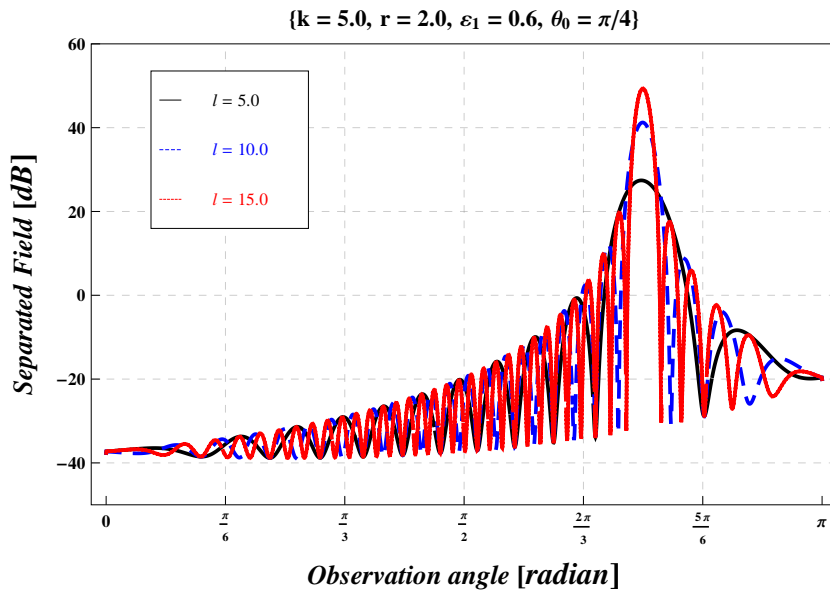


(b)

Figure 6.4: The separated field for k in the (a) isotropic and (b) an-isotropic medium.



(a)



(b)

Figure 6.5: The separated field for $2l$ in the (a) isotropic and (b) an-isotropic medium.

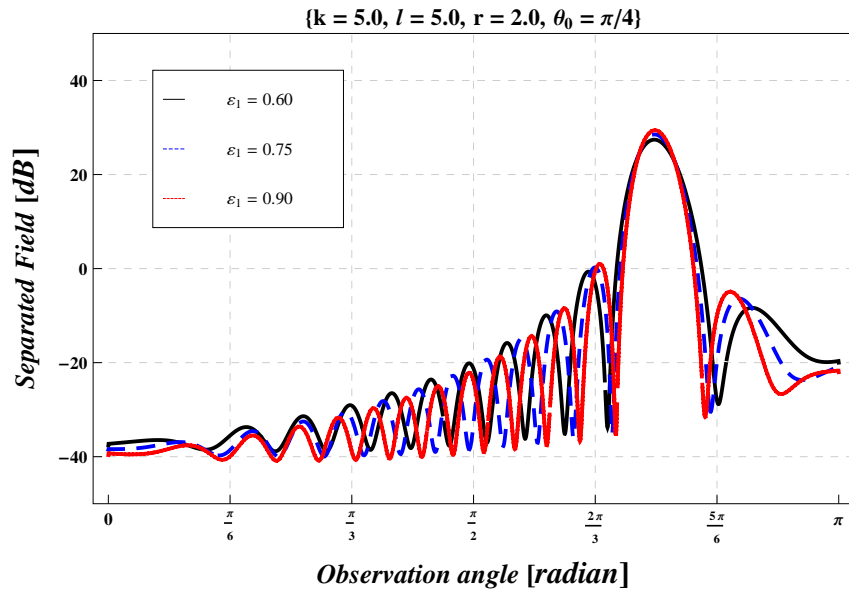


Figure 6.6: The separated field for ε_1 .

6.6 Conclusions

From above analysis, it is concluded that the diffraction behavior of H_z^{inc} on finite-width slit with Dirichlet surface is affected rigorously by parameters controlling behavior in the existence of non-thermal plasma. It is deeply figured out that the function H^{sep} is amplified by different θ_0 , k , $2l$, ε_1 and reduced by ε_2 .

Chapter 7

EM-Wave Incident on Finite-Width Slit with Neumann Conditions in An-isotropy of Non-thermal Plasma

This chapter thoroughly investigate the interaction of wave field due to finite-width slit by assuming the Neumann boundary conditions in the context of non-thermal plasma. After applying the Fourier transform to the Helmholtz equation, the boundary value problem is established. To solve the challenge stated for this model, the Wiener-Hopf analysis is used. At the completion of the analysis, the separated field computed along with its numerical findings are elaborated to further investigate the impacts of variation in physical parameters in an an-isotropic medium.

7.1 Problem Statement

We have investigated the diffraction pattern of plane electromagnetic waves due to a finite-width slit in non-thermal plasma, as illustrated in Fig. 7.1. Furthermore, Neumann conditions are assumed on the slit and angle of incidence is θ_0 . The total

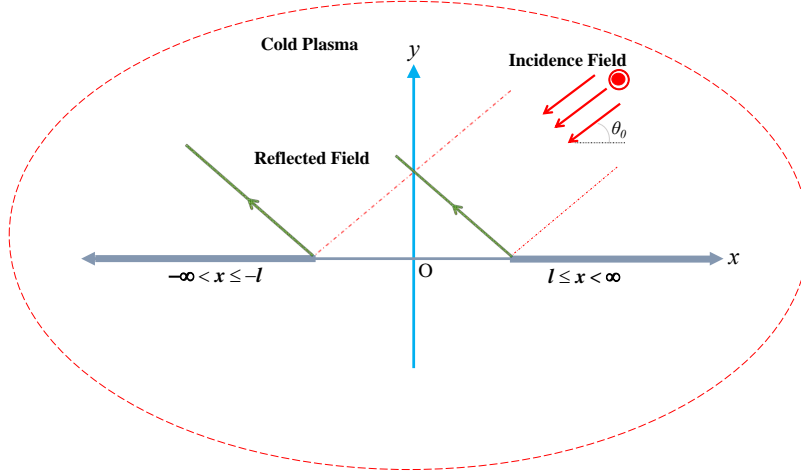


Figure 7.1: **Simplified figure of the problem.**

field can be represented in terms of incident, refracted and diffracted fields as:

$$H_z^{tot}(x, y) = H_z^{inc}(x, y) - H_z^{ref}(x, y) + H_z(x, y), \quad (7.1)$$

where the incident and refracted fields are defined as

$$H_z^{inc}(x, y) = e^{-ik_{eff}(x \cos \theta_0 + y \sin \theta_0)}, \quad (7.2)$$

$$H_z^{ref}(x, y) = e^{-ik_{eff}(x \cos \theta_0 - y \sin \theta_0)}. \quad (7.3)$$

Suppose that medium is slightly lossy, and constant K_{eff} appearing in above equations is complex in such a way ($0 < \Im\{k_{eff}\} \ll \Re\{k_{eff}\}$). At the end, for real K_{eff} solution could be determine by taking its imaginary part to zero. The entire field $H_z^{tot}(x, y)$ meeting the Helmholtz equation is

$$[\partial_{xx} + \partial_{yy} + k_{eff}^2]H_z^{tot}(x, y) = 0, \quad (7.4)$$

Substituting the value of $H_z^{tot}(x, y)$ from (7.1), we get the equation for diffracted field as:

$$[\partial_{xx} + \partial_{yy} + k_{eff}^2]H_z(x, y) = 0, \quad (7.5)$$

In order to establish the Wiener-Hopf equation, conditions at $x = \pm l$ in conjunction with continuity relations are used. Neumann boundary conditions on a finite-width slit are specified as

$$H_z^{tot} = 0, \text{ for } -l \geq x \geq l, \text{ and } y = 0^\pm, \quad (7.6)$$

along with

$$H_z^{tot}(x, 0^+) = H_z^{tot}(x, 0^-) = 0, \quad \text{at } |x| < l, \quad y = 0, \quad (7.7)$$

7.2 Problem Transformation

Following results can be obtained with the use of Fourier Transforms.

$$\begin{aligned} \mathcal{F}(\beta, y) &= \frac{1}{\sqrt{2\pi}} \int_{-\infty}^{\infty} e^{i\beta x} H_z(x, y) dx \\ &= e^{i\beta l} \mathcal{F}_+(\beta, y) + e^{-i\beta l} \mathcal{F}_-(\beta, y) + \mathcal{F}_l(\beta, y), \end{aligned} \quad (7.8)$$

where $\beta = \sigma + i\tau$.

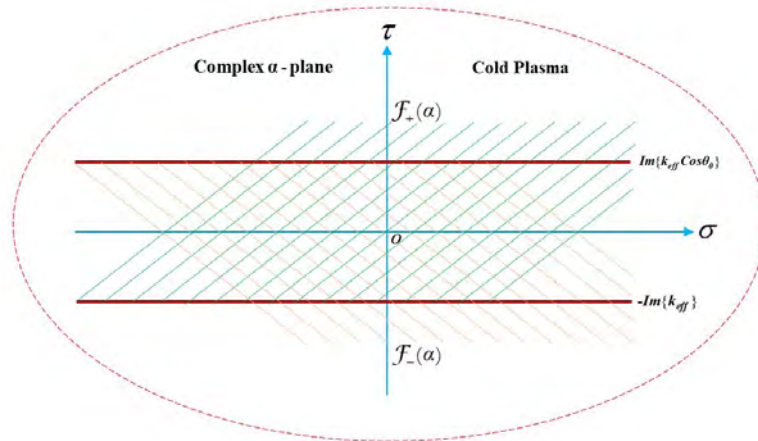


Figure 7.2: Illustration of Analytic-Continuation.

For high values of x , the diffracted field is interpreted as follows:

$$H_z(x, y) = \begin{cases} O(e^{-ik_{eff}x}), \\ O(e^{-k_{eff}x \cos \theta_0}). \end{cases} \quad (7.9)$$

The regions of regularity in the complex plane for $\mathcal{F}_+(\beta, y)$ and $\mathcal{F}_-(\beta, y)$ are $\Im\{\beta\} > -\Im\{k_{eff}\}$ and $\Im\{\beta\} < \Im\{k_{eff} \cos \theta_0\}$. From Fig 7.2, we can see the common region $-\Im\{k_{eff}\} < \Im\{\beta\} < \Im\{k_{eff} \cos \theta_0\}$ of analyticity, where the functions $\mathcal{F}_l(\beta, y)$ are also analytic and hence, we can define

$$\mathcal{F}_\pm(\beta, y) = \pm \frac{1}{\sqrt{2\pi}} \int_{\pm l}^{\pm\infty} e^{i\beta(x \mp l)} H_z(x, y) dx \quad (7.10)$$

$$\mathcal{F}_l(\beta, y) = \frac{1}{\sqrt{2\pi}} \int_{-l}^l e^{i\beta x} H_z(x, y) dx \quad (7.11)$$

$$\mathcal{F}^{inc}(\beta, y) = \frac{\exp(-iyk_{eff} \sin \theta_0)}{\sqrt{2\pi}} \left(\frac{\exp[i\beta(\beta - k_{eff} \cos \theta_0)] - \exp[-i\beta(\beta - k_{eff} \cos \theta_0)]}{i(\beta - k_{eff} \cos \theta_0)} \right). \quad (7.12)$$

$$\mathcal{F}^{ref}(\beta, y) = \frac{\exp(iyk_{eff} \sin \theta_0)}{\sqrt{2\pi}} \left(\frac{\exp[i\beta(\beta - k_{eff} \cos \theta_0)] - \exp[-i\beta(\beta - k_{eff} \cos \theta_0)]}{(\beta - k_{eff} \cos \theta_0)} \right). \quad (7.13)$$

The following transformed boundary value problem could be obtained by applying the Fourier transformation to Eqs. (7.5 – 7.7) .

$$\left(\frac{d^2}{dy^2} + \gamma^2 \right) \mathcal{F} = 0 \quad (7.14)$$

where $\gamma(\beta) = \sqrt{k_{eff}^2 - \beta^2}$.

$$\begin{aligned} \mathcal{F}(\beta, 0^+) &= \mathcal{F}^{ref}(\beta, 0) - \mathcal{F}^{inc}(\beta, 0), \\ \mathcal{F}(\beta, 0^-) &= 0 \end{aligned}, \quad (7.15)$$

and

$$\mathcal{F}_\pm(\beta, 0^+) = 0 = \mathcal{F}_\pm(\beta, 0^-). \quad (7.16)$$

7.3 Solution of the Wiener-Hopf Equation

The solution of transformed boundary value problem (7.14), fulfilling the radiation conditions is,

$$\mathcal{F}(\beta, y) = \begin{cases} A_1(\beta) \exp(-i\gamma y) & y \geq 0, \\ A_2(\beta) \exp(i\gamma y) & y < 0. \end{cases} \quad (7.17)$$

Now using Eqs. (7.15 – 7.17), following Wiener-Hopf equation is obtained.

$$\exp(i\beta l)\mathcal{F}'_+(\beta, 0) + \exp(-i\beta l)\mathcal{F}'_-(\beta, 0) + \mathcal{K}(\beta)\tilde{\mathcal{F}}_l(\beta, 0) = -i\mathcal{G}(\beta), \quad (7.18)$$

where,

$$\mathcal{K}(\beta) = i\gamma, \quad (7.19)$$

$$\tilde{\mathcal{F}}_l(\beta, 0) = \frac{1}{2} (\mathcal{F}_l(\beta, 0^+) - \mathcal{F}_l(\beta, 0^-)) \quad (7.20)$$

$$\mathcal{G}(\beta) = \frac{\exp[i\beta(\beta - k_{eff} \cos \theta_0)] - \exp[-i\beta(\beta - k_{eff} \cos \theta_0)]}{\sqrt{2\pi(\beta - k_{eff} \cos \theta_0)}}, \quad (7.21)$$

The Kernel function defined in Eq. 7.19 can be written as:

$$\mathcal{K}(\beta) = \frac{1}{i\gamma(\beta)} = \mathcal{K}_\pm(\beta) \text{ with } \gamma(\beta) = \gamma_\pm(\beta), \quad (7.22)$$

where $\mathcal{K}_\pm(\beta)$ are,

$$\mathcal{K}_\pm(\beta) = \frac{\exp(-i\frac{\pi}{4})}{\gamma_\pm(\beta)} \text{ with } \gamma_\pm(\beta) = \sqrt{k_{eff} \pm \beta}. \quad (7.23)$$

It must be noted that the functions, $\mathcal{K}_\pm(\beta)$ have region of regularity are $\Im\{\beta\} > -\Im\{k_{eff}\}$ and $\Im\{\beta\} < \Im\{k_{eff} \cos \theta_0\}$ and similarly for $\gamma_\pm(\beta)$. From Eq. (7.18), equating the terms which are regular in their corresponding regions, creates a common region of analyticity. Hence, by analytic continuation, we get an entire function $\mathcal{P}(\beta)$ and by Liouville's theorem, $\mathcal{P}(\beta)$ must be equal to zero[12], yielding the following results.

$$\mathcal{F}_{\pm}(\beta, 0) = \frac{\mathcal{A}}{\sqrt{2\pi}} [\mathcal{K}_{\pm}(\beta)\mathcal{G}_{1,2}(\pm\beta) + \mathcal{K}_{\pm}(\beta)\mathcal{T}(\pm\beta)\mathcal{C}_{1,2}], \quad (7.24)$$

where

$$\mathcal{G}_{1,2}(\beta) = \frac{\exp(\mp ik_{eff}l \cos \theta_0)}{\alpha \mp k_{eff} \cos \theta_0} \left(\frac{1}{\mathcal{K}_{+}(\beta)} - \frac{1}{\mathcal{K}_{+}(\pm k_{eff} \cos \theta_0)} \right) - \exp(\pm ik_{eff}l \cos \theta_0) \mathcal{R}_{1,2}(\beta), \quad (7.25)$$

$$\mathcal{C}_{1,2} = \mathcal{K}_{+}(k_{eff}) \frac{\mathcal{G}_{2,1}(k_{eff}) + \mathcal{K}_{+}(k_{eff})\mathcal{G}_{1,2}(k_{eff})\mathcal{T}(k_{eff})}{1 - \mathcal{K}_{+}^2(k_{eff})\mathcal{T}^2(k_{eff})}, \quad (7.26)$$

$$\mathcal{R}_{1,2}(\beta) = \frac{E_{-1}}{2\pi i(\beta \mp k_{eff} \cos \theta_0)} [\mathcal{W}_{-1}(-i(k_{eff} \pm k_{eff} \cos \theta_0)) - \mathcal{W}_{-1}(-i(k_{eff} + \beta))], \quad (7.27)$$

$$\mathcal{T}(\beta) = \frac{E_{-1}}{2\pi} \mathcal{W}_{-1}[-i(k_{eff} + \beta)l], \quad E_{-1} = 2\sqrt{\frac{l}{i}} e^{ik_{eff}\beta}, \quad (7.28)$$

$$\mathcal{W}_{n-1/2}(q) = \int_0^{\infty} \frac{v^n e^{-v}}{v+q} dv = \Gamma(n+1) e^{(\frac{q}{2})} q^{(n-1)/2} \mathcal{W}_{-(n+1)/2, n/2}(q), \quad (7.29)$$

where $q = -i(k_{eff} + \beta)l$, $n = -\frac{1}{2}$ and \mathcal{W} is the Whittaker function. Solving Eqs. 7.17 and 7.18, diffracted field is,

$$\mathcal{F}(\beta, y) = -\frac{1}{\mathcal{K}(\beta)} [\exp(i\beta l)\mathcal{F}_{+}(\beta, 0) + \exp(-i\beta l)\mathcal{F}_{-}(\beta, 0) + \mathcal{F}_l(\beta, 0)] e^{-i\gamma|y|}, \quad (7.30)$$

where

$$\mathcal{F}_l(\beta, 0) = i\mathcal{G}(\beta), \quad (7.31)$$

Inverse Fourier transformation of Eq. (7.30), yeilds the diffracted field as:

$$H_z(x, y) = \frac{1}{\sqrt{2\pi}} \int_{-\infty}^{\infty} \mathcal{F}(\beta, y) \exp(-i\beta x - i\gamma|y|) d\beta. \quad (7.32)$$

Inserting (7.30) in (7.32), we get

$$H_z(x, y) = -\frac{1}{\sqrt{2\pi}} \int_{-\infty}^{\infty} \frac{1}{\mathcal{K}(\beta)} \left\{ \begin{array}{l} \exp(i\beta l)\mathcal{F}_{+}(\beta, 0) + \exp(-i\beta l)\mathcal{F}_{-}(\beta, 0) + \\ + \tilde{\mathcal{F}}_l(\beta, 0) \end{array} \right\} \exp(-i\beta x - i\gamma|y|) d\beta. \quad (7.33)$$

Diffracted field $H_z(x, y)$ further bifurcate in the separated and interaction fields $H_z^{sep}(x, y)$ and $H_z^{int}(x, y)$, respectively as,

$$H_z(x, y) = H_z^{sep}(x, y) + H_z^{int}(x, y), \quad (7.34)$$

where

$$H_z^{sep}(x, y) = \frac{1}{2\pi} \int_{-\infty}^{\infty} \frac{\mathcal{A}}{\mathcal{K}(\beta)} \left\{ \begin{array}{l} \frac{\mathcal{K}_+(\beta) \exp[i(\beta - k_{eff} \cos \theta_0)l]}{\mathcal{K}_+(k_{eff} \cos)(\beta - k_{eff} \cos \theta_0)} \\ - \frac{\mathcal{K}_+(-\beta) \exp[-i(\beta - k_{eff} \cos \theta_0)l]}{\mathcal{K}_+(-k_{eff} \cos)(\beta - k_{eff} \cos \theta_0)} \end{array} \right\} \exp(-i\beta x - i\gamma|y|) d\beta, \quad (7.35)$$

$$H_z^{int}(x, y) = \frac{1}{2\pi} \int_{-\infty}^{\infty} \frac{\mathcal{A}}{\mathcal{K}(\beta)} \left\{ \begin{array}{l} \exp(i\beta l) \mathcal{K}_+(\beta) \mathcal{T}(\beta) \mathcal{C}_1 \\ - \exp[i(\beta + k_{eff} \cos \theta_0)l] \mathcal{K}_+(\beta) \mathcal{R}_1(\beta) \\ + \exp(-i\beta l) \mathcal{K}_-(\beta) \mathcal{T}(-\beta) \mathcal{C}_2 \\ - \exp[-i(\beta + k_{eff} \cos \theta_0)l] \mathcal{K}_-(\beta) \mathcal{R}_2(-\beta) \end{array} \right\} \exp(-i\beta x - i\gamma|y|) d\beta. \quad (7.36)$$

The separated field given by (7.35) depicts diffraction separately at the edges. The H_z^{int} represented by Eq. (7.36) explains the interaction of one end with the other.

7.4 Diffracted Field

The diffracted field due to slit of finite width for the far field can be obtained asymptotically by coping with the integral appearing in (7.32). Polar coordinates are introduced for the evaluation of Eq. 7.32 with the following transformation.

$$\beta = -k_{eff} \cos(\phi + i\eta), \quad 0 < \phi < \pi, \quad -\infty < \eta < \infty. \quad (7.37)$$

Now when the method of stationary phase [32] is used for (7.32), the following result are obtained:

$$H_z(r, \phi) = \frac{ik_{eff}}{\sqrt{k_{eff}r}} \mathcal{F}(-k_{eff} \cos \phi, \pm r \sin \phi) \sin \phi \exp\left(ik_{eff}r + i\frac{\pi}{4}\right). \quad (7.38)$$

Using the same polar coordinates, the transformation and subsequently the method of stationary phase are used to assess and yield the separated field and interaction fields as follows:

$$\{H_z^{sep}, H_z^{int}\}(r, \phi) = \frac{1}{\sqrt{2\pi}} \frac{ik_{eff}}{\sqrt{k_{eff}r}} \{f_{sep}, -f_{int}\}(-k_{eff} \cos \phi) \sin \phi \exp\left(ik_{eff}r + i\frac{\pi}{4}\right), \quad (7.39)$$

where

$$f_{sep}(-k_{eff} \cos \phi) = \frac{\mathcal{A}}{\mathcal{K}(-k_{eff} \cos \phi)} \left\{ \begin{array}{l} \frac{\mathcal{K}_+(-k_{eff} \cos \phi) \exp[-ik_{eff}l(\cos \phi + \cos \theta_0)]}{\mathcal{K}_+(k_{eff} \cos \theta_0)(-k_{eff} \cos \phi - k_{eff} \cos \theta_0)} \\ - \frac{\mathcal{K}_+(k_{eff} \cos \phi) \exp[ik_{eff}l(\cos \phi + \cos \theta_0)]}{\mathcal{K}_+(-k_{eff} \cos \theta_0)(-k_{eff} \cos \phi - k_{eff} \cos \theta_0)} \end{array} \right\} \quad (7.40)$$

$$f_{int}(-k_{eff} \cos \phi) = \frac{\mathcal{A}}{\mathcal{K}(-k_{eff} \cos \phi)} \left\{ \begin{array}{l} \exp(-ik_{eff}l \cos \phi) \mathcal{K}_+(-k_{eff} \cos \phi) \\ \times \mathcal{T}(-k_{eff} \cos \phi) \mathcal{C}_1 \\ - \exp[il(-k_{eff} \cos \phi + k_{eff} \cos \theta_0)] \\ \times \mathcal{K}_+(-k_{eff} \cos \phi) \mathcal{R}_1(-k_{eff} \cos \phi) \\ + \mathcal{K}_-(-k_{eff} \cos \phi) \exp(ik_{eff}l \cos \phi) \\ \times \mathcal{T}(k_{eff} \cos \phi) \mathcal{C}_2 \\ - \exp[-il(-k_{eff} \cos \phi + k_{eff} \cos \theta_0)] \\ \times \mathcal{K}_-(-k_{eff} \cos \phi) \mathcal{R}_2(k_{eff} \cos \phi) \end{array} \right\} \quad (7.41)$$

From Eq. (7.38), we can clearly see that the asymptotic expressions for far field can be obtained by letting $k_{eff}r \rightarrow \infty$ and the resulting expressions will be holds true for any observational angle. The separated field of an EM-wave is investigated in order to characterise both the field diffracted by the corners of a slit and the influence of the geometrical wave field. The separated field that results gives physical evidence

for the non-thermal plasma concept. Separated-field, on the other hand, provides no physical information due to contact at one edge with the other, which has already been enumerated by separated-field. As a result, we've only talked about the separated field because it conveys a full physical comprehension of EM-wave diffraction at the established boundaries. Additionally, we discovered that the interaction field is created by diffraction from the corners of slit at $x = \pm l$. Furthermore, when the slit width is increased up to ∞ , the contribution of H_z^{int} terms disappears, leaving just the separated field terms in the diffracted field. As a consequence, we merely examine the separated field, as illustrated visually in the next section.

7.5 Discussion and Numerical Results

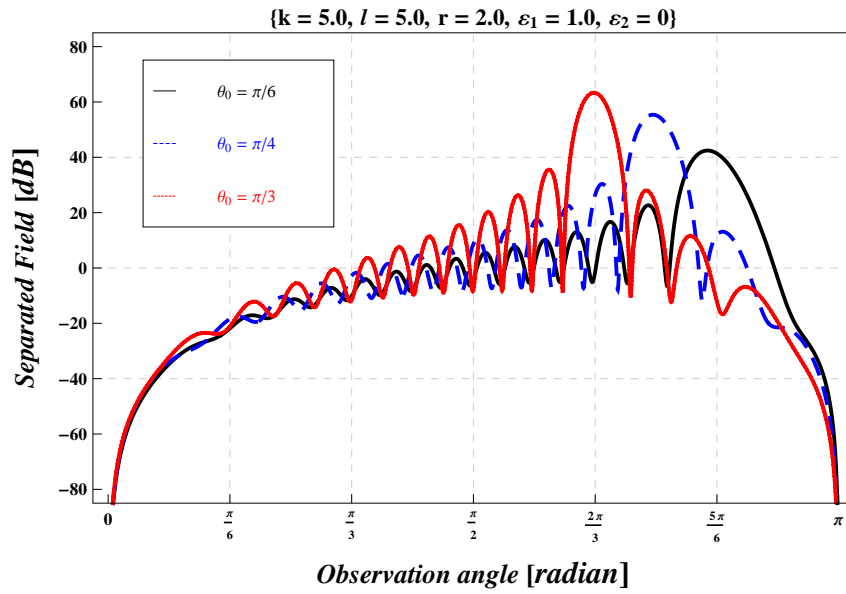
In this section, we examined the EM-waves by finite-width slit as graphically by the variation of physical parameters in an anisotropic media with Neumann conditions versus the observational angle. For the ionosphere, we take the value of ω_p as $56.4MHz$ and ω_c as $8.78MHz$. Now, the values of ε_1 and ε_2 are computed numerically against ω to verify the considered model. Also, the values of ω are taken between $80MHz$ and $600MHz$ given in Table-7.1. It can be notice from Table-7.1, that the value of ε_2 is comparably very small from ε_1 with the boost up of ω in the frequency range. For isotropic medium, we can take $\varepsilon_1 = 1$ and $\varepsilon_2 = 0$, While the parameters ε_1 and ε_2 for the anisotropic media (non-thermal plasma) can indeed be selected from Table-1.

ω (in MHz)	ε_1	ε_2
80.15	0.504834	0.054242
99.50	0.678699	0.028352
145.75	0.850259	0.009020
245.15	0.947071	0.001895
375.50	0.97744	0.000527
480.50	0.986222	0.000251
599.75	0.991157	0.000129

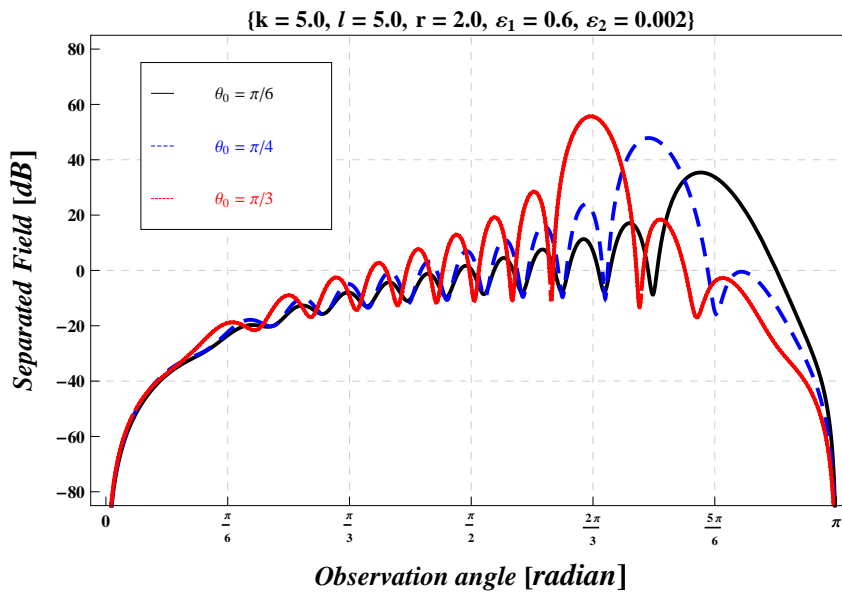
Table 7.1: Values of ε_1 and ε_2 for corresponding ω .

The graphical analysis is elaborated to explore the influence of physical parame-

ters on diffracted field due to a finite-width slit lying in the ionosphere of non-thermal plasma. These physical parameters are θ_0 , k , $2l$ and ε_1 . Fig. ?? represents the pattern of the separated field for variation of θ_0 , and it gets maxima for $\theta_0 = \pi/3, \pi/4, \pi/6$ occurring at $\theta = 2\pi/3, 3\pi/4, 5\pi/6$, respectively. These maxima actually predict the shadow of reflected field. Fig. ?? reveals the separated field for k . It is notable that the field has a direct dependence upon k because the field gets amplified for k . Since the frequency is directly related to k , so it excites the frequency of wave towards the high range. As extension of the slit-width is actually the expansion of aperture which is responsible for the diffraction of electromagnetic radiations, and so, separated field gets amplified as well as more oscillated as can be seen in Fig. ?. This amplified amplitude could be controlled by introducing the ionosphere as can be observed through Fig.?.?. By comparing Figs. ??, ?? and ?? of the separated field in the anisotropic medium with their respective Figs. ??, ?? and ?? in the isotropic medium. It is explained that anisotropy of the medium caused by non-thermal plasma influenced the separation field, in both amplitude reduction and wavelength contraction. Fig. ?? explores the trend of the field for ε_1 , while its mathematical interpretation predicts its physical nature. It is expressed by Eq. (??) and can be described as ω_c has no big difference in the values in the different parts of Earth and ω_p has direct relation with the square root of N_e (ion concentration), which fluctuates massively with the variation of seasons and days to night. Therefore, without fluctuation on ω , ε_1 can be fluctuate. Since ε_1 has inverse relation with ω , so increase in N_e with fixed ω , ε_1 declines and wavelength will be increase. It means that the separated field with longer wavelength will occur for increasing number of free charges in the medium.

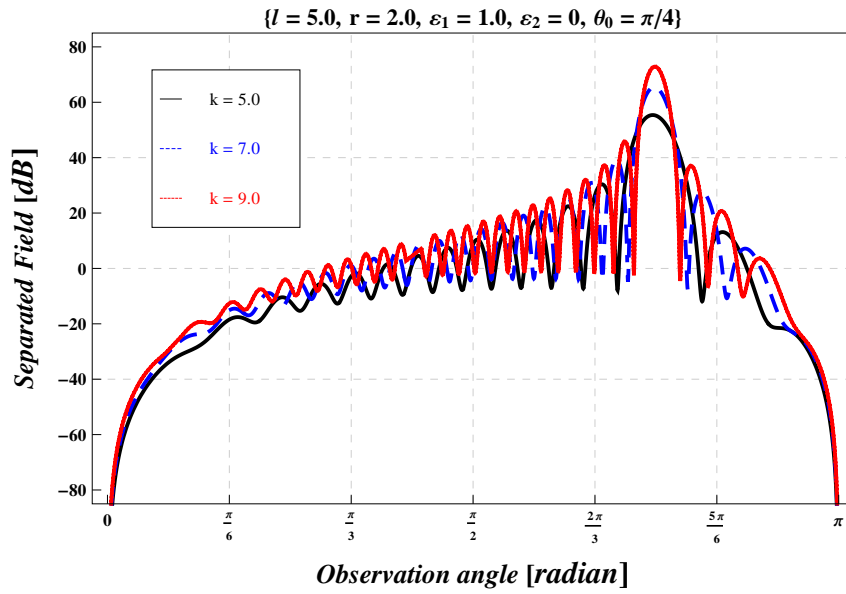


(a)

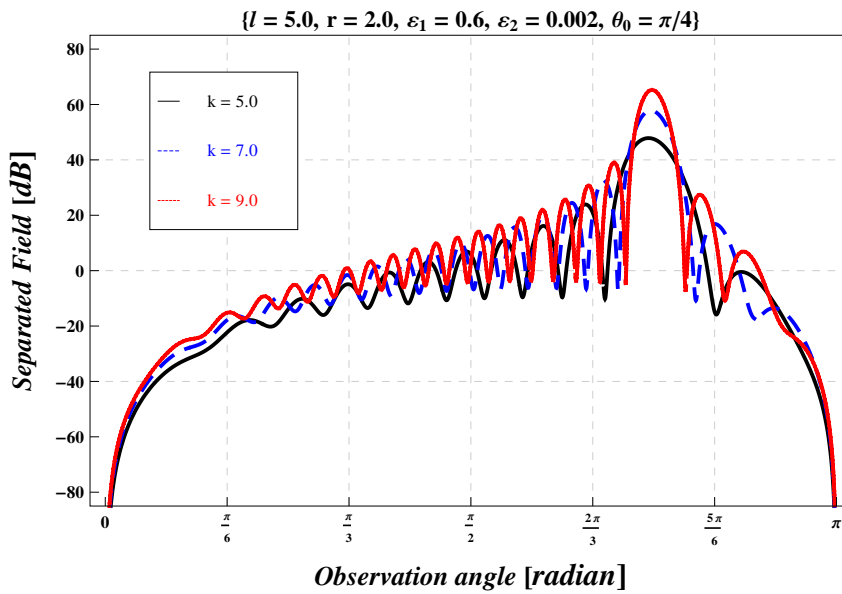


(b)

Figure 7.3: The separated field for θ_0 in the (a) isotropic and (b) an-isotropic medium.

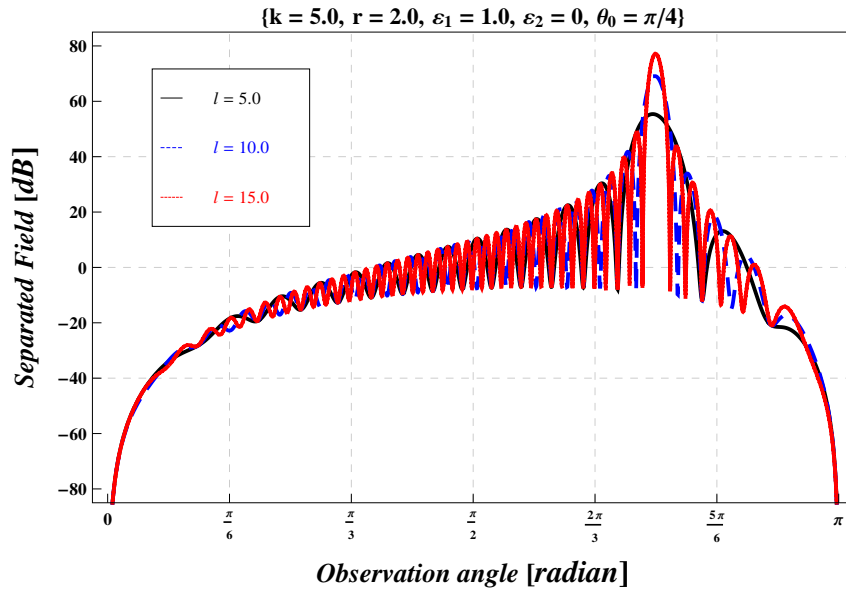


(a)

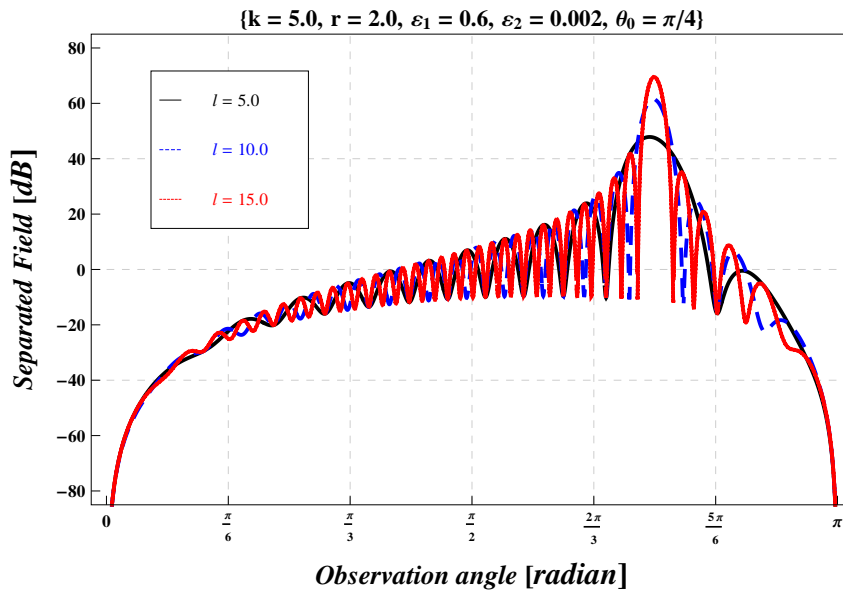


(b)

Figure 7.4: The separated field for k in the (a) isotropic and (b) an-isotropic medium.



(a)



(b)

Figure 7.5: The separated field for $2l$ in the (a) isotropic and (b) an-isotropic medium.

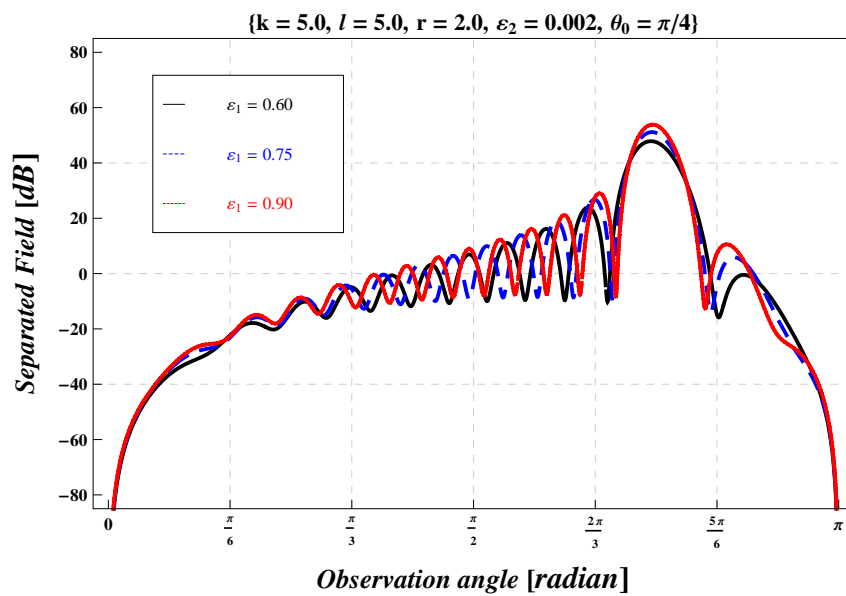


Figure 7.6: The separated field for ε_1 .

7.6 Conclusions

On the basis of deep analysis, it is concluded that the diffraction behavior of H_z^{inc} incident on finite-width slit under the assumptions of Neumann surface is affected rigorously by parameters controlling behavior in the existence of non-thermal plasma. It is deeply figured out that the function H^{sep} is amplified by different θ_0 , k , $2l$, ε_1 and reduced by ε_2 .

References

- [1] H. Poincare, Sur la polarization par diffraction, *Acta. Math.* 16 (1892) 297–339.
- [2] A. Sommerfeld, Mathematische theorie der diffraction. *Math. Ann.* 47 (1896) 317–374.
- [3] B. Nobel, *Methods Based on the Wiener–Hopf Technique*, Pergamon, London, (1958).
- [4] R. Mittra and S. W. Lee, *Analytical Technique in the Theory of Guided Waves*, Macmillan, New York, 1971.
- [5] V. P. Shestopalov, *The Riemann-Hilbert Method in the Theory of Diffraction and Propagation of Electromagnetic Waves*, Kharkov University Press, Kharkov, 1971.
- [6] Y. Okuno, *Analysis Methods for Electromagnetic Wave Problems*, Artech House, Boston, 1990.
- [7] K. Kobayashi, Plane wave diffraction by a strip: Exact and asymptotic solutions, *J. Phys. Soc. Japan*, 60 (1991) 1891–1905.
- [8] J. B. Lawrie and I. D. Abrahams, A brief historical perspective of Wiener–Hopf technique. *Journal of Engineering Mathematics* 59 (2007) 351–358.
- [9] R. Nawaz, M. Ayub and Javaid, Plane wave diffraction by a finite plate with impedance boundary conditions, *PloS ONE* 9 (2014) 1–13.

- [10] P. M. Morse and P. J. Rubenstein, The diffraction of waves by ribbon and slits, *Phys. Rev.* (1938) 895.
- [11] P. C. Clemmow, *The Plane Wave Spectrum Representation of Electromagnetic Field*, Pergamon, New York, (1966).
- [12] K. Hongo, Diffraction of electromagnetic plane wave by two parallel infinitely long slits in a thin conducting screen, *Trans. Inst. Electronics and Comm. Engrg. in Japan* 57-B (1974) 565–572.
- [13] A. Imran, Q. A. Naqvi and K. Hongo, Diffraction of plane wave by two parallel slits in an infinitely long impedance plane using the method of Kobayashi potential, *Progress In Electromagnetic Research* 63 (2006) 107 – 123.
- [14] M. K. Tippett and R. W. Ziolkowski, A Bidirectional Wave Transformation of The Cold-Plasma Equations, *Journal of Mathematical Physics* 32 (1991) 488 – 492.
- [15] A. D. Avdeev, On the Special Function of the Problem of Diffraction by a Wedge in an Anisotropic-Plasma, *Radio Tekhnika I Elektronika* 39 (1994) 885 – 892.
- [16] S. L. Dvorak, R. W. Ziolkowski and D. G. Dudley, Ultra-Wide-Band Electromagnetic Pulse Propagation in a Homogeneous Cold Plasma, *Radio Science* 32 (1997) 239 – 250.
- [17] S. Yener and A. H. Serbest, Diffraction of Plane Wave by an Impedance Half-Plane in Cold Plasma, *J. of Electromagn. Waves and Appl.* 16 (2002) 995 – 1005.
- [18] Tufail A. Khan, M. Ayub and K. Jilani, E-polarized plane wave diffraction by an impedance loaded parallel-plate waveguide located in cold plasma, *Phys. Scr* 89 (2014) 01 – 09.
- [19] M. Ayub, T. A. Khan and K. Jilani, Effect of cold plasma permittivity on the radiation of the dominant TEM-wave by an impedance loaded parallel-plate waveguide radiator, *Math. Meth. Appl. Sci.* 39 (2015) 134 – 143.

- [20] S. Hussain, M. Ayub and G. Rasool, EM-Wave Diffraction by a Finite Plate with Dirichlet Conditions in the Ionosphere of Cold Plasma, *Physics of Wave Phenomena* 26 (2018) 342 – 350.
- [21] C. E. Pearson, G. F. Carrier and M. Krook, *Functions of a Complex Variable: Theory and Technique*, McGraw-Hill, New York, (1966).
- [22] E.T. Copson, *Asymptotic Expansions*, University Press, Cambridge, (1967).

Turnitin Originality Report

Exact and Asymptotic Analysis of EM-Wave Scattering in Cold Plasma
Javaid .

by Ayesha



From CL QAU (DRSML)

- Processed on 28-Jun-2022 09:04 PKT
- ID: 1864000888
- Word Count: 21076

Prof. Dr. Muhammad Ayub
(Supervisor)

Similarity Index

16%

Similarity by Source

Internet Sources:

10%

Publications:

12%

Student Papers:

3%

Focal Person (Turnitin)
Quaid-i-Azam University
Islamabad

sources:

1

1% match ()

[Toru EIZAWA. "有限幅正弦波状格子による電磁波散乱に関する解析的研究", 中央大学理工学部事務室, 2017](#)

2

1% match (publications)

[Toru Eizawa, Kazuya Kobayashi. "WIENER-HOPF ANALYSIS OF THE H-POLARIZED PLANE WAVE DIFFRACTION BY A FINITE SINUSOIDAL GRATING \(Invited Paper\)", Progress In Electromagnetics Research, 2014](#)

3

1% match (publications)

[S. Hussain, M. Ayub. "EM-Wave Diffraction by a Finite Plate with Neumann Conditions Immersed in Cold Plasma", Plasma Physics Reports, 2020](#)

4

1% match (publications)

[Sajjad Hussain, Muhammad Ayub, Rab Nawaz. "Analysis of high frequency EM-waves diffracted by a finite strip with impedance in anisotropic medium", Waves in Random and Complex Media, 2021](#)

5

1% match (Internet from 31-Jan-2013)

<http://aw.twi.tudelft.nl/~koekoek/documents/wi4006/watson.pdf>

6

1% match (Internet from 12-Jan-2017)

<http://cdmbuntu.lib.utah.edu/utils/getfile/collection/etd3/id/4034/filename/4032.pdf>

7

< 1% match (publications)

[Kazuya Kobayashi. "Solutions of Wave Scattering Problems for a Class of the Modified Wiener-Hopf Geometries", IEEJ Transactions on Fundamentals and Materials, 2013](#)

8

< 1% match (publications)

[Rolf Busam, Eberhard Freitag. "Complex Analysis", Springer Science and Business Media LLC, 2009](#)